Search for Charged Lepton Flavor Violation at J-PARC — COMET Phase-II Experiment

TingSam Wong
Osaka University of Japan

Based on Dr B. Krikler thesis

4st May, 2018

Overview

- Lepton Flavor Violation
- Muonic atom and muon electron conversion
- The COMET Phase-II experiment
  - Optimisation
  - Sensitivity
  - Background
- COMET status and R&D

Standard model

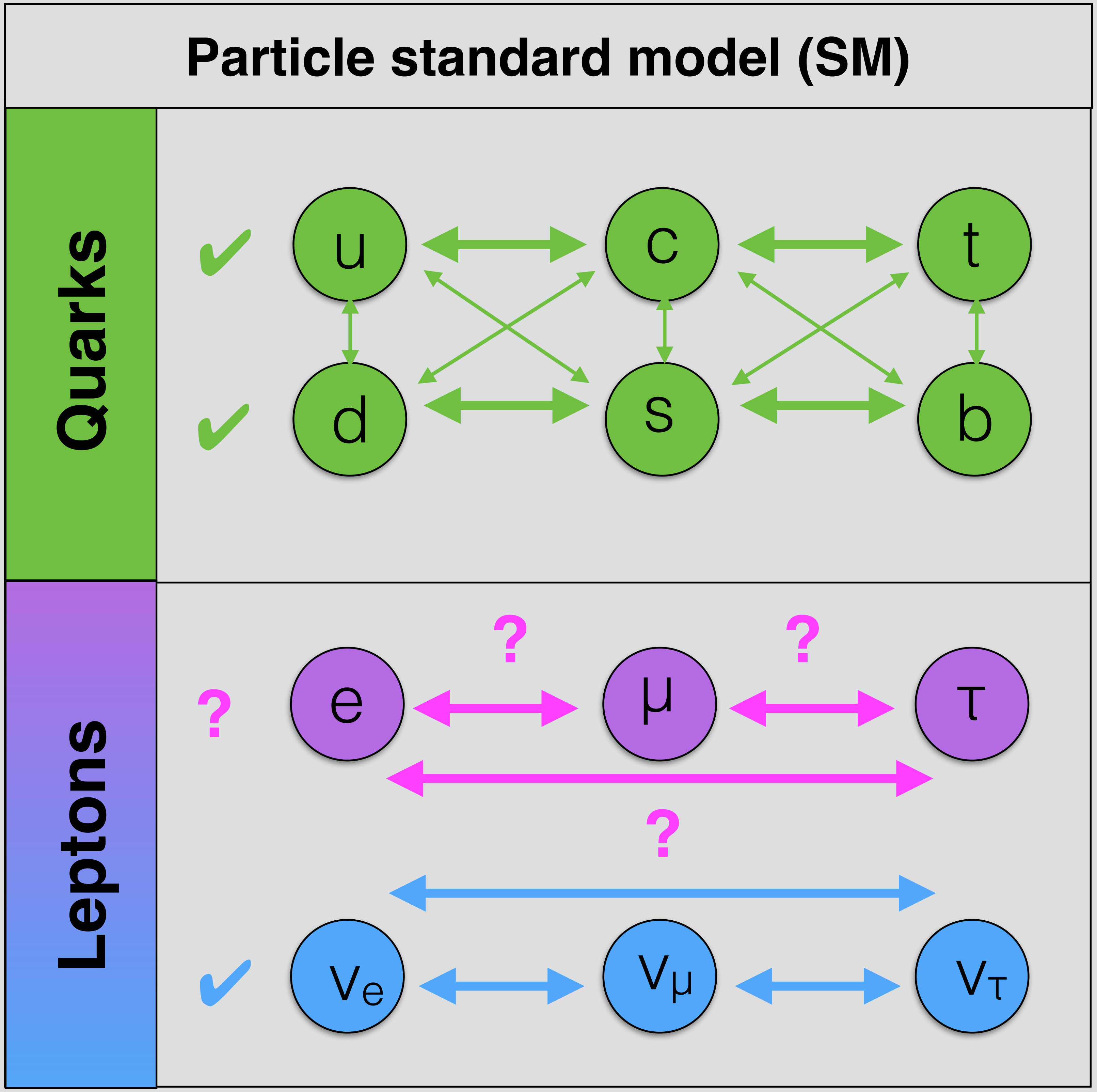

CKM matrx

PMNS matrx

Lepton Flavor Violation

What is Lepton Flavor?

Muon Decay in Flight

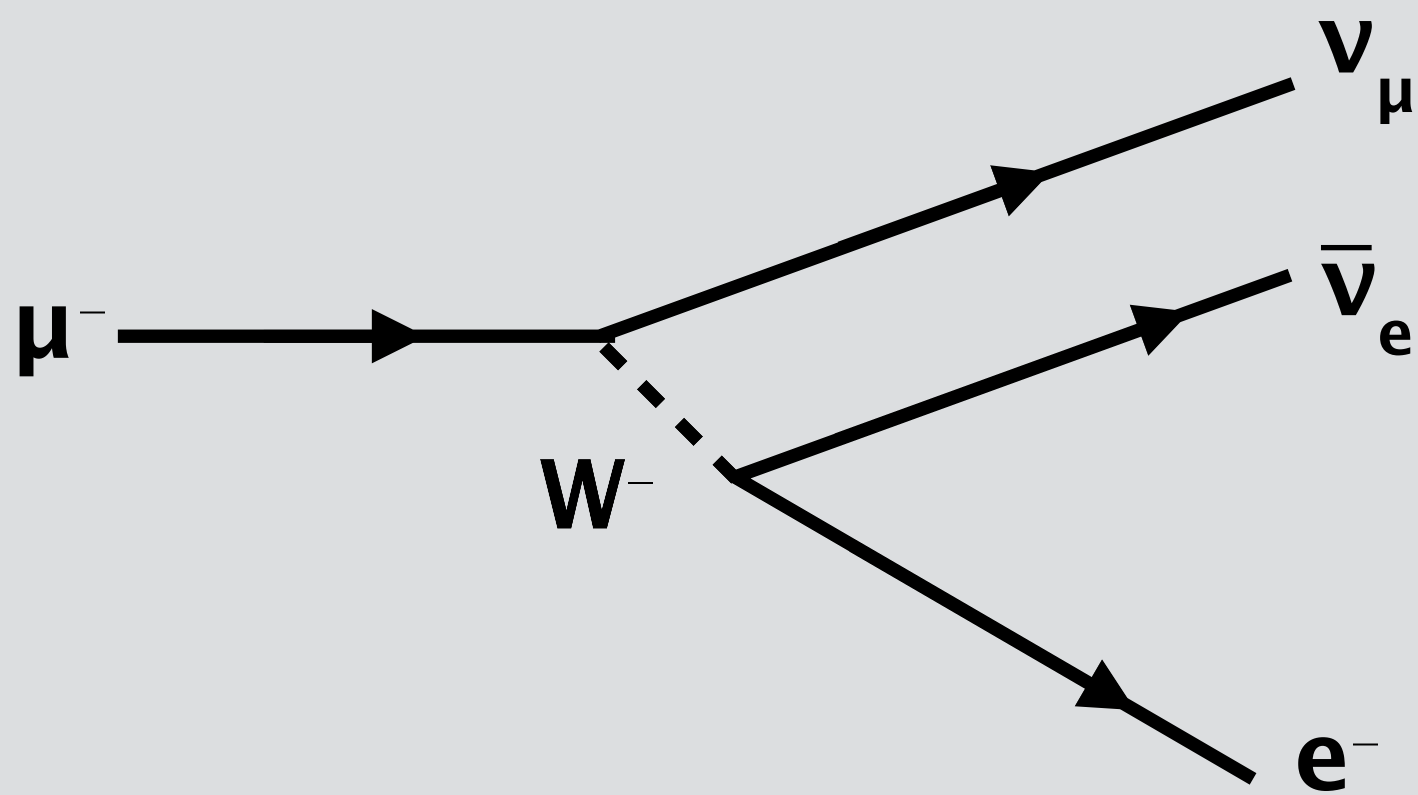

- **Standard model : Conversion of Lepton Flavor**

First guess of Lepton Flavor Violation (LFV)

Intermediate state: Neutrino oscillation

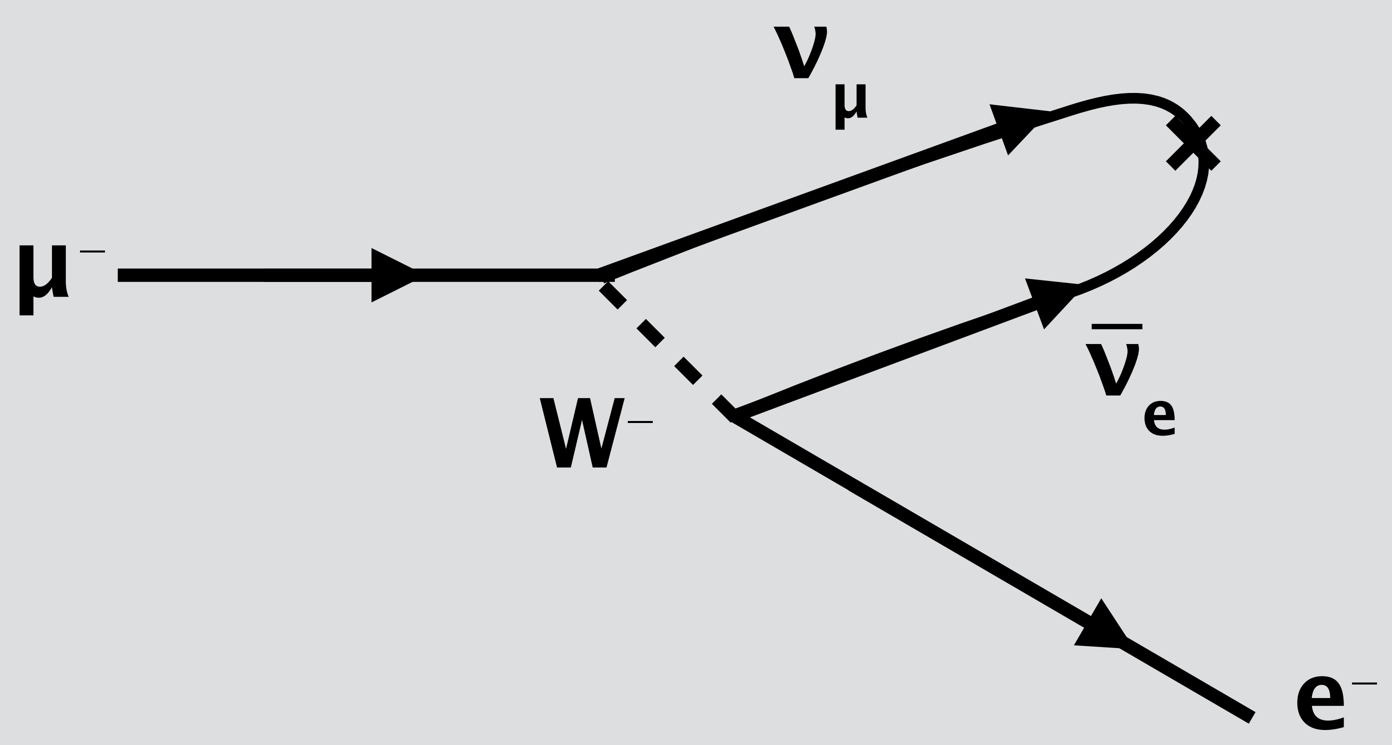

- **Unfortunately, the energy and momentum DO NOT converse**
- **We need something to provide energy → An ATOM will help us**

Muon electron conversion in nucleus field

Conversion of bounded muons via neutrino oscillation

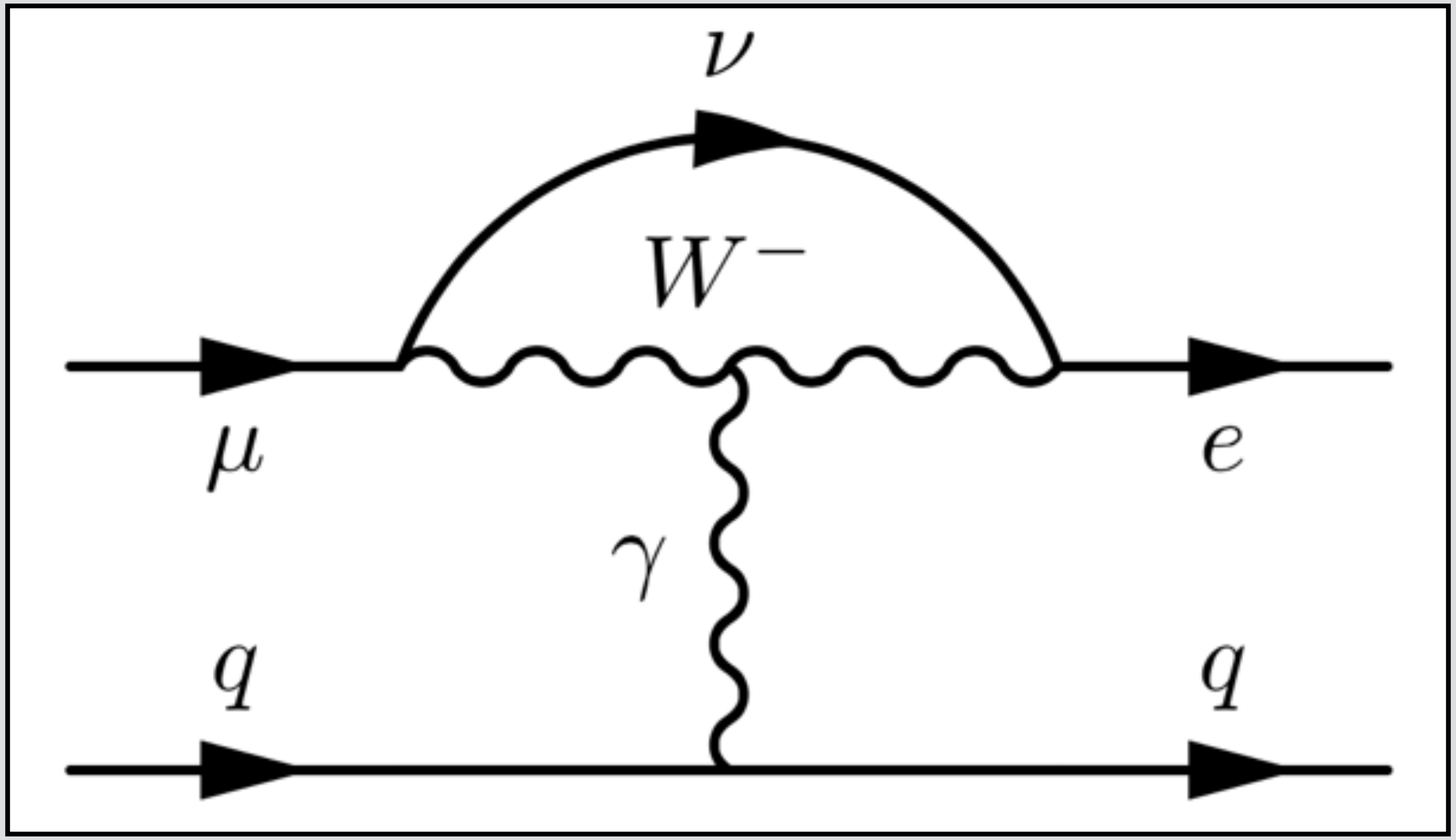

- **No outgoing neutrinos**
- **Now everything is good!**
- **Momentum && Energy conversed**
- **Charged Lepton Flavour Violation!**

$$\mu^- + N(A,Z) \to e^- + N(A,Z)$$

Muon electron conversion in nucleus field

Conversion of bounded muons via neutrino oscillation

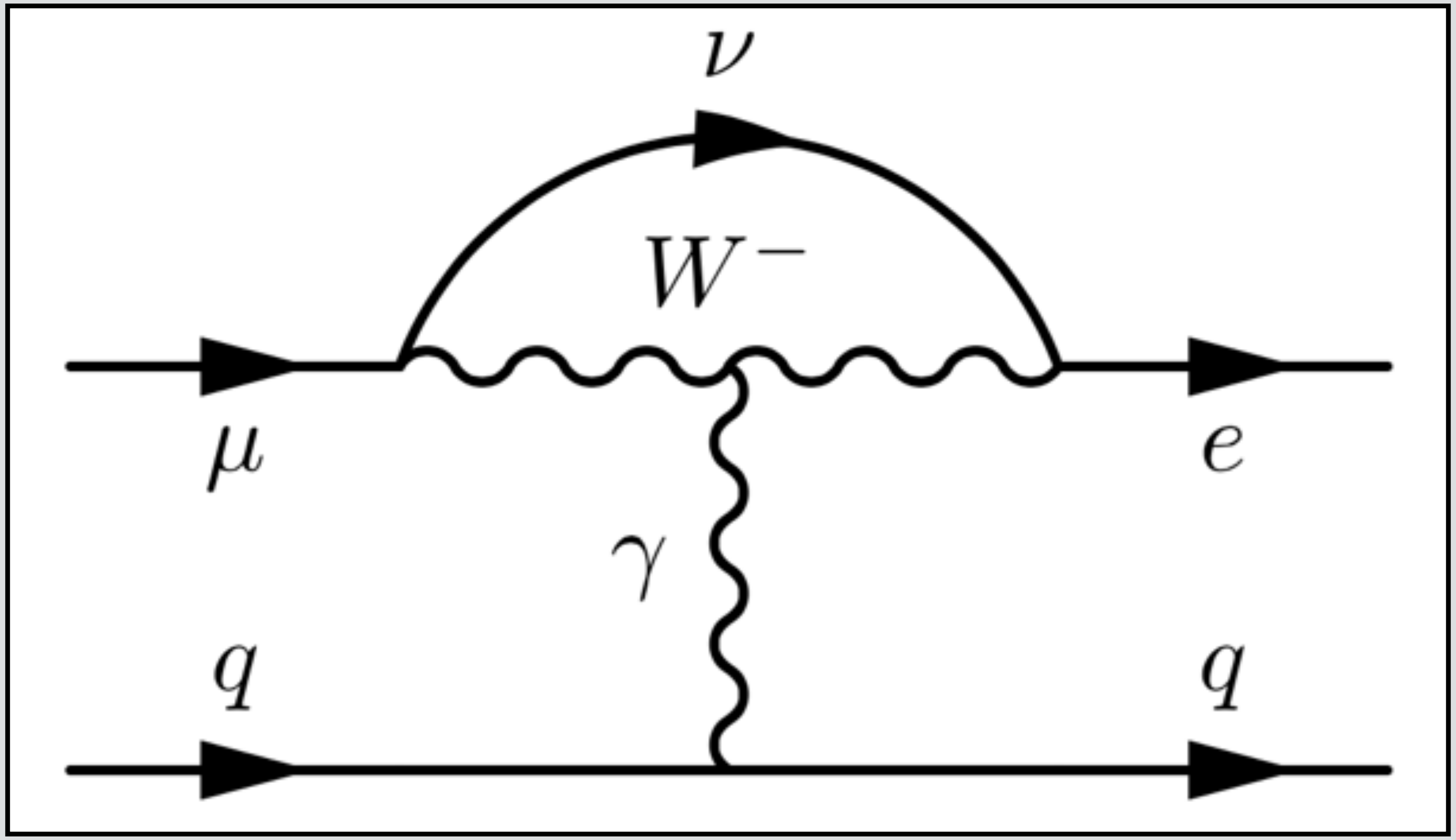

BUT…

Conversion Rate:

GIM Suppressed

$$\mathcal{R} = \mathcal{O}\left(\frac{(\Delta M_\nu^2)^2}{(M_W^2)^2}\right) \sim 10^{-54}$$

μ-e conversion beyond standard model

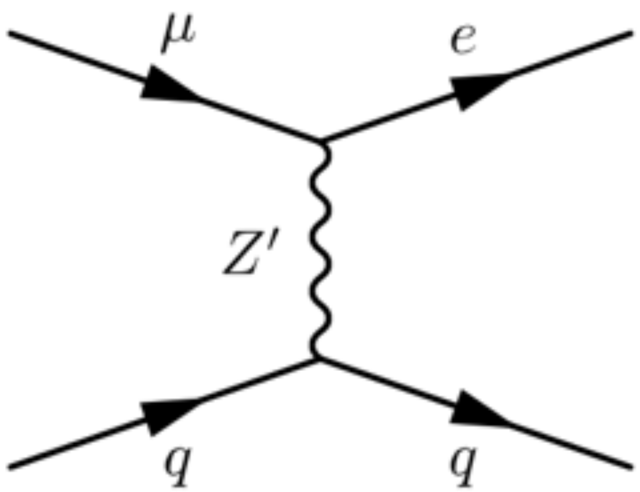

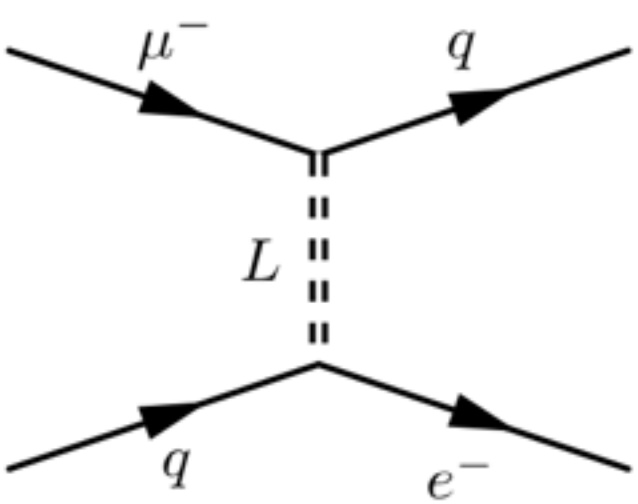

- Predicted in many Beyond the Standard Model theories
- Rate is model dependent

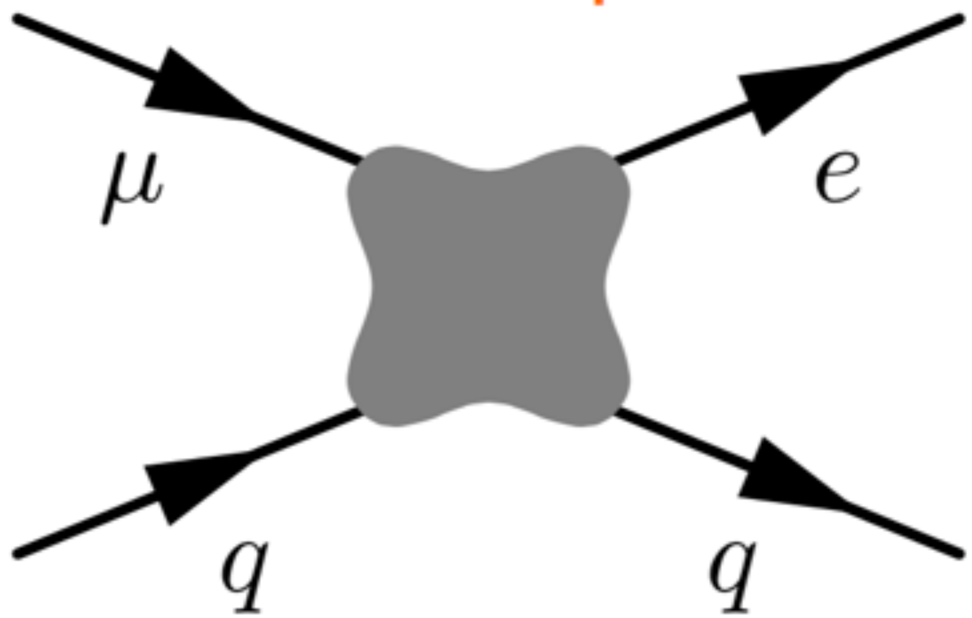

$\mathcal{R} < \mathcal{O}(10^{-14})$

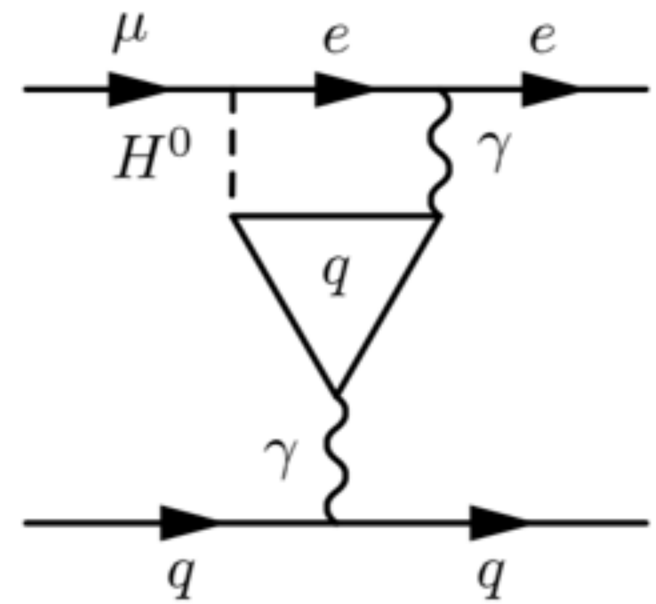

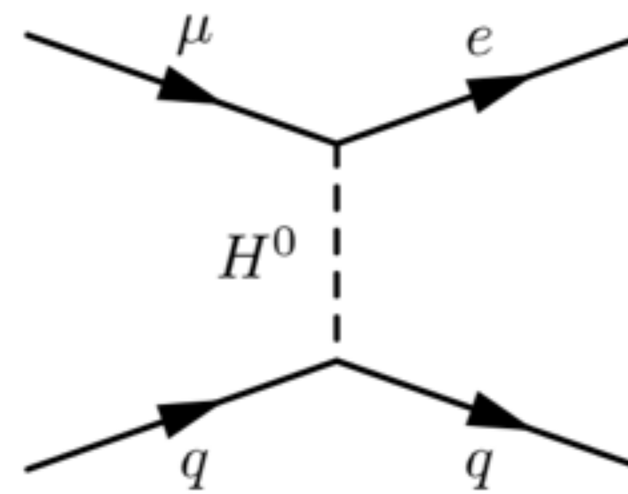

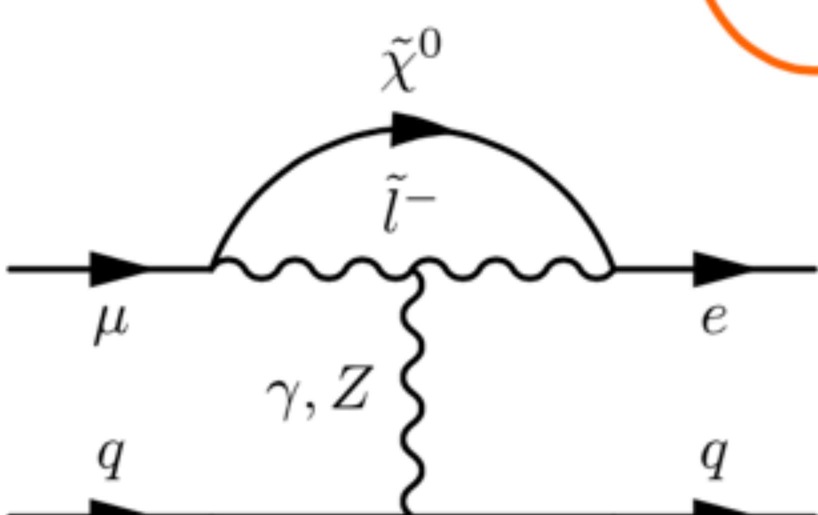

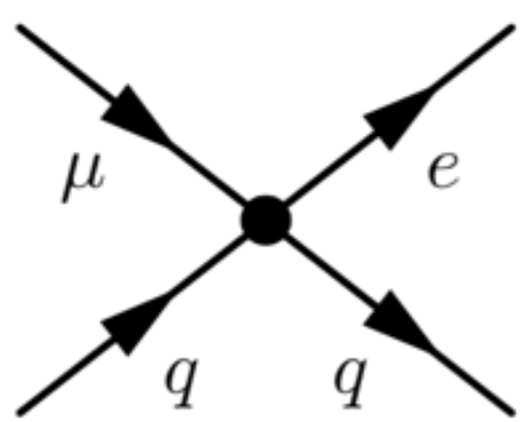

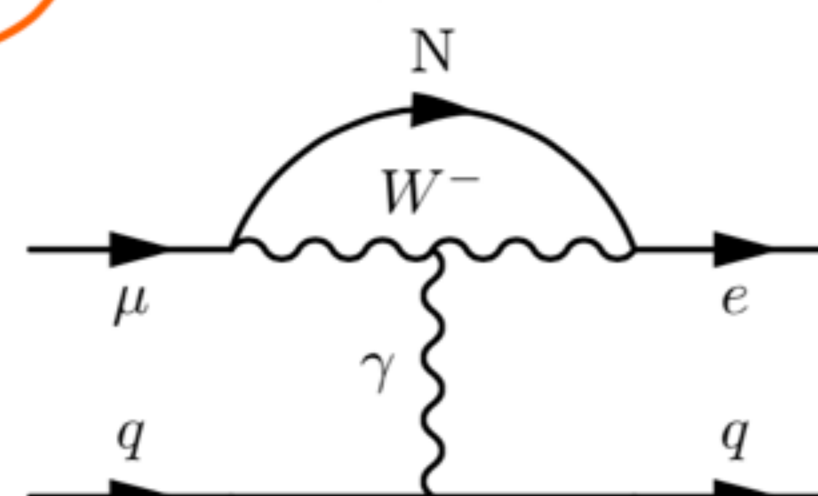

History of CLFV experiment

First CLFV : Bruno Pontecorvo at 1948

Producing muons by accelerator

Future experiment COMET/Mu2e

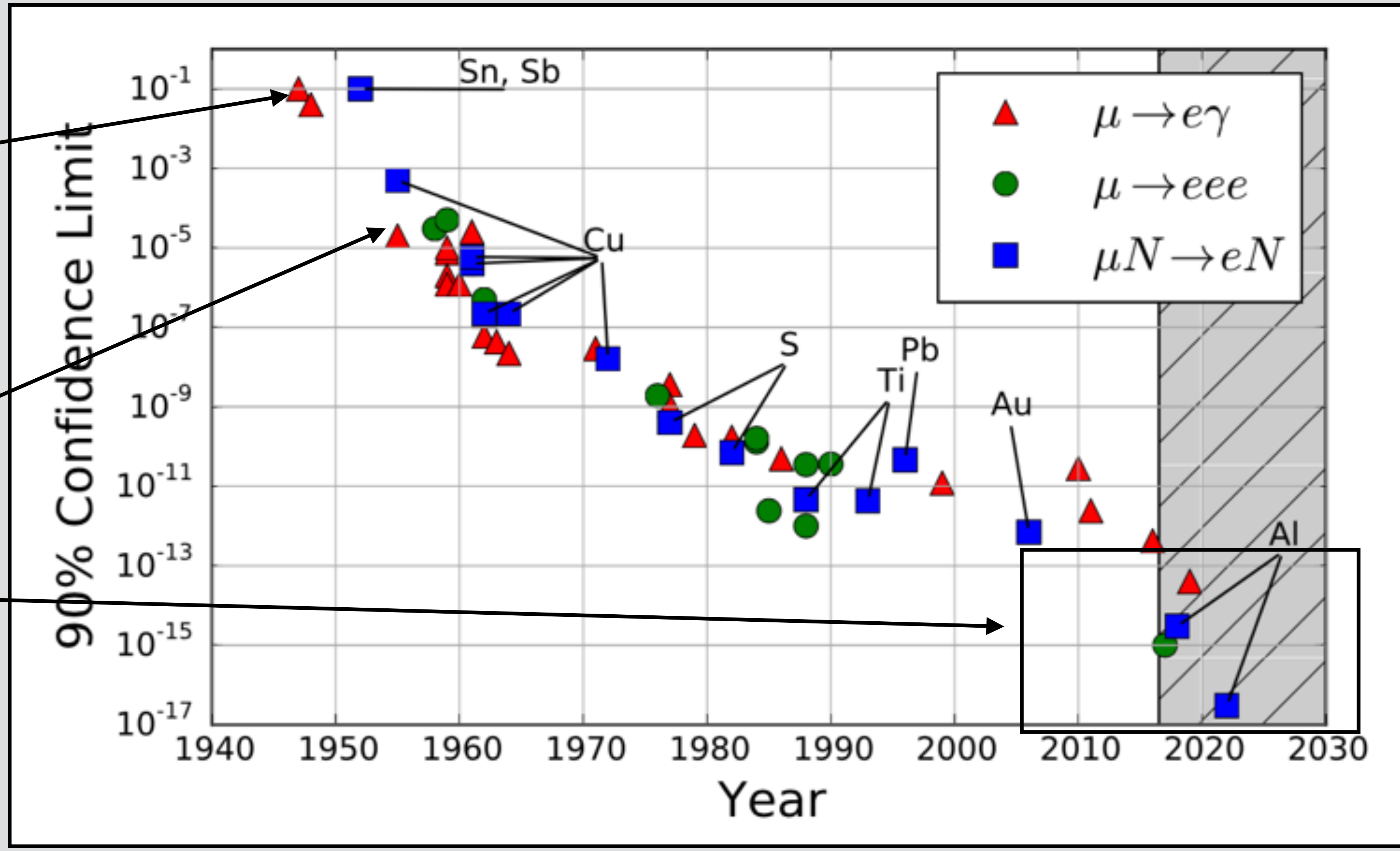

Every decade, the sensitivity increase by a factor 100

ref: https://arxiv.org/pdf/1307.5787.pdf

μ-e conversion channels

Experiments

- COMET
- DeMee
- Mu2e

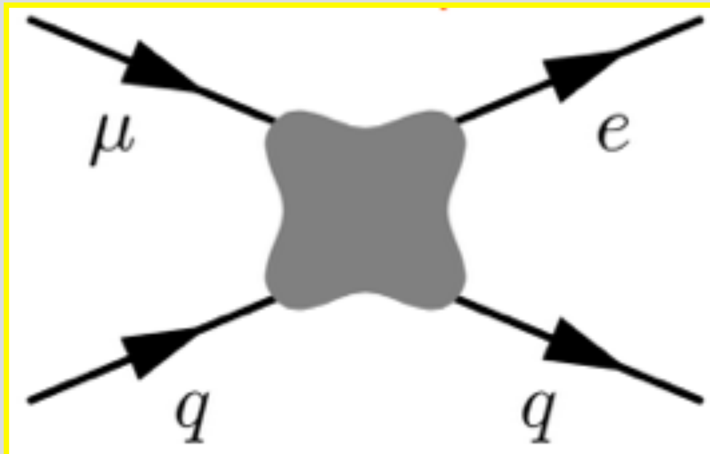

- MEG
- MEGII

- Mu3e

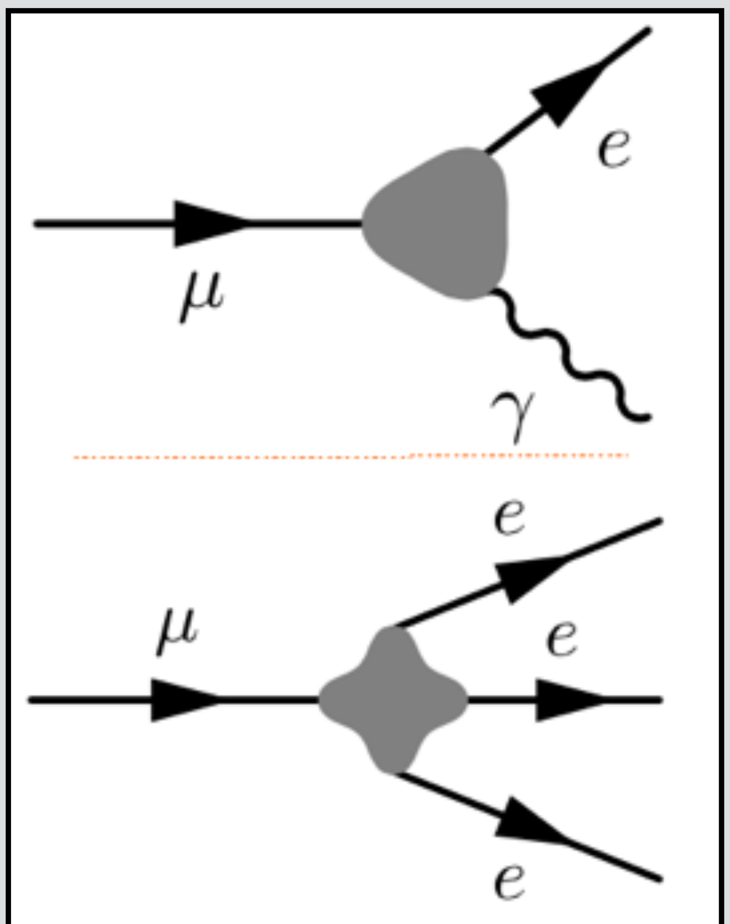

Current/Future Limit

Group	Process	Current	Future
$\Delta(L_e - L_\mu) = 2$	$\mu \to e\gamma$	4.2×10^{-13} [15]	4×10^{-14}[16]
	$\mu \to e\bar{e}e$	1.0×10^{-12} [17]	10^{-16} [18]
	$\mu \to e$ conv.	$\mathcal{O}(10^{-12})$ [19]	10^{-17} [20, 21]
	$h \to e\bar{\mu}$	3.5×10^{-4} [22]	2×10^{-4} [23]
	$Z \to e\bar{\mu}$	7.5×10^{-7} [24]	–
	had$\to e\bar{\mu}$(had)	4.7×10^{-12} [25]	10^{-12} [26]
$\Delta(L_e - L_\tau) = 2$	$\tau \to e\gamma$	3.3×10^{-8} [27]	10^{-9} [28]
	$\tau \to e\bar{e}e$	2.7×10^{-8} [29]	10^{-9} [28]
	$\tau \to e\bar{\mu}\mu$	2.7×10^{-8} [29]	10^{-9} [28]
	$\tau \to e$ had	$\mathcal{O}(10^{-8})$ [30]	10^{-9} [28]
	$h \to e\bar{\tau}$	6.9×10^{-3} [22]	5×10^{-3} [23]
	$Z \to e\bar{\tau}$	9.8×10^{-6} [31]	–
	had$\to e\bar{\tau}$(had)	$\mathcal{O}(10^{-6})$ [32, 33]	–
$\Delta(L_\mu - L_\tau) = 2$	$\tau \to \mu\gamma$	4.4×10^{-8} [27]	10^{-9} [28]
	$\tau \to \mu\bar{e}e$	1.8×10^{-8} [29]	10^{-9} [28]
	$\tau \to \mu\bar{\mu}\mu$	2.1×10^{-8} [29]	10^{-9} [28]
	$\tau \to \mu$ had	$\mathcal{O}(10^{-8})$ [30]	10^{-9} [28]
	$h \to \mu\bar{\tau}$	1.2×10^{-2} [7]	5×10^{-3} [23]
	$Z \to \mu\bar{\tau}$	1.2×10^{-5} [34]	–
	had$\to \mu\bar{\tau}$(had)	$\mathcal{O}(10^{-6})$ [32, 33]	–

reference : https://arxiv.org/pdf/1610.07623

Muonic atom and μ-e conversion

Muonic atom — Processes

Muonic nuclear capture

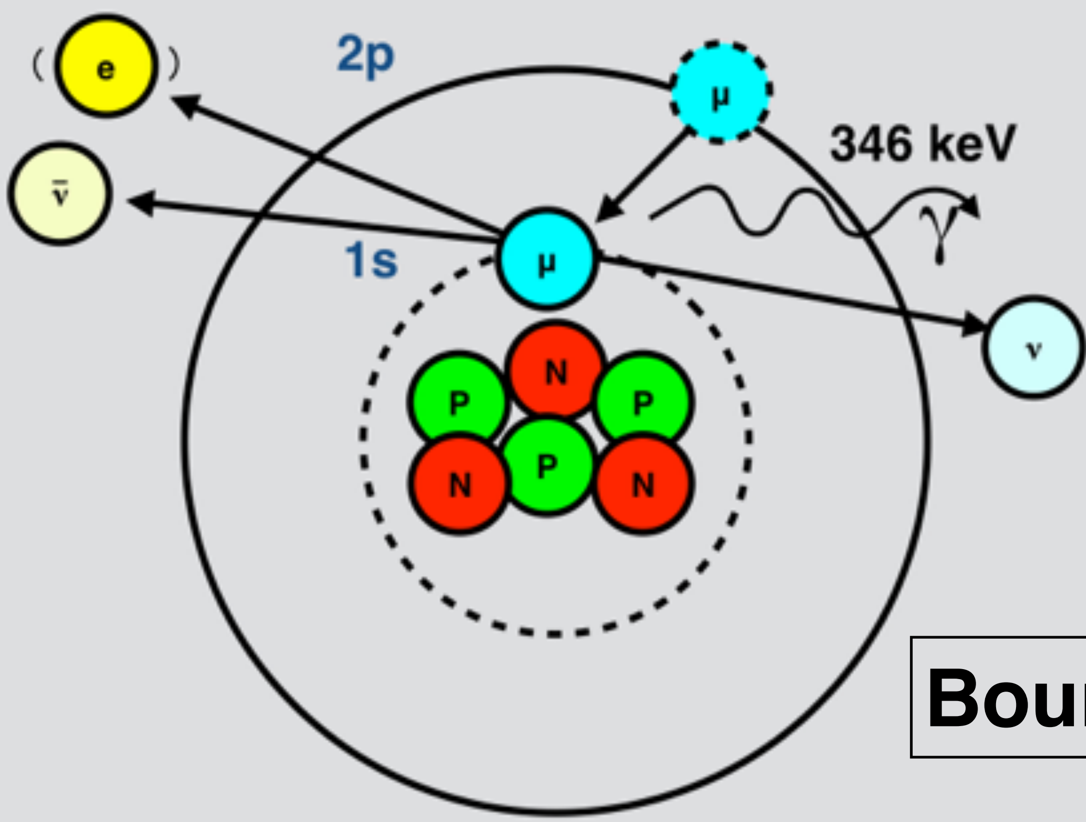

μ e Conversion

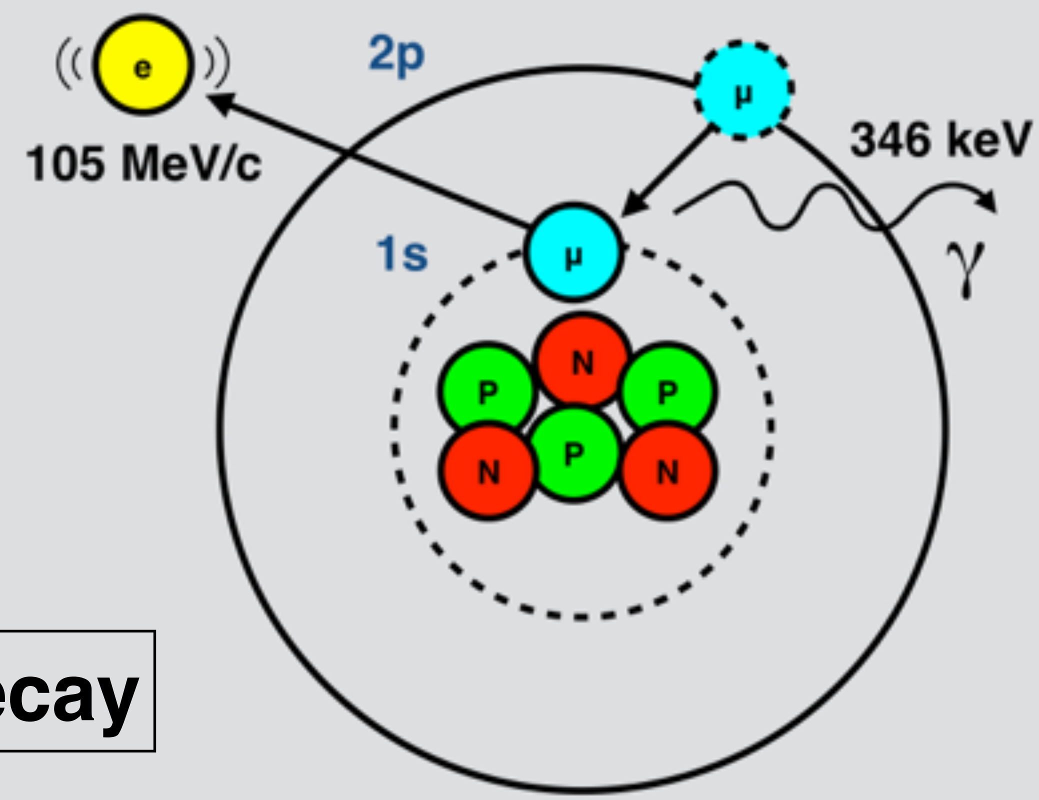

Bound Muon decay

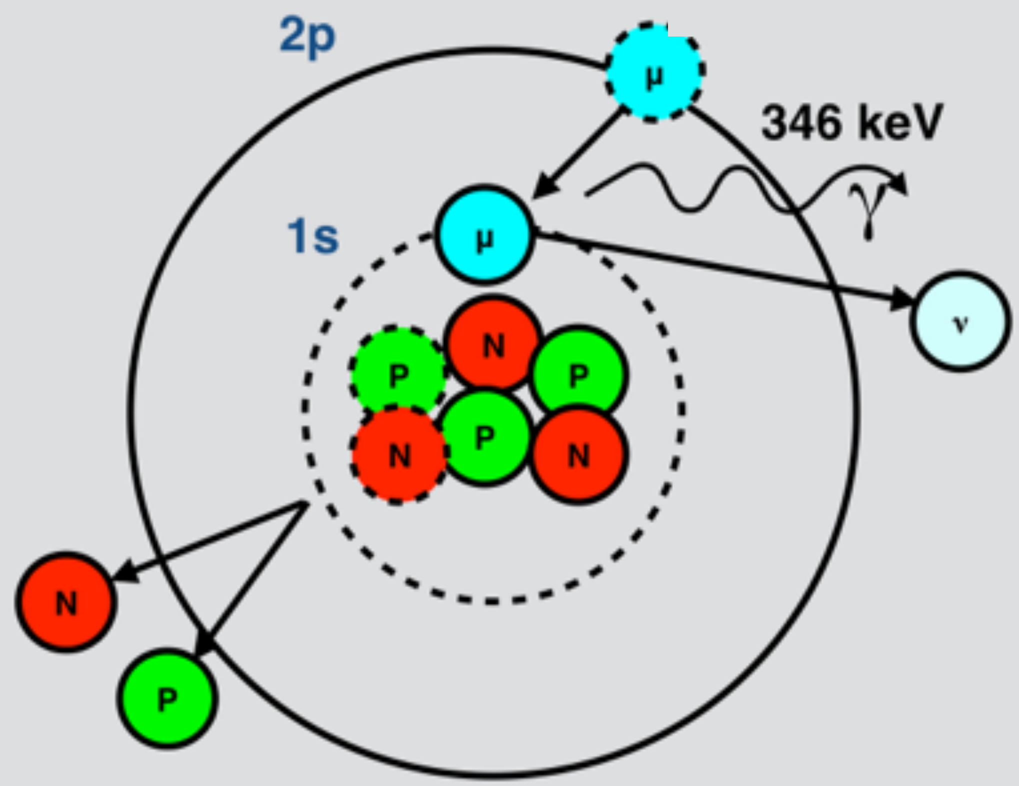

Muon decay-in-orbit (DIO)

- Main background source
- Up to mass of muon, but usually ~ falls to 60 MeV (Decay-in-flight)
  - Depending on Z, the shape of DIO changes [0]

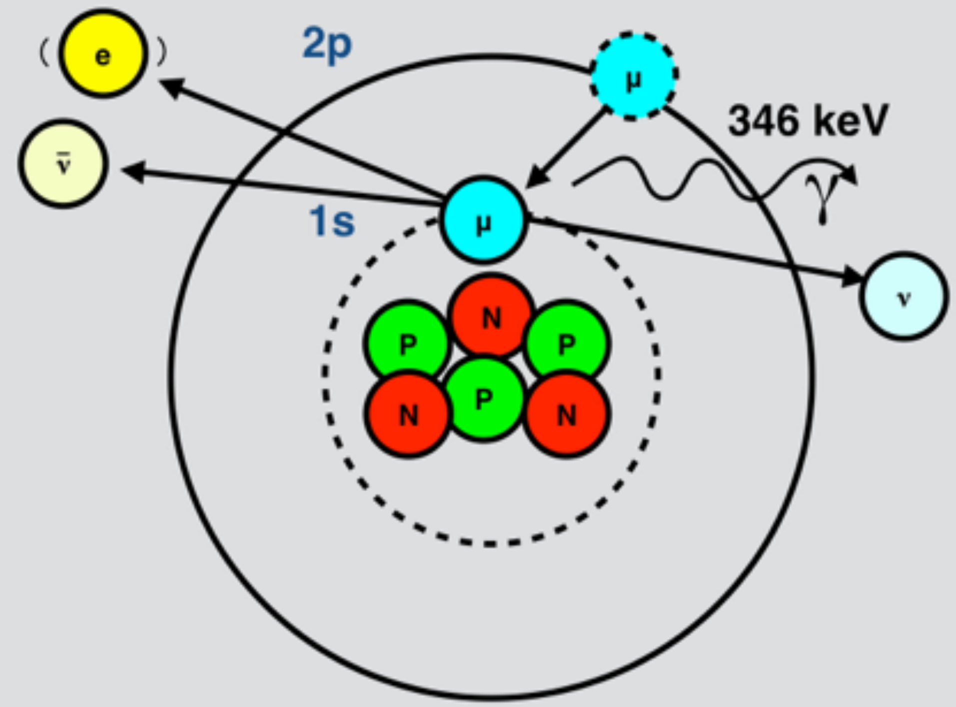

- Currently, no accurate measurement of end point
  - SINDRUM 10^{-14} for Gold nucleus [1].

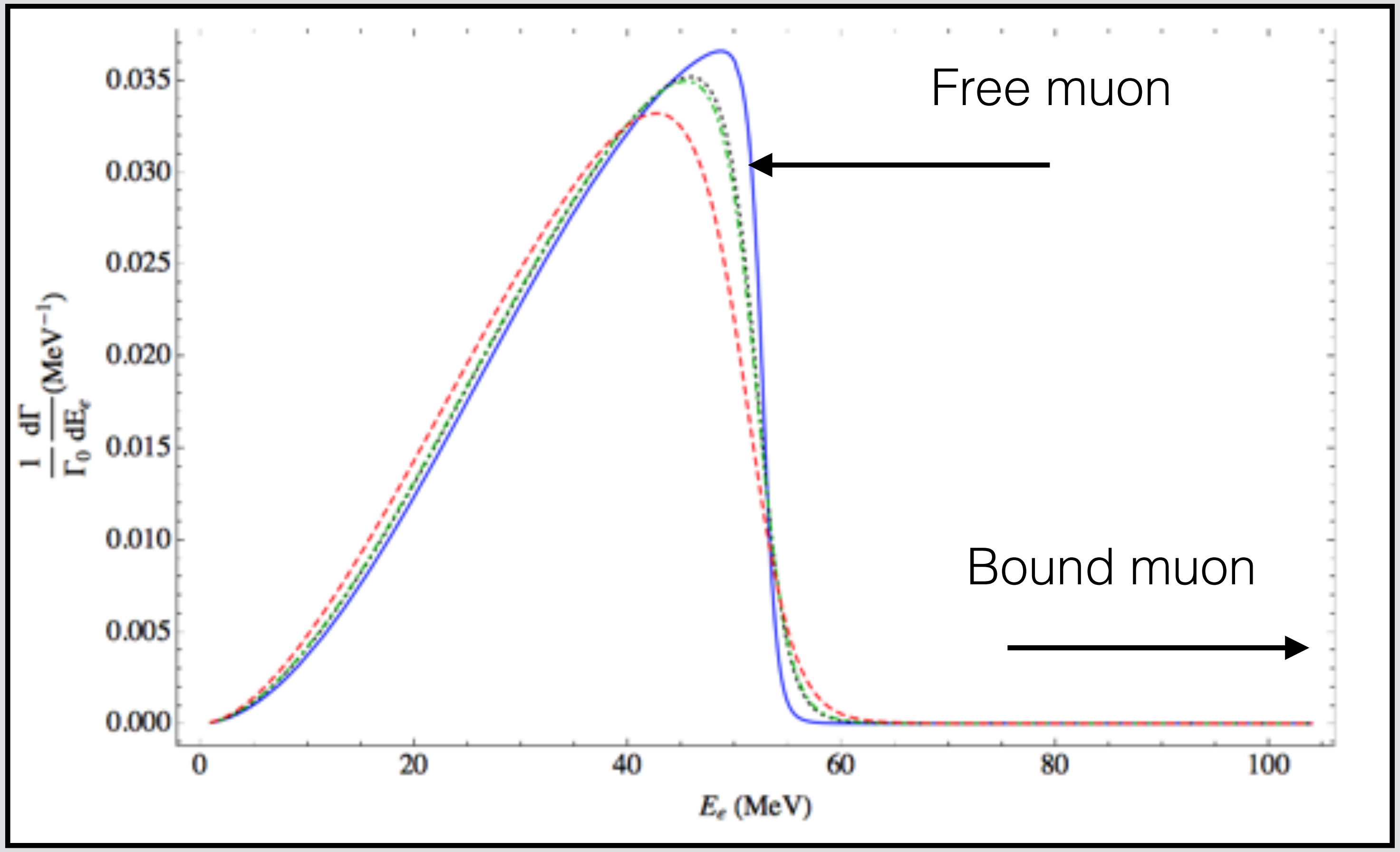

[1] W. H. Bertl, et al. (SINDRUM II). "A Search for muon to electron conversion in muonic gold." *Eur. Phys. J.*, C47:337, 2006. doi:10.1140/epjc/s2006-02582-x.

Muon nuclear capture

- **Basically ~50MeV all go to nucleus!**
- **Emitted particles:**
  - **Photon, Protons, neutrons, alpha**
- **Measurement**
  - **Alcap experiment (2013)**
  - **Alcap experiment (2015)**

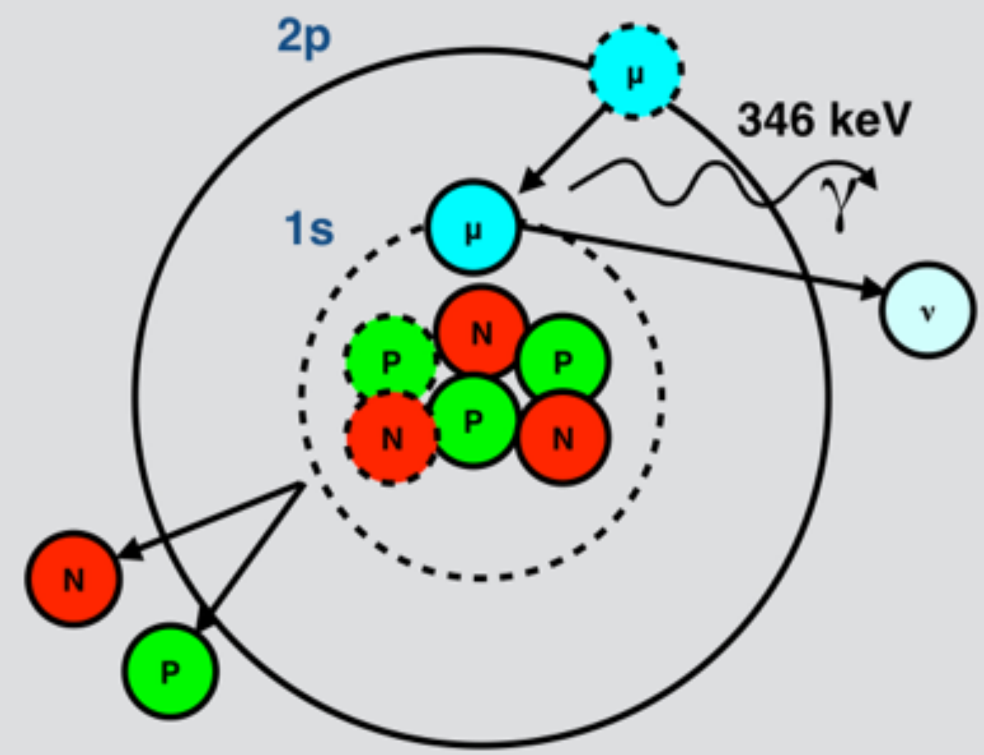

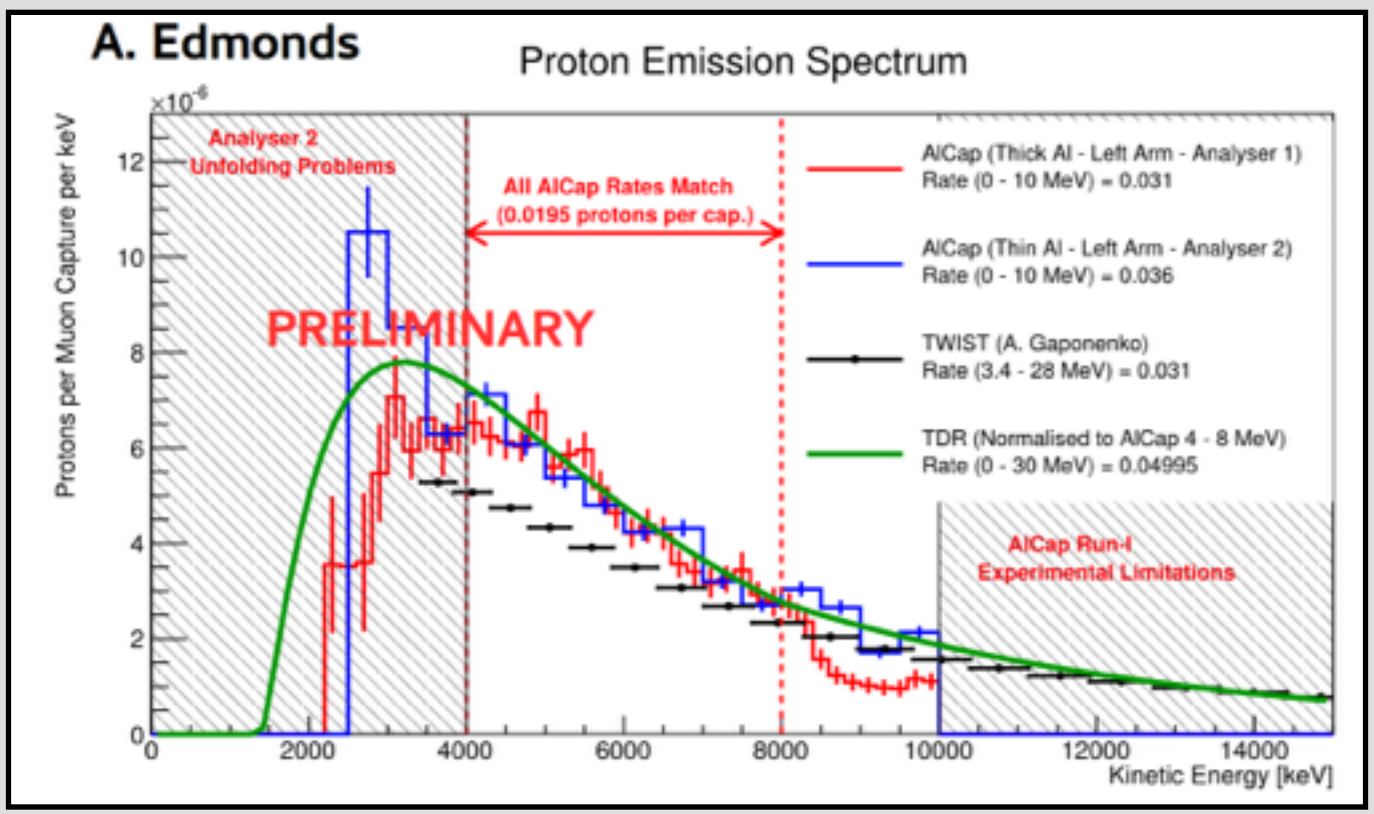

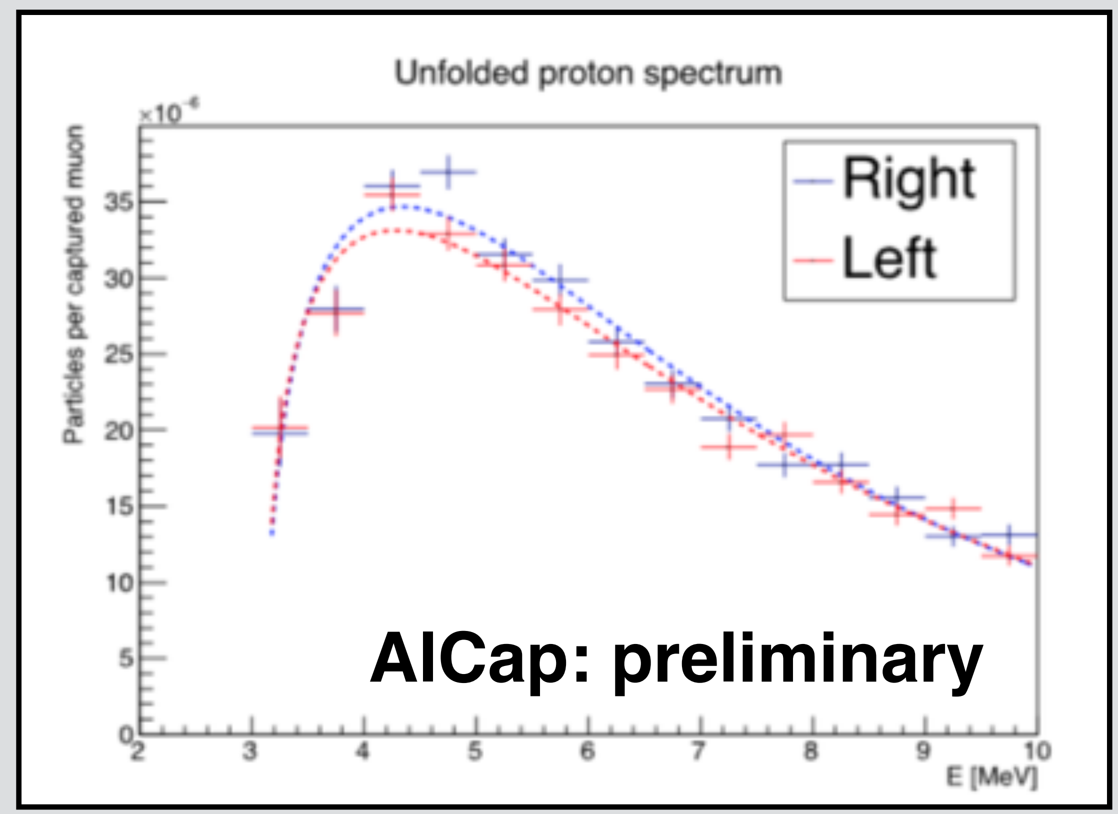

[2]: Kuno laboratory, Dr. Wong Ming Liang PhD thesis (unpublished)

Muon electron conversion

- **Charged lepton flavour violation**

$$\mu^- + N(A,Z) \rightarrow e^- + N(A,Z)$$

- **Nucleus unchanged → Coherent Process**

$$E_e = m_\mu - B_\mu - E_{recoil}$$

- **Current Limit on <u>Gold</u> (90% C.L) SINDRUM-II**

$$Rate = \frac{Br(\mu\text{–}e\ conversion)}{Br(\mu\ capture)} < 7 \times 10^{-13}$$

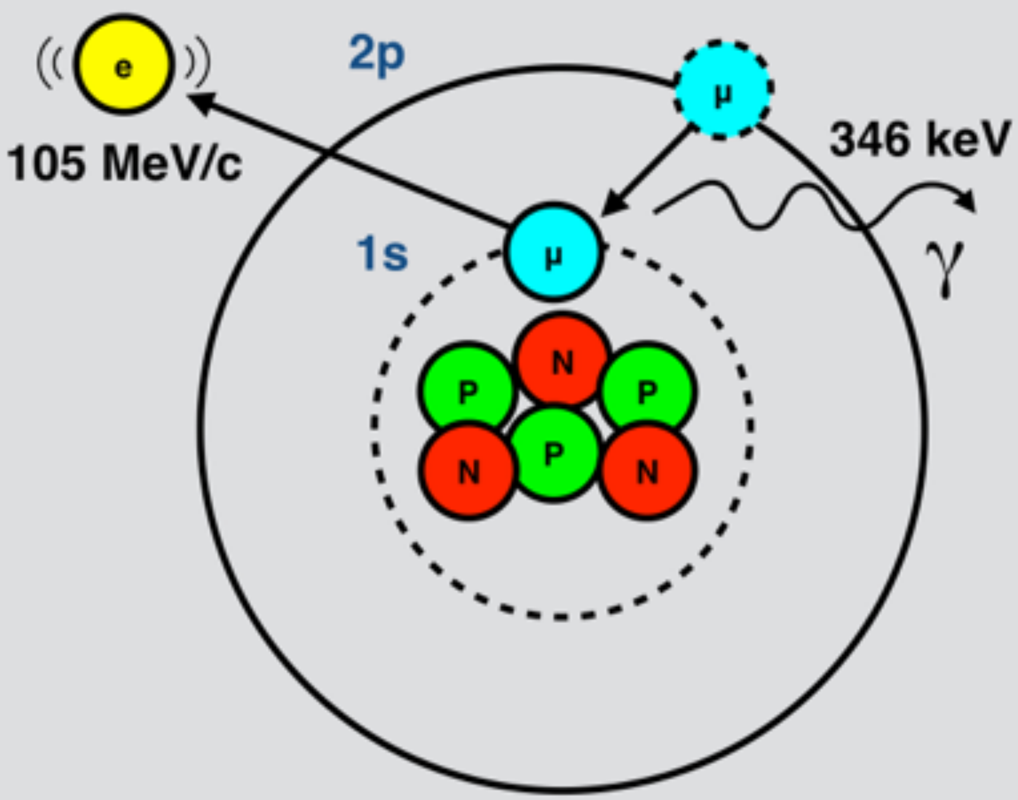

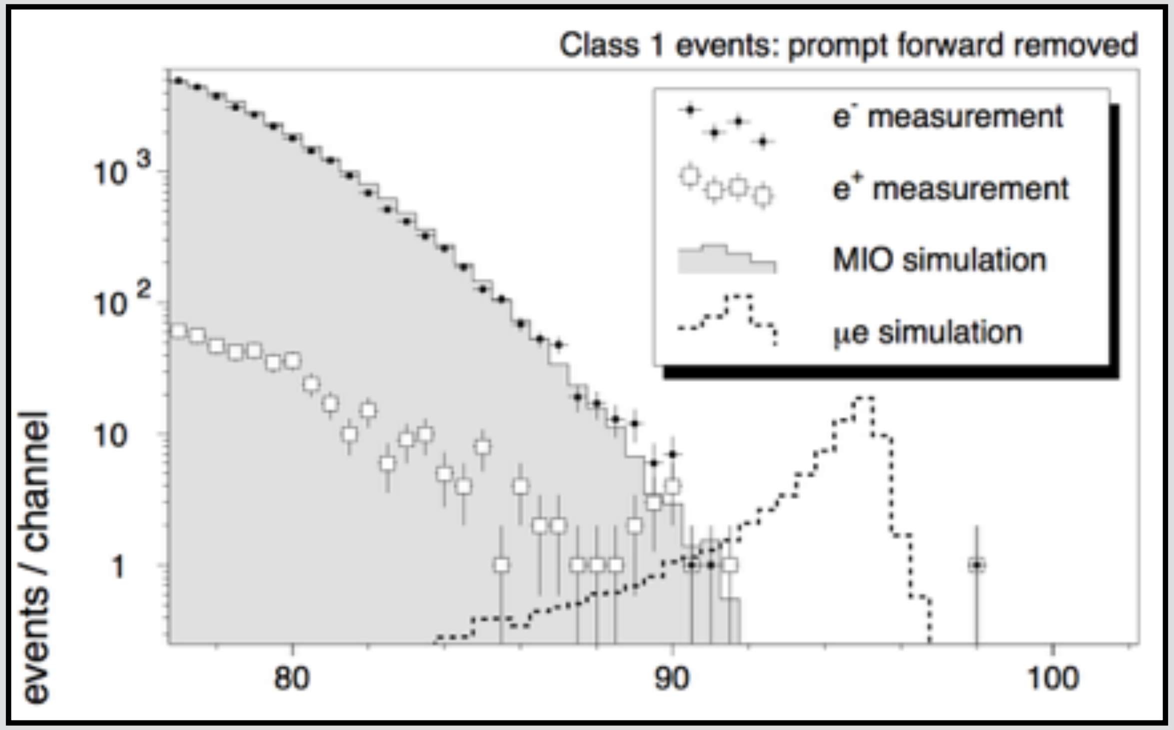

PSI: Muon beam intensity ~ $10^{7\text{-}8}$

- **How to overcome this limit?**
  - **<u>Increase</u> the intensity!!**
- **Future exp. : Mu2e/COMET**
  - **Aluminium**
  - **Ee = 104.97 MeV (Mono-energetic)**
  - **Expected Single Event Sensitivity = O(10^{-17})**

Design of the COMET experiment

Achieving High Sensitivity

HIGH Muons flux at targets

Pion Capture and Muon Capture by Superconducting solenoid System

LOW signal-like background

Beam-related background : Pulse Beam with good extinction factor

Curved Solenoid : Selection of electron energy (>75MeV/c)

HIGH signal acceptance

Low mass High energy resolution detector

Low detector occupancy

The COMET experiment

COMET: COherent Muon to Electron Transition

E21 J-PARC, Tokai, Japan
Staged approach w/ Sensitivity:

- Phase-I : $O(10^{-15})$
- Phase-II : $O(10^{-17})$

Proton beam
8GeV
56kW, 7μA

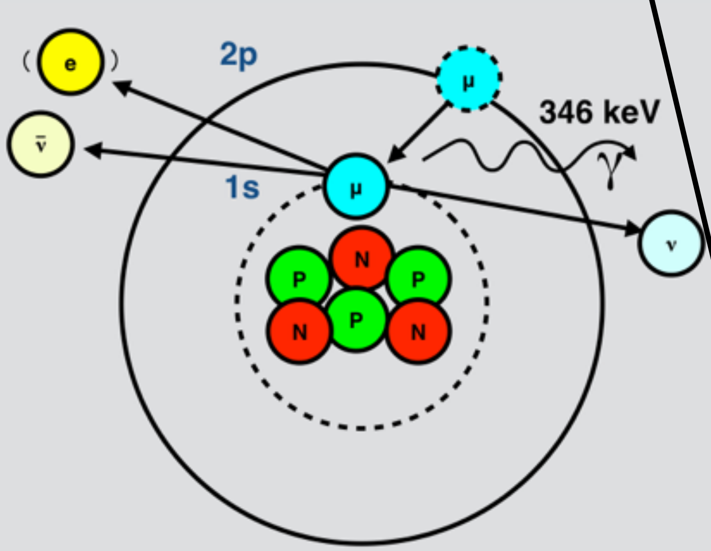

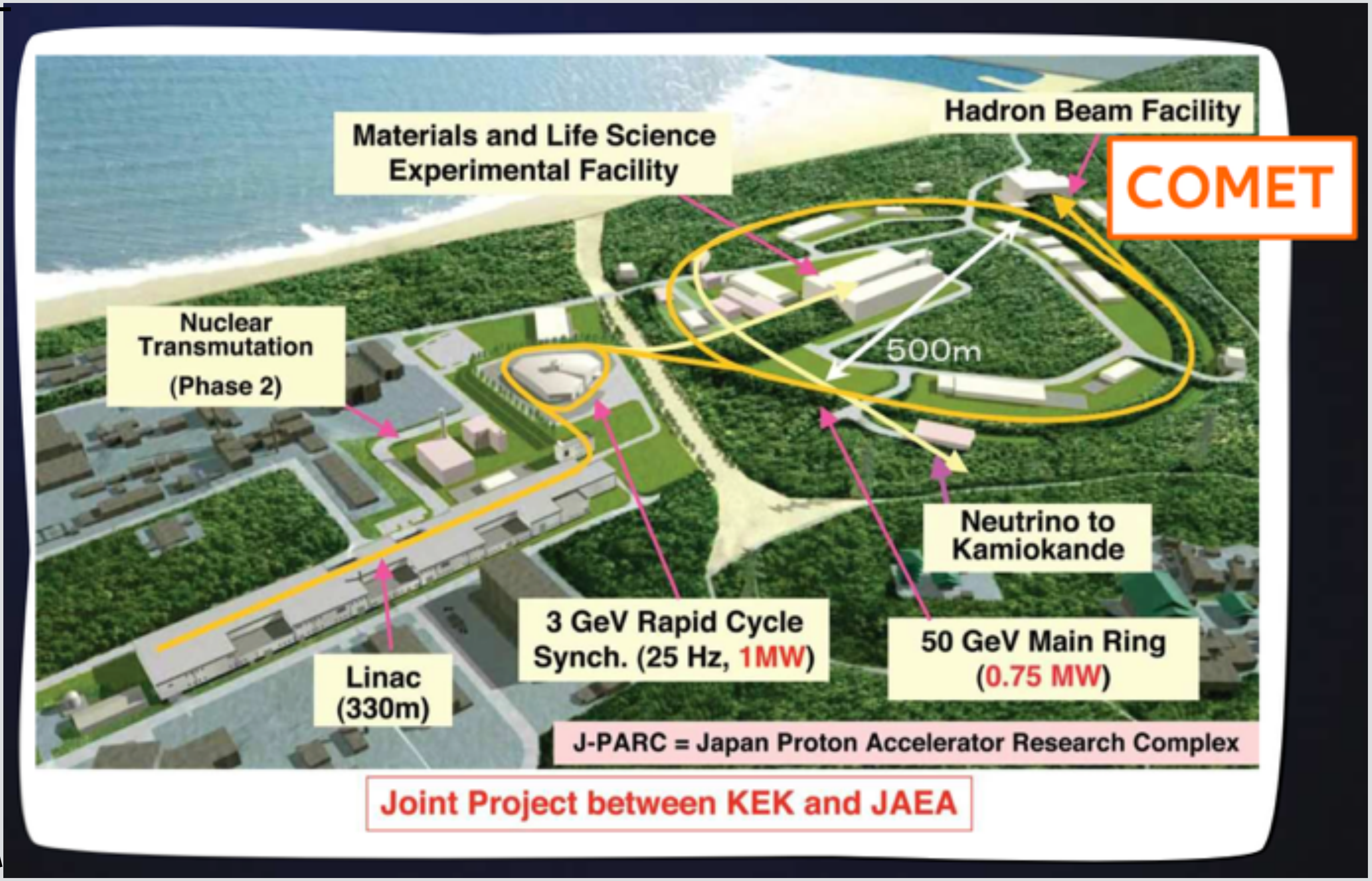

$$\mu^- + N(A,Z) \rightarrow e^- + N(A,Z)$$

The COMET experiment

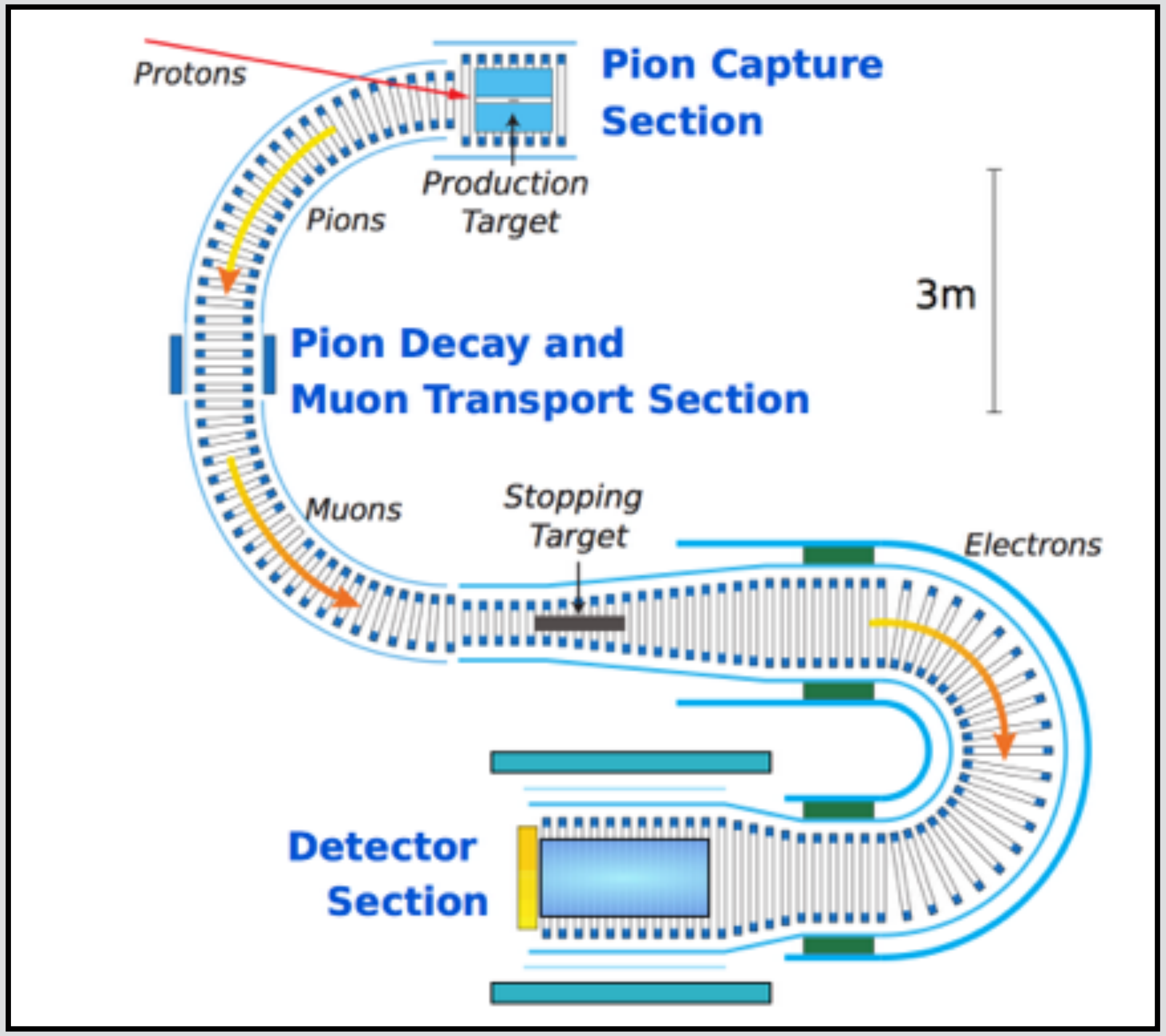

Staged approach

COMET Phase-II

Sensitivity: 2.6 x 10^{-17}

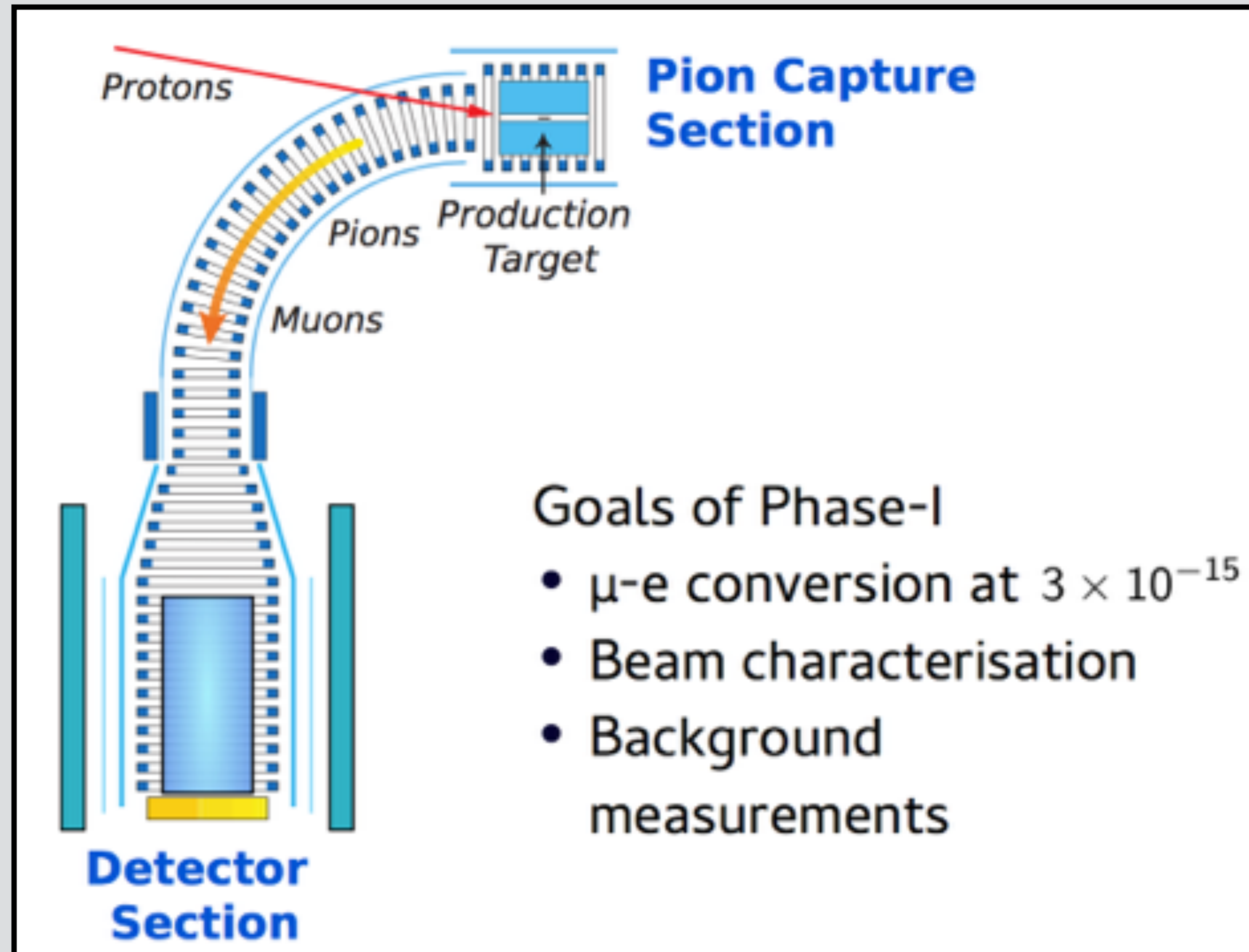

Staged approach

COMET Phase-I

Sensitivity: 3.1 x 10^{-15}

COMET Experimental Hall

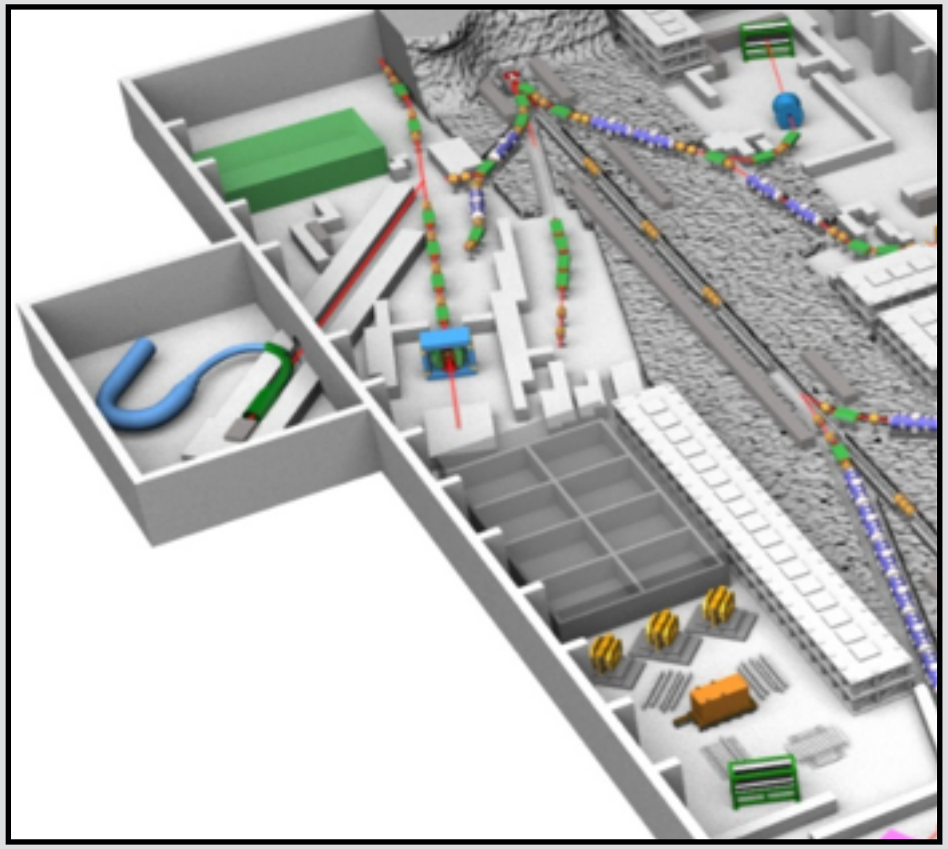

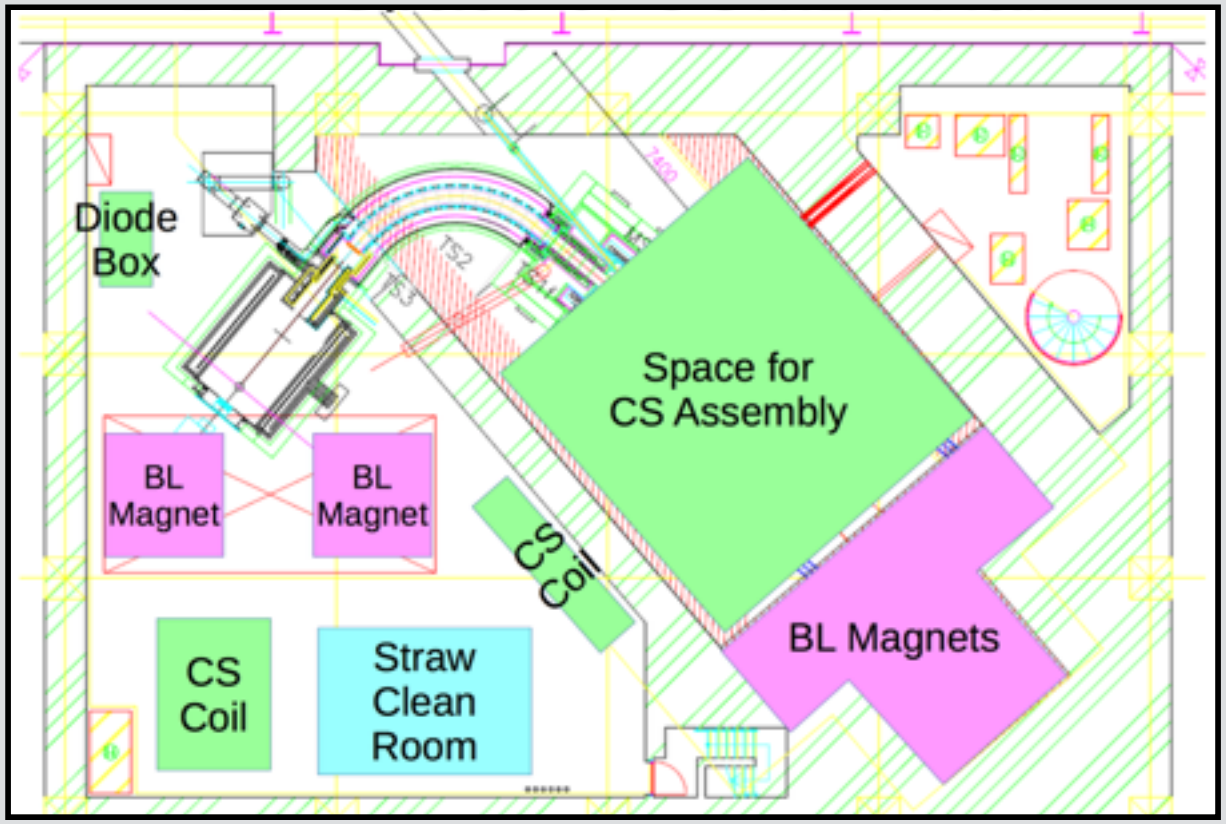

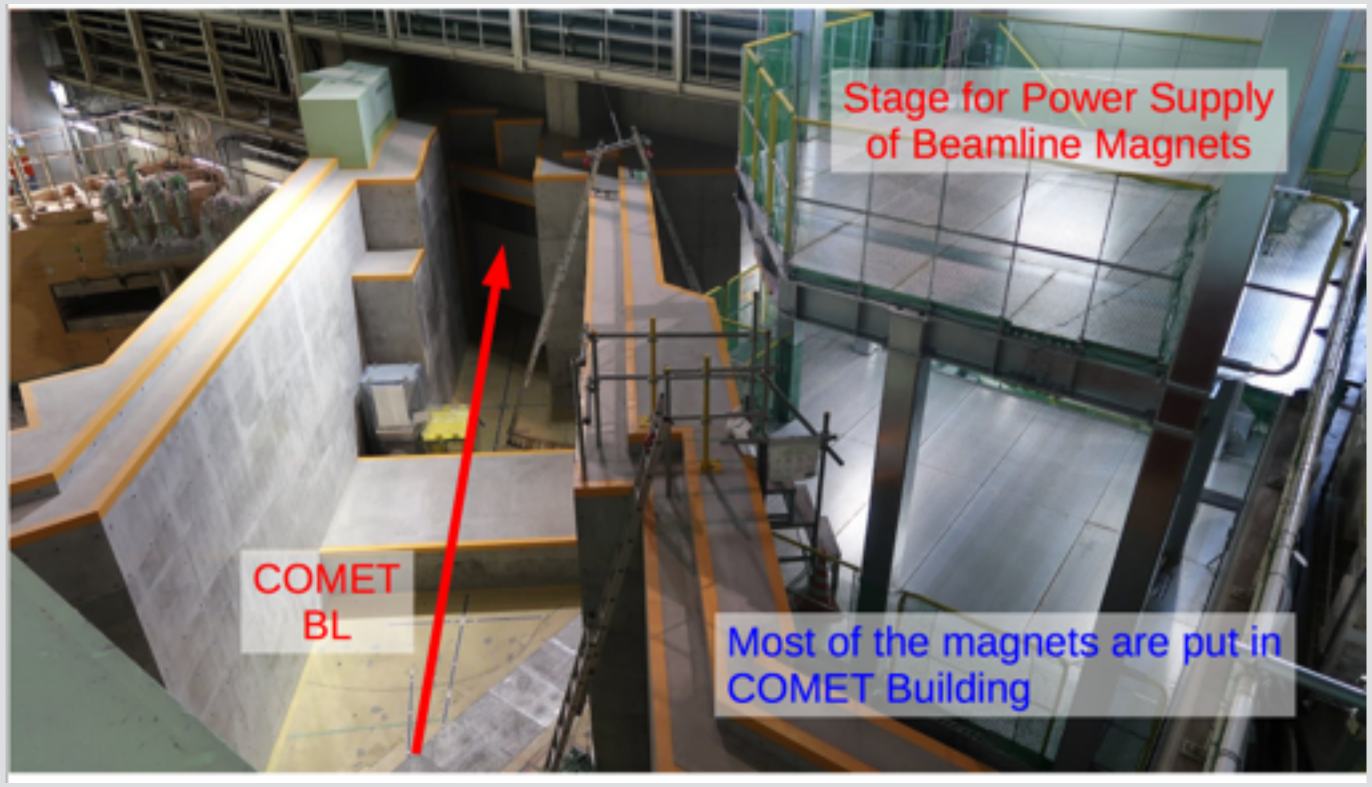

Idea of COMET Phase-II

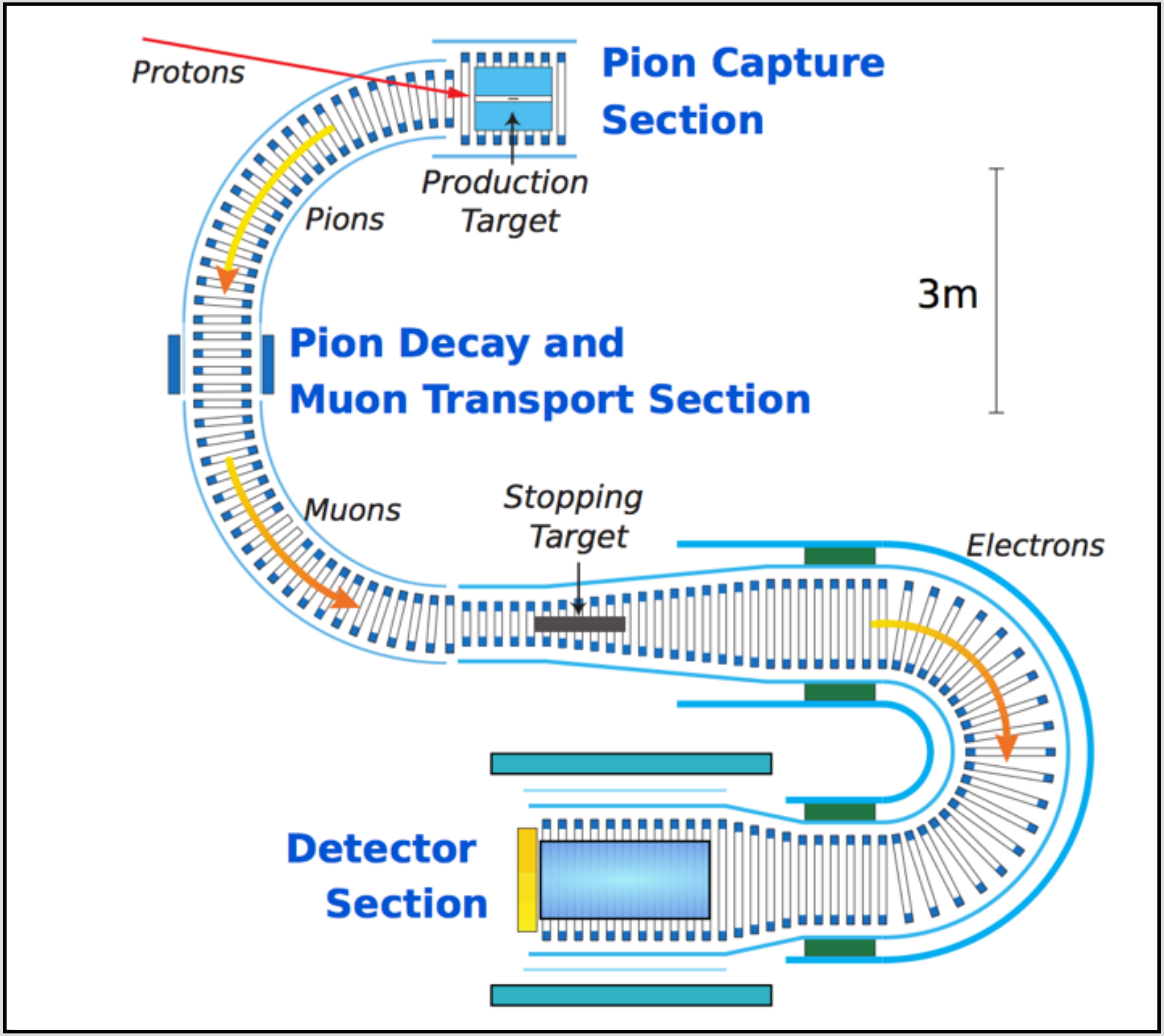

COMET Phase-II Geometry

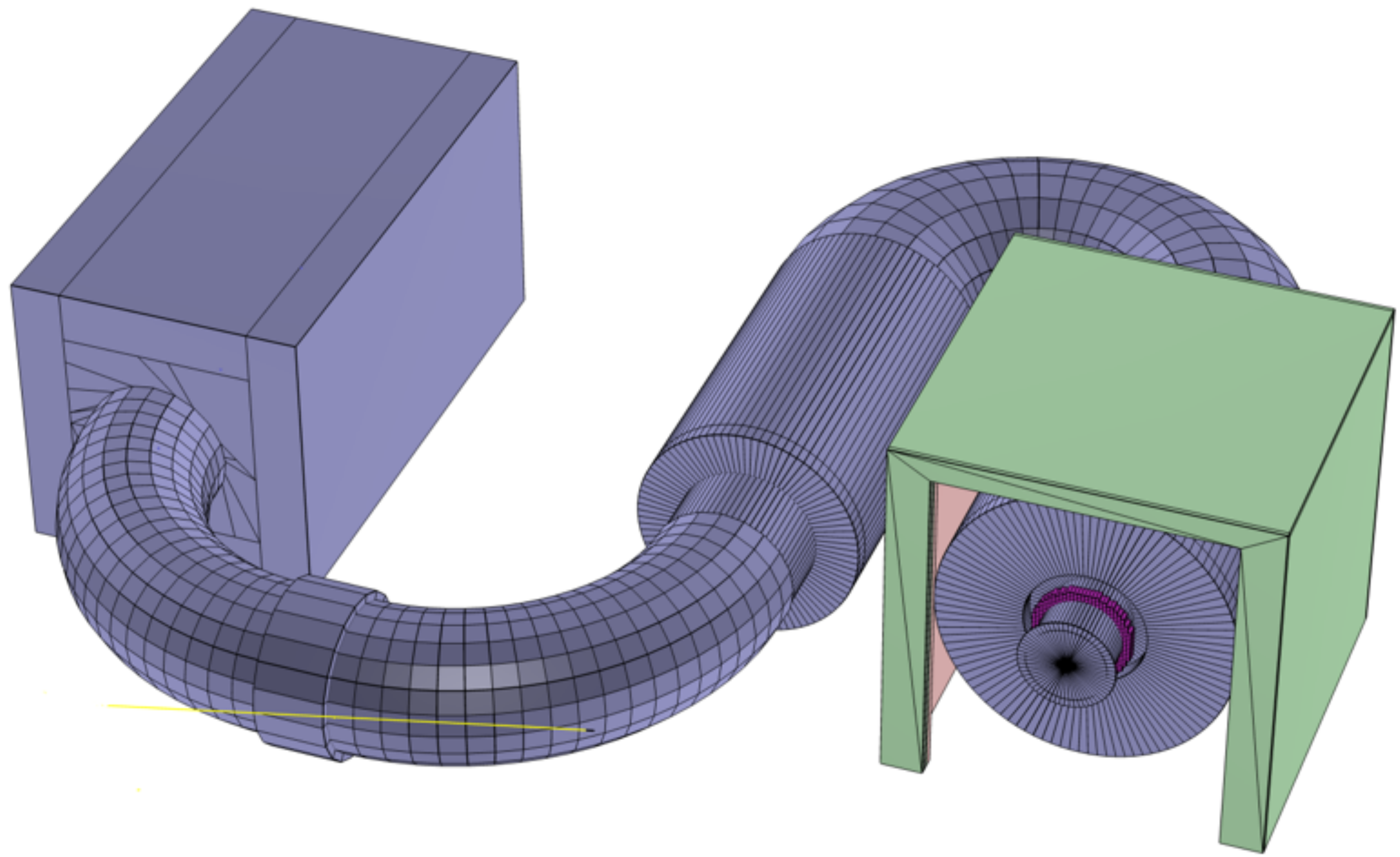

COMET Phase-II (Cross-Section)

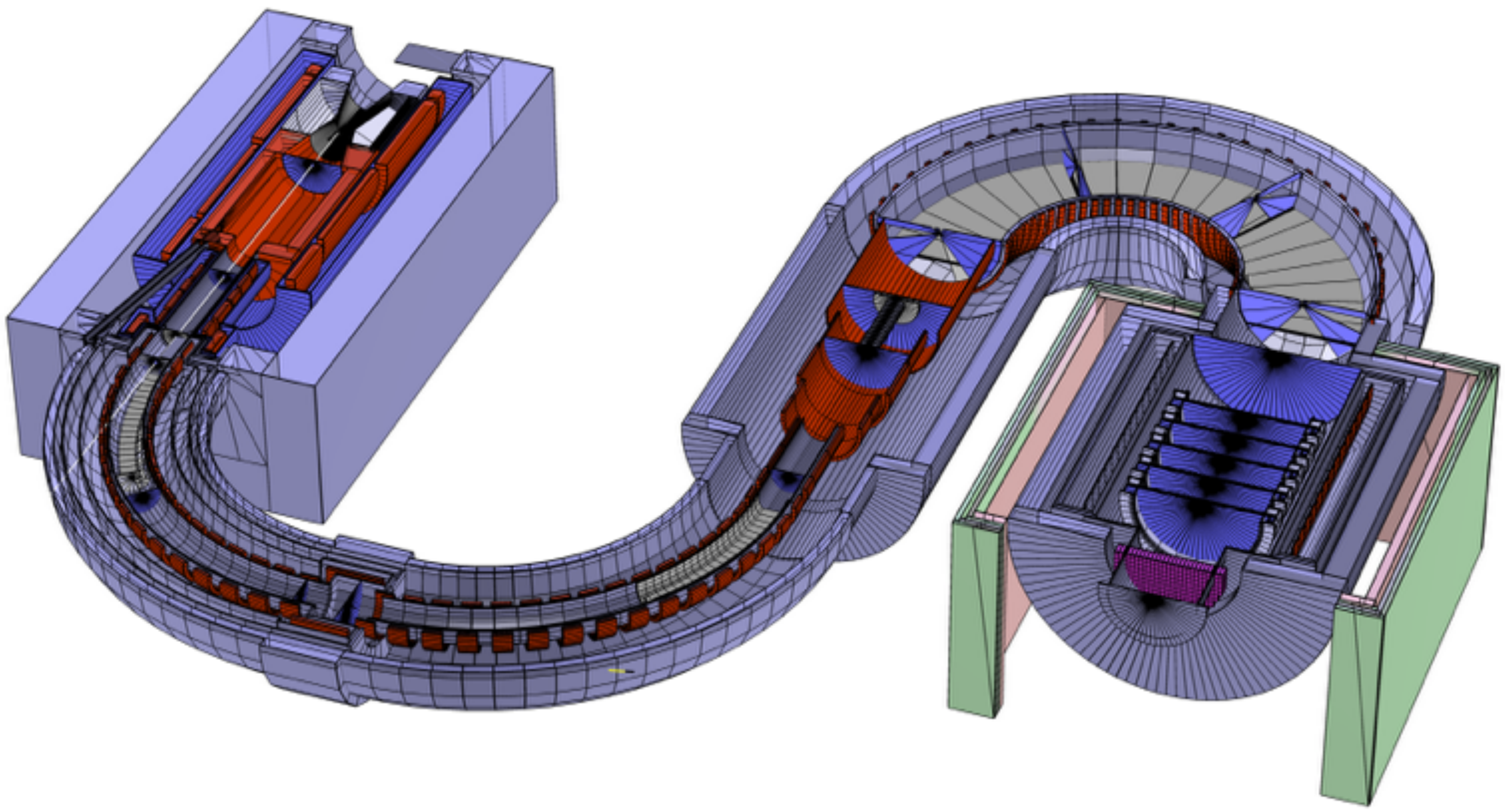

COMET Phase-II (With buildings)

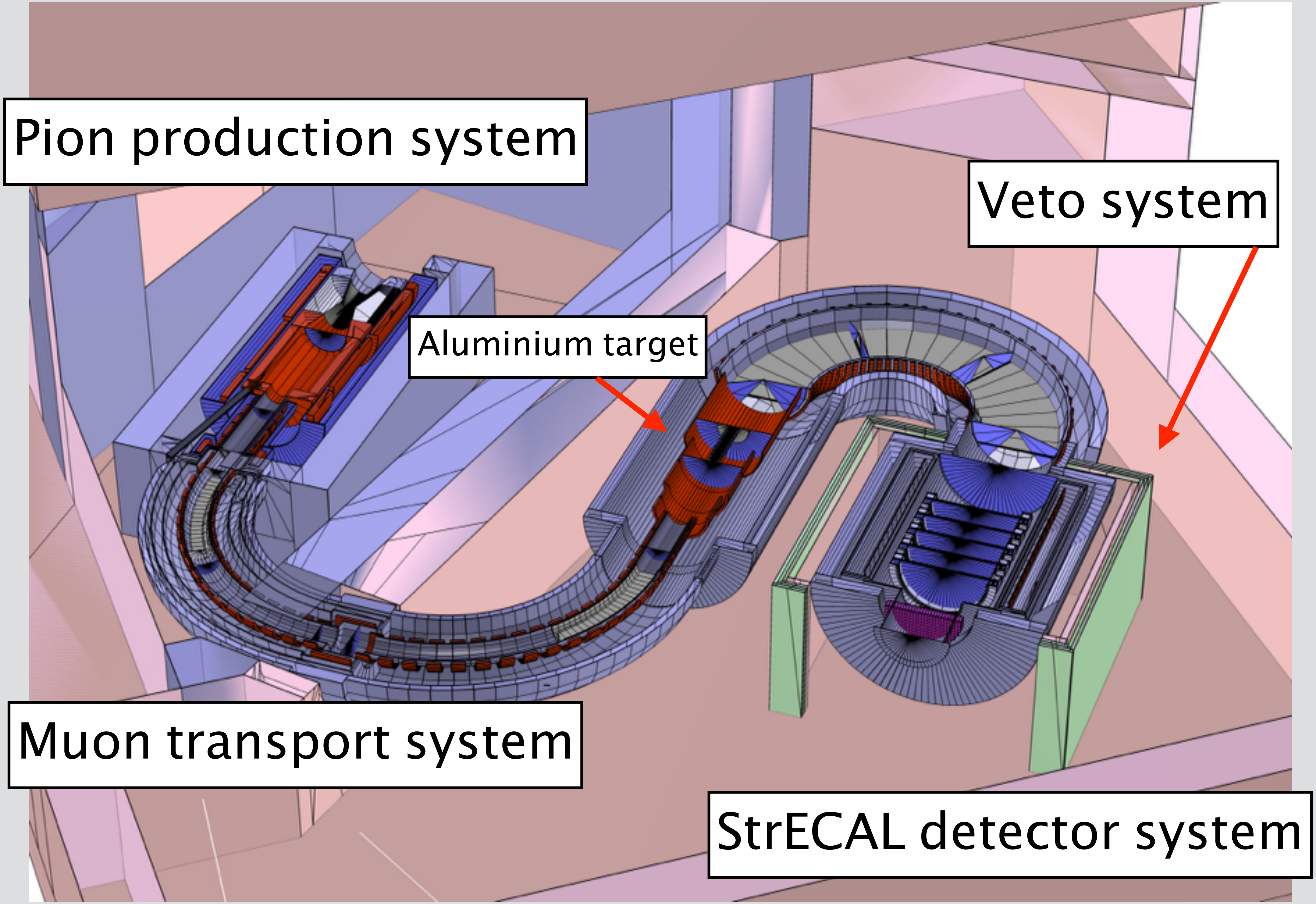

The COMET Beam line

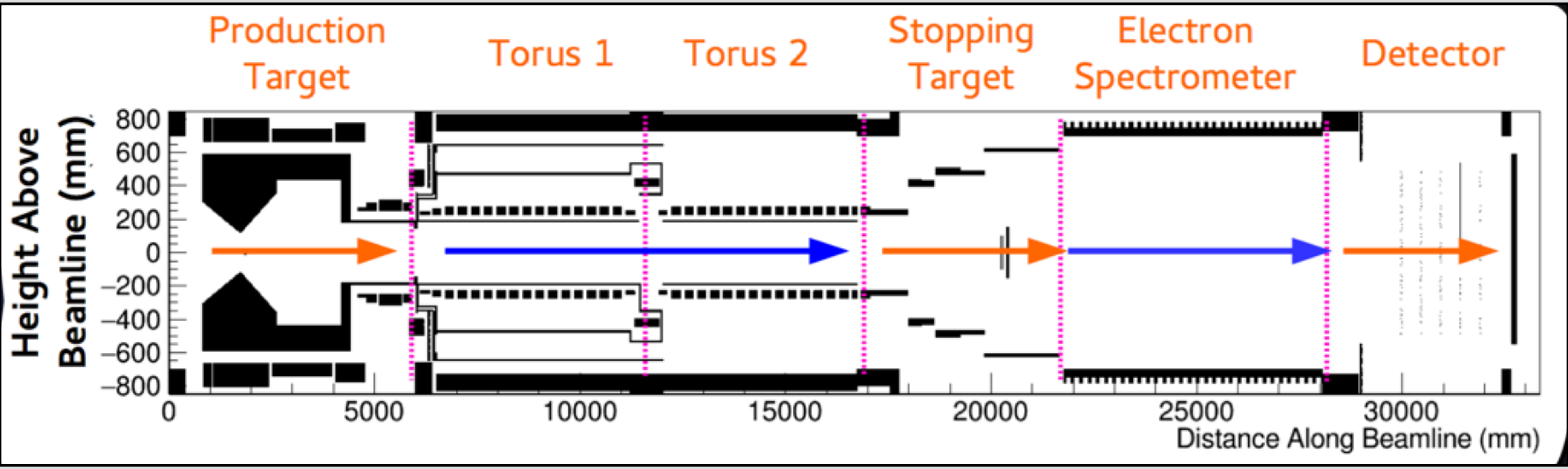

- **Main components**
  - **Capture Solenoid + production targets**
  - **Torus 1&2 Solenoids (180 degrees)**
  - **Stopping targets (Al)**
  - **Electron spectrometers**
  - **Straw tracks and Electromagnetic Calorimeter**

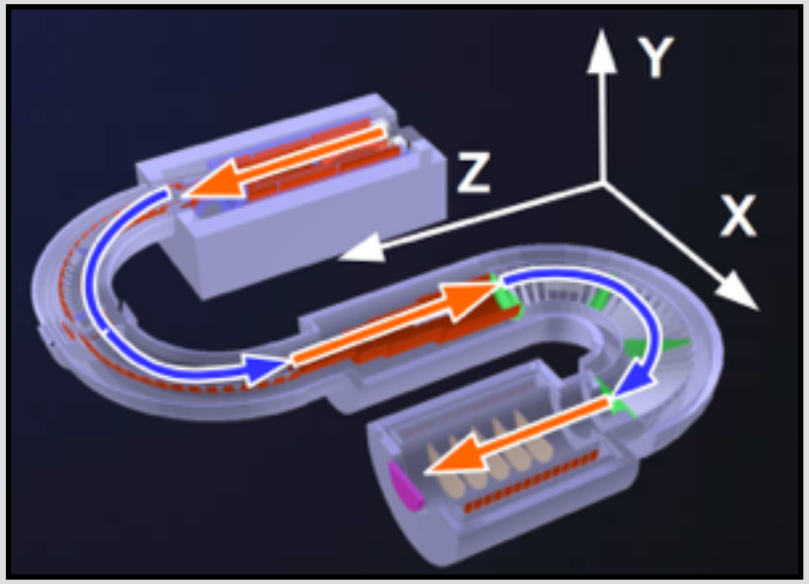

How are the muons generated and stopped?

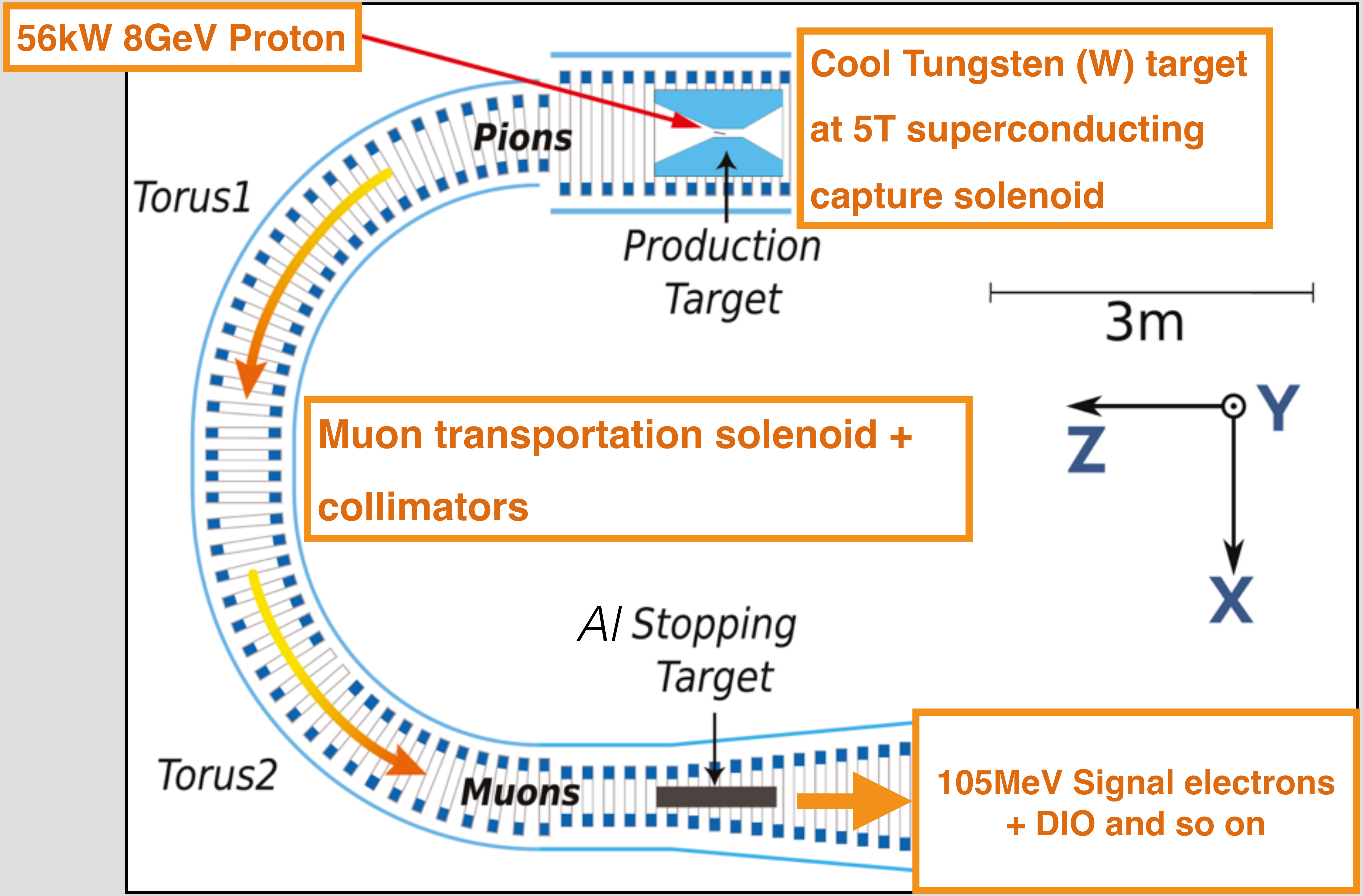

Pion Production at production target

- **Backward Pions**
  - **Cross-section Tungsten is 2 times larger than Graphite**
- **Consideration**
  - **Stable**
  - **Cost**
- **Tungsten is the best choice**
- **However, cooling is needed**

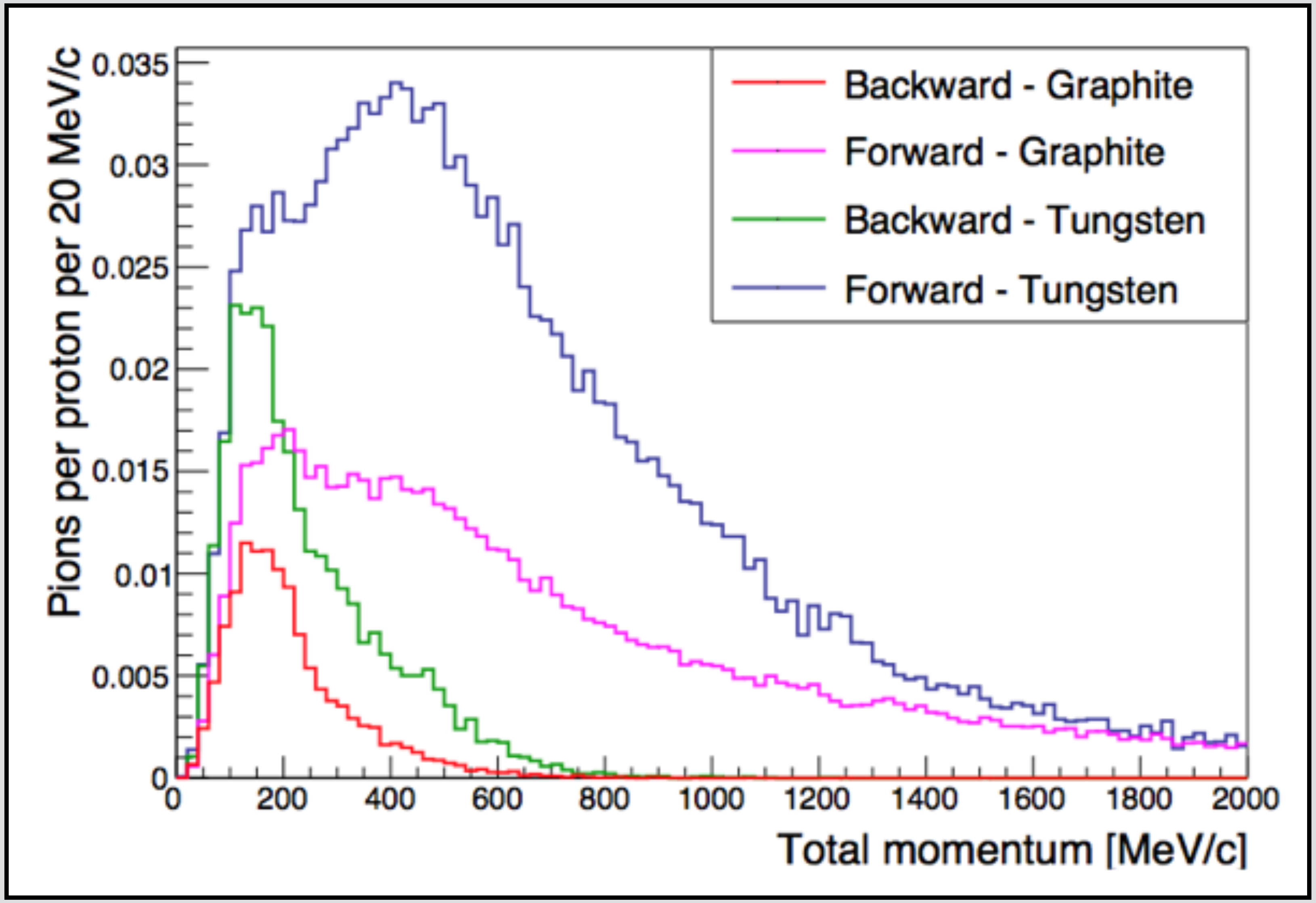

Muon transport solenoid design

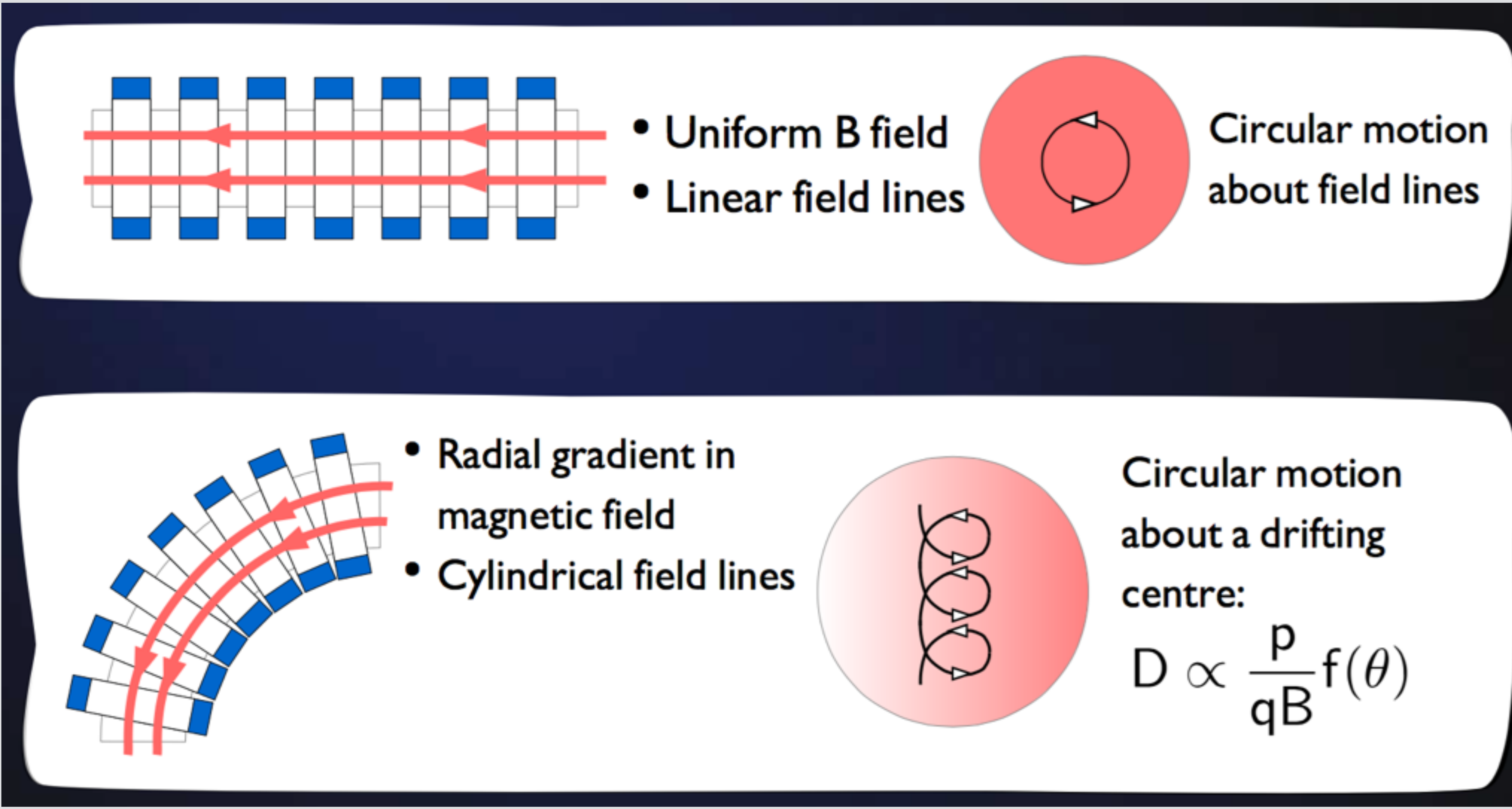

Muon transport solenoid design

- Consist of 2 Toruses
  - Bore radius : 175mm
  - Magnetic field : 2T
  - Bending : 180 degree
  - Radius Curvature : 3m
- Eliminating most high energy muons

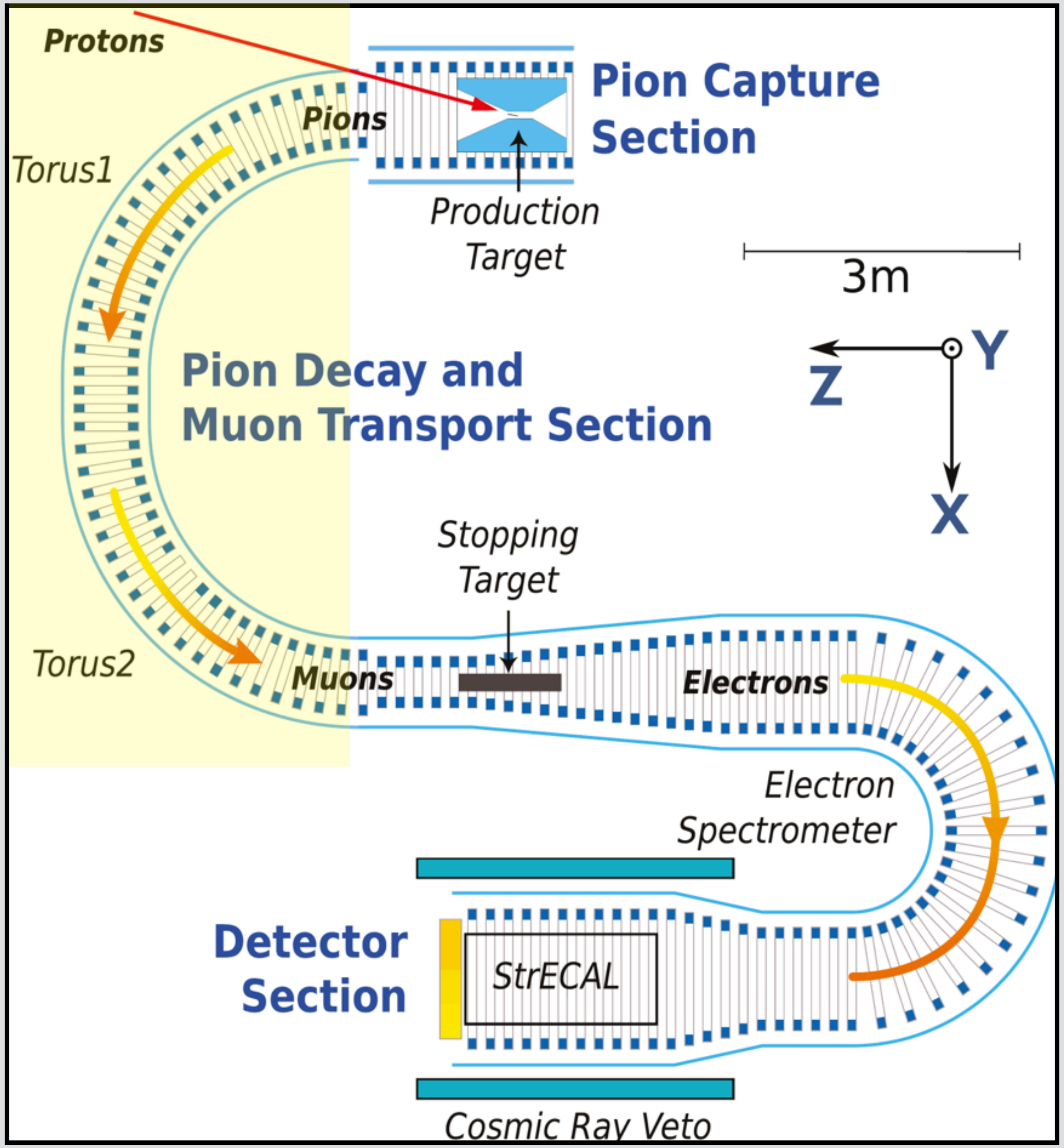

Optimisation of the field map along beam line

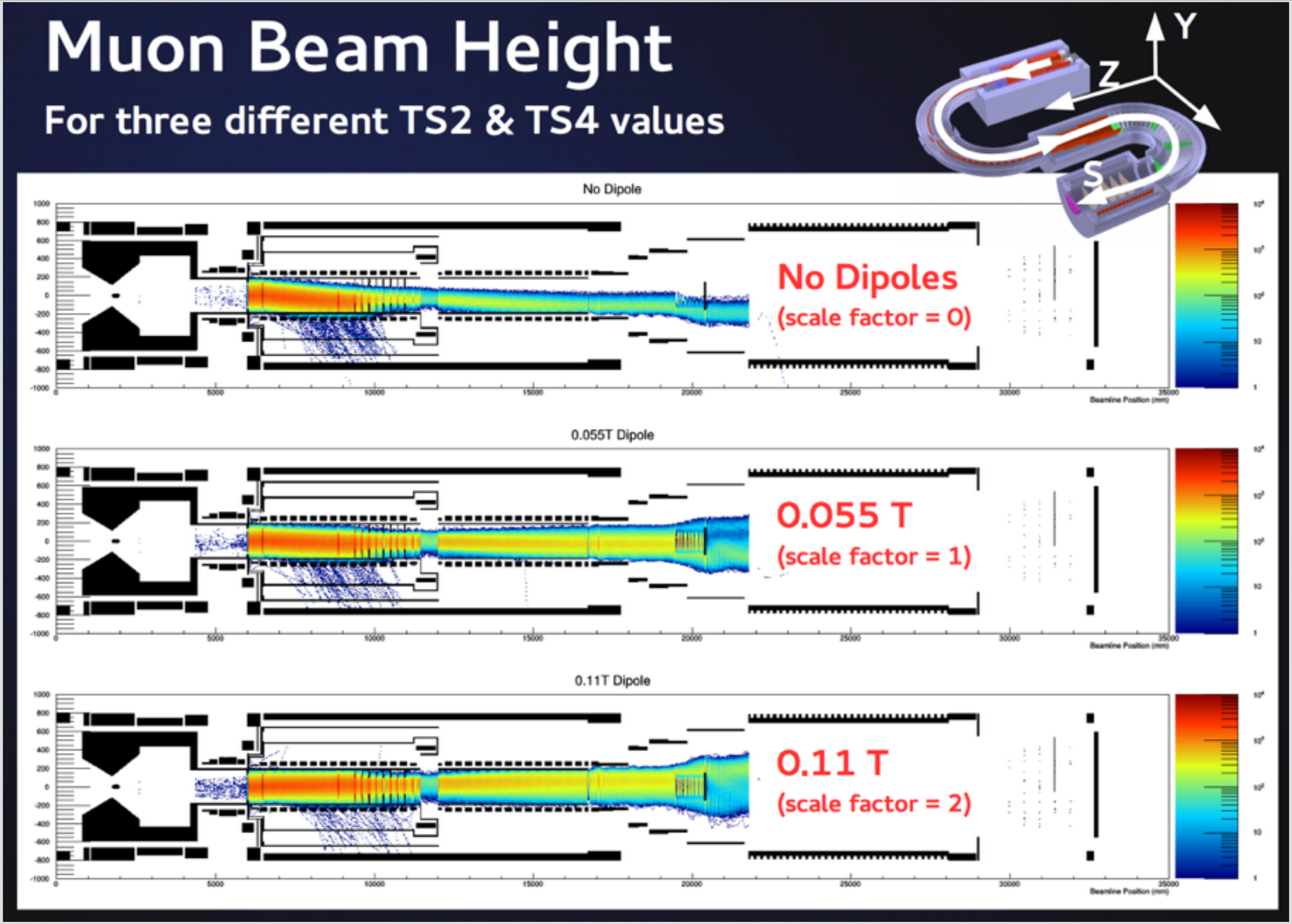

Optimisation of the field map along beam line

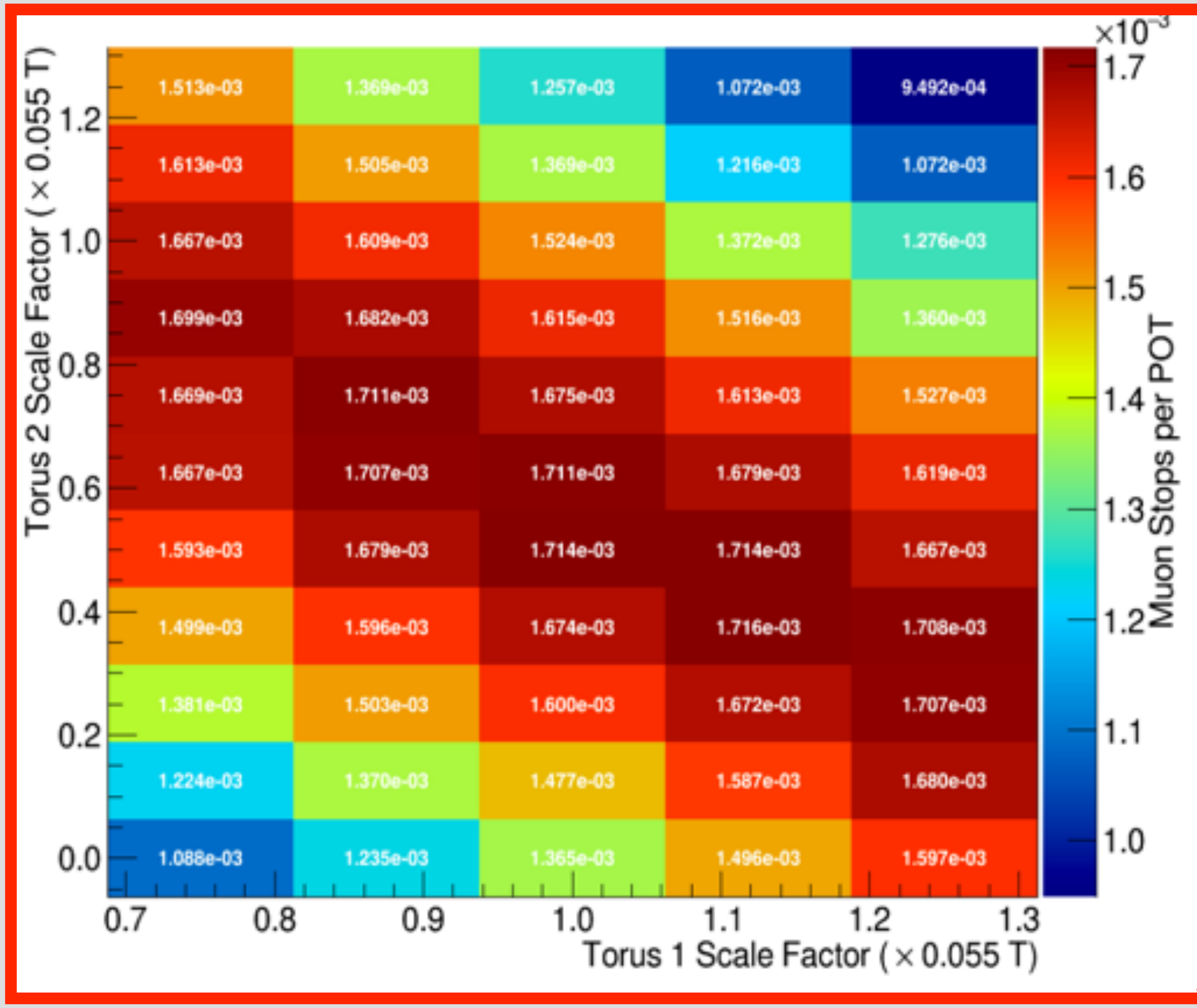

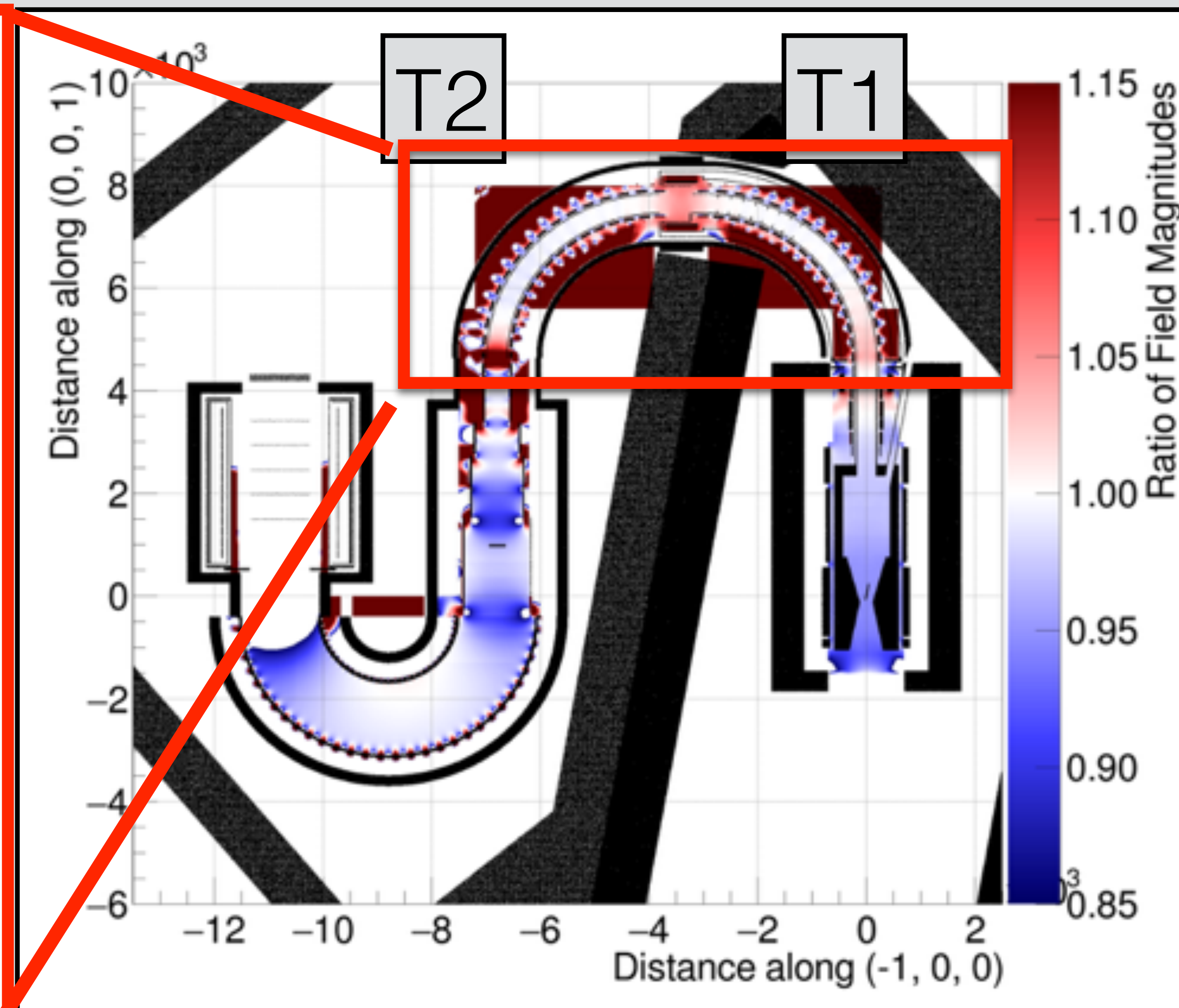

- Optimised results of Muon Transported solenoid :
  - T1: 0.055 T
  - T2: 0.0275 T

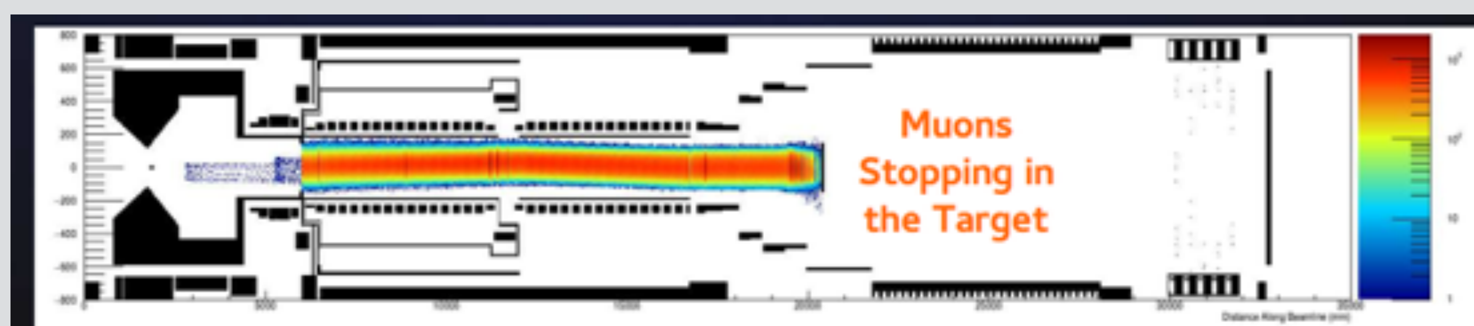

Muon transport solenoid design

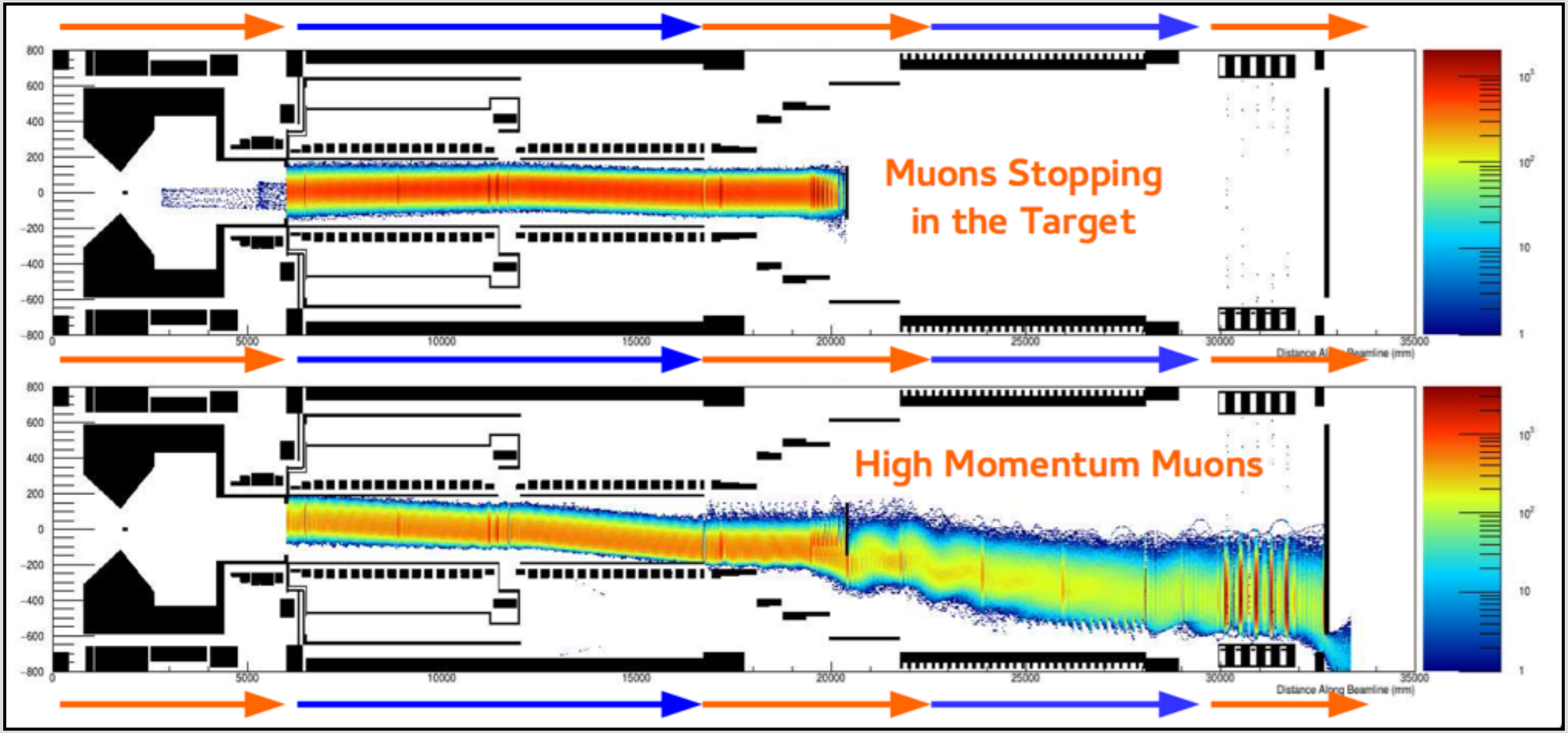

Muon transport solenoid design

- Consist of 2 Toruses
  - Bore radius : 175mm
  - Magnetic field : 2T
  - Bending : 180 degree
  - Radius Curvature : 3m
- Eliminating most high energy muons

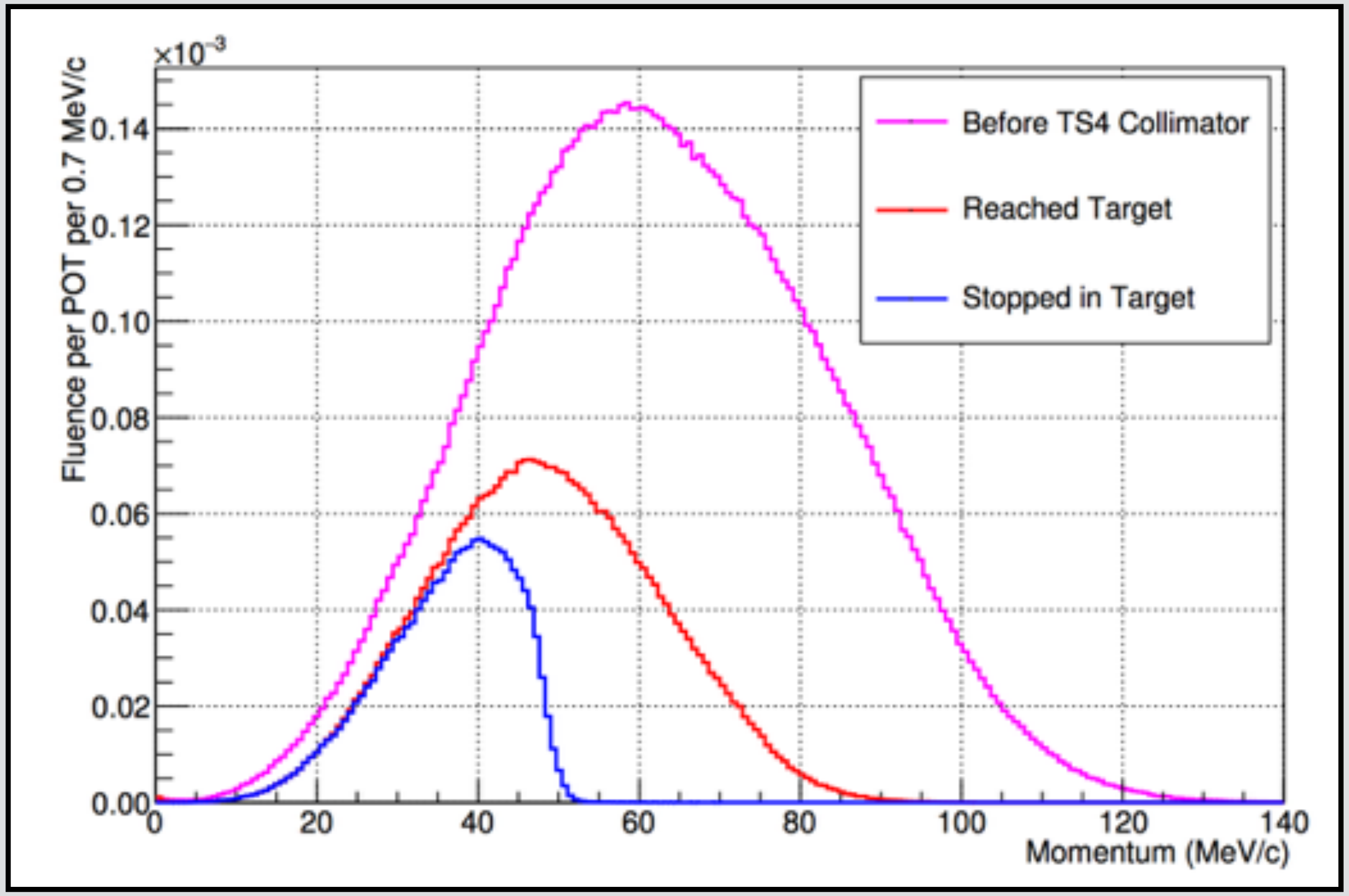

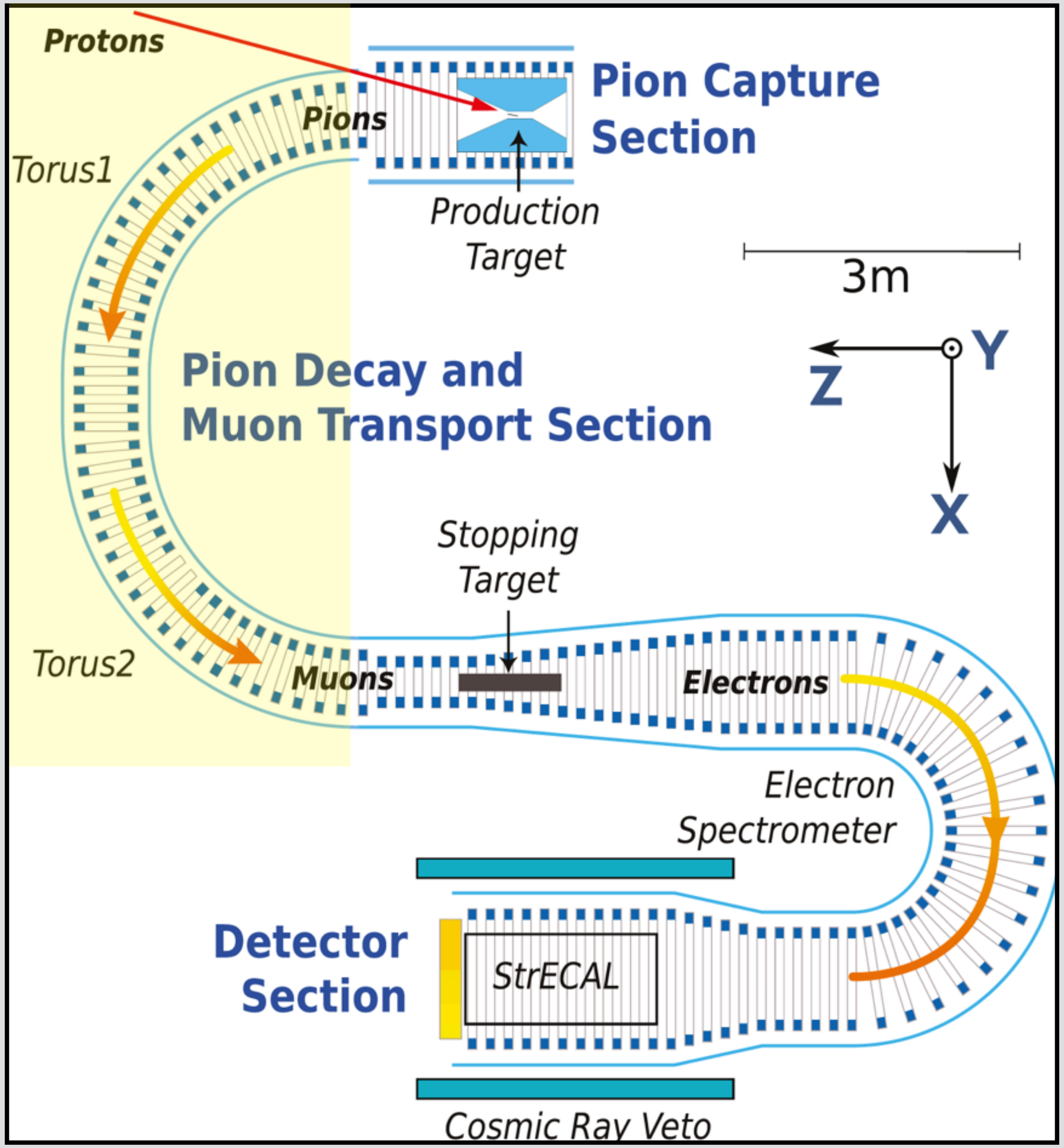

Muon transport solenoid design

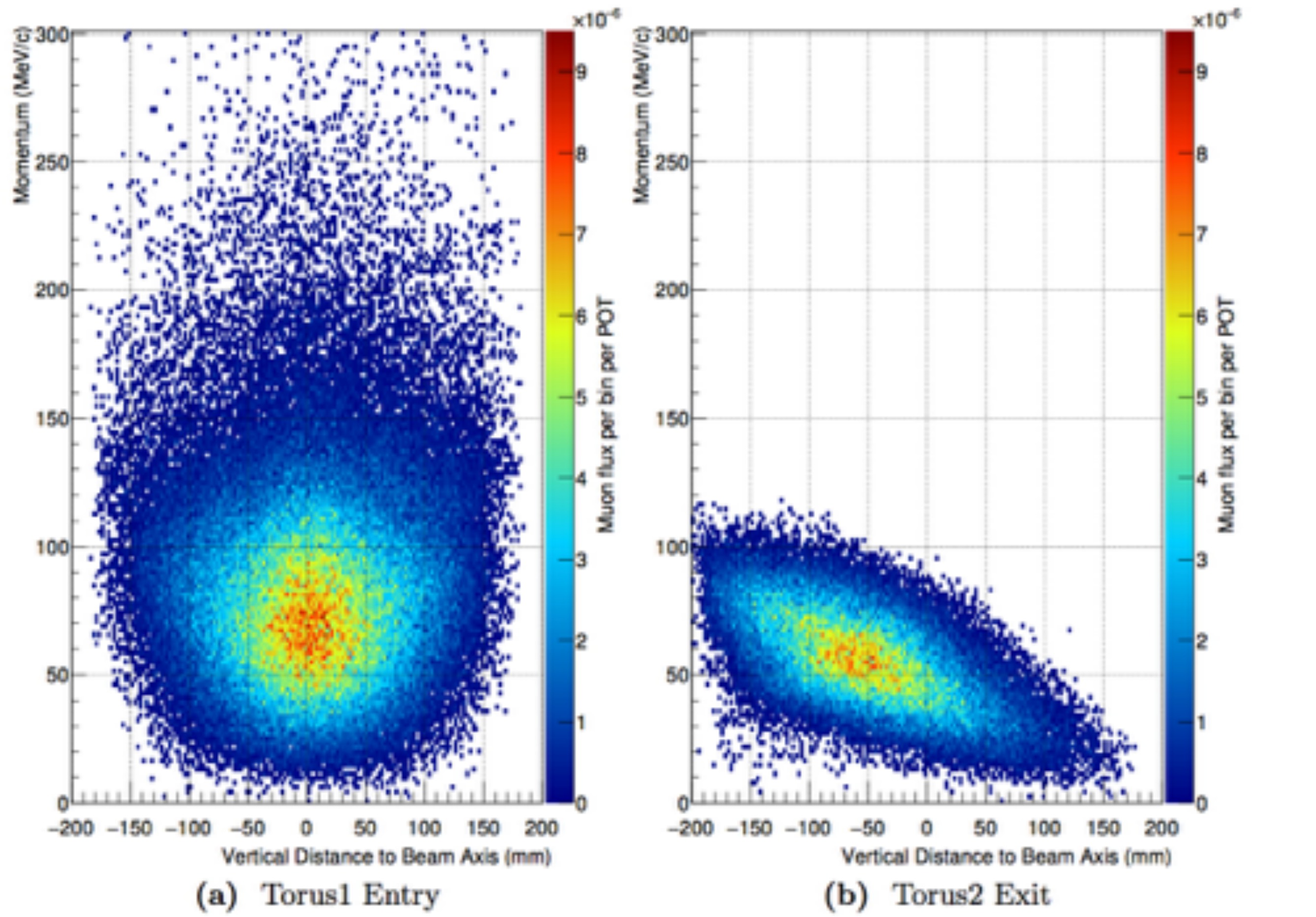

Figure 5.20: Dispersive effect of the 180° bent transport solenoid and dipole field on muons. No collimating material is yet included, so the high-energy muons being removed is due purely to the beam-pipe itself.

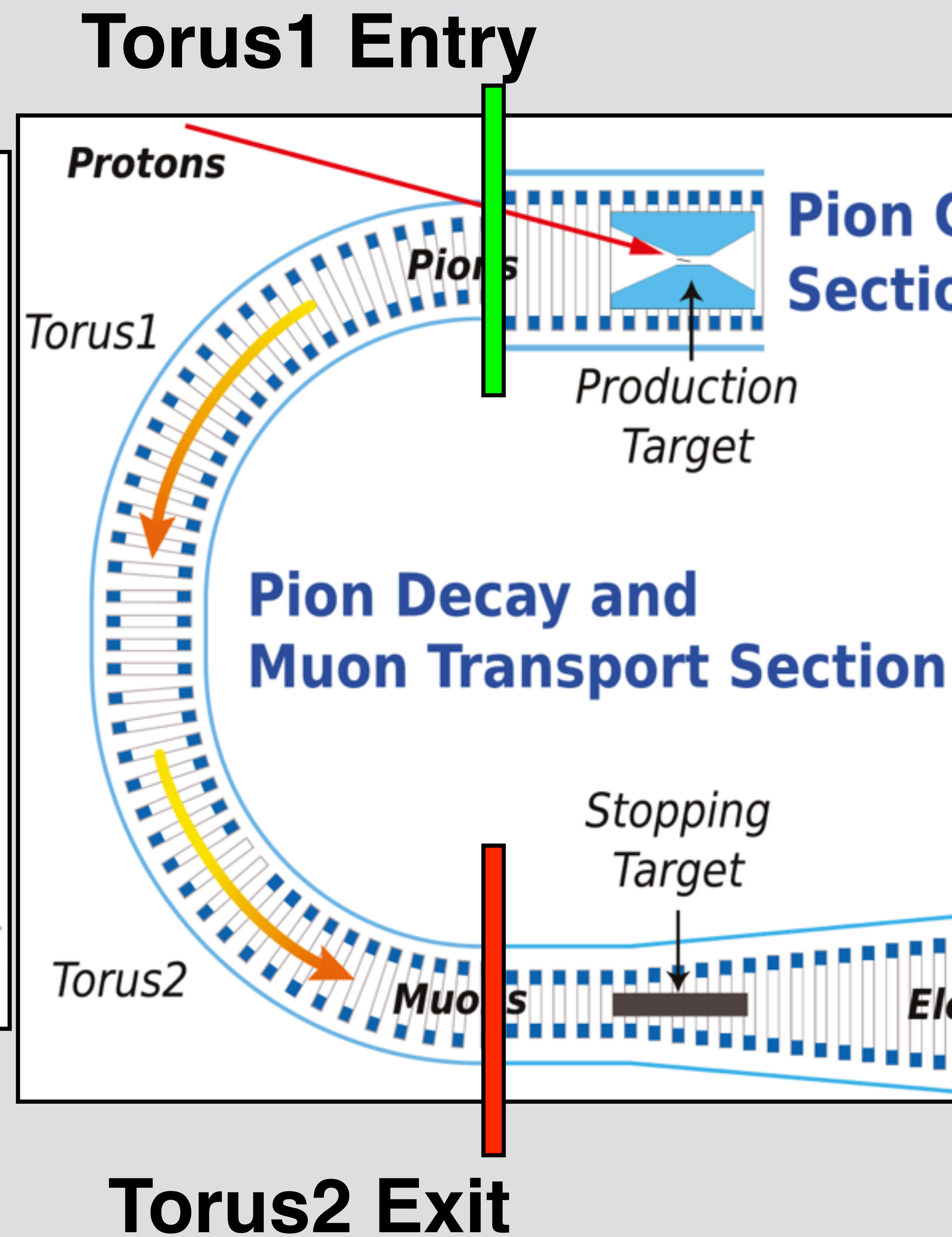

Design Beam collimator

- **Dangerous particle**
  - **High momentum pions**
  - **High momentum muons**
- **At 180 degree, separation is the best, Collimator should be installed here**

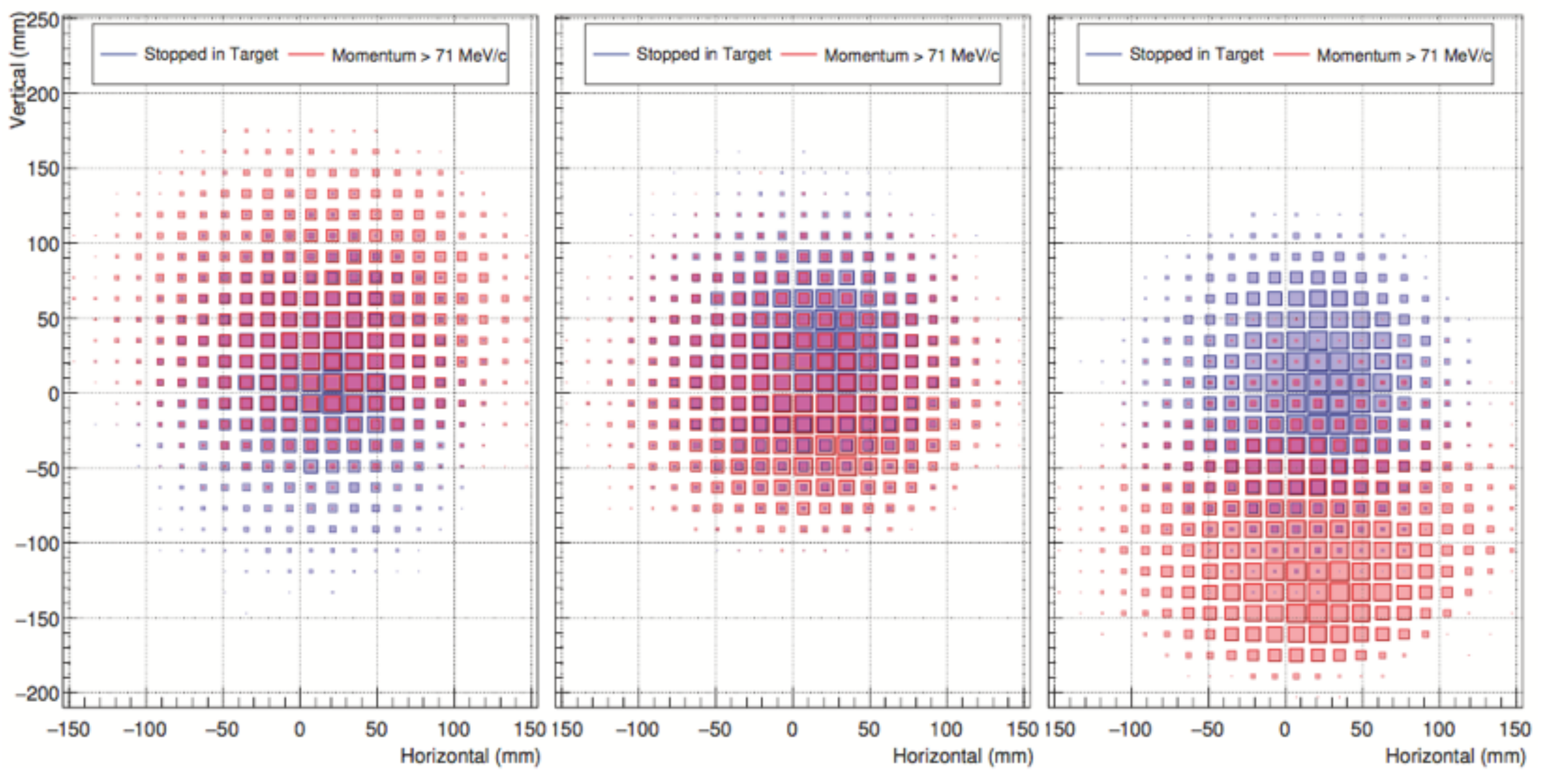

(a) At 0°　(b) At 90°　(c) At 180°

Design of beam collimator

- Cut at 120 mm height from the beam height axis
  - Suppress
    - 14% of >71MeV/c pions
    - 24% of >71MeVc/ c muons
    - 3% of the stopping rate
  - Using Phase-I design decrease further more

Phase-I design

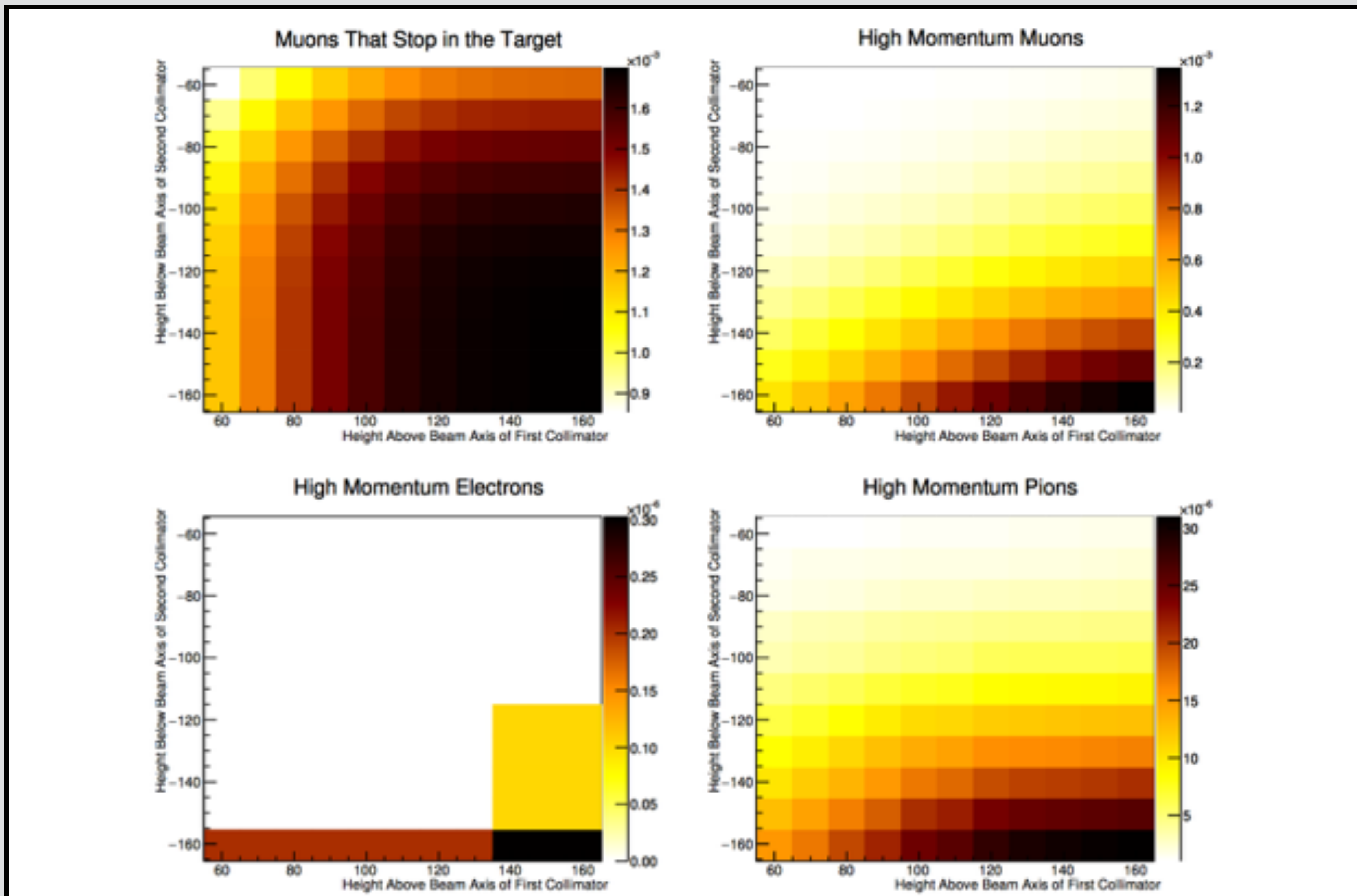

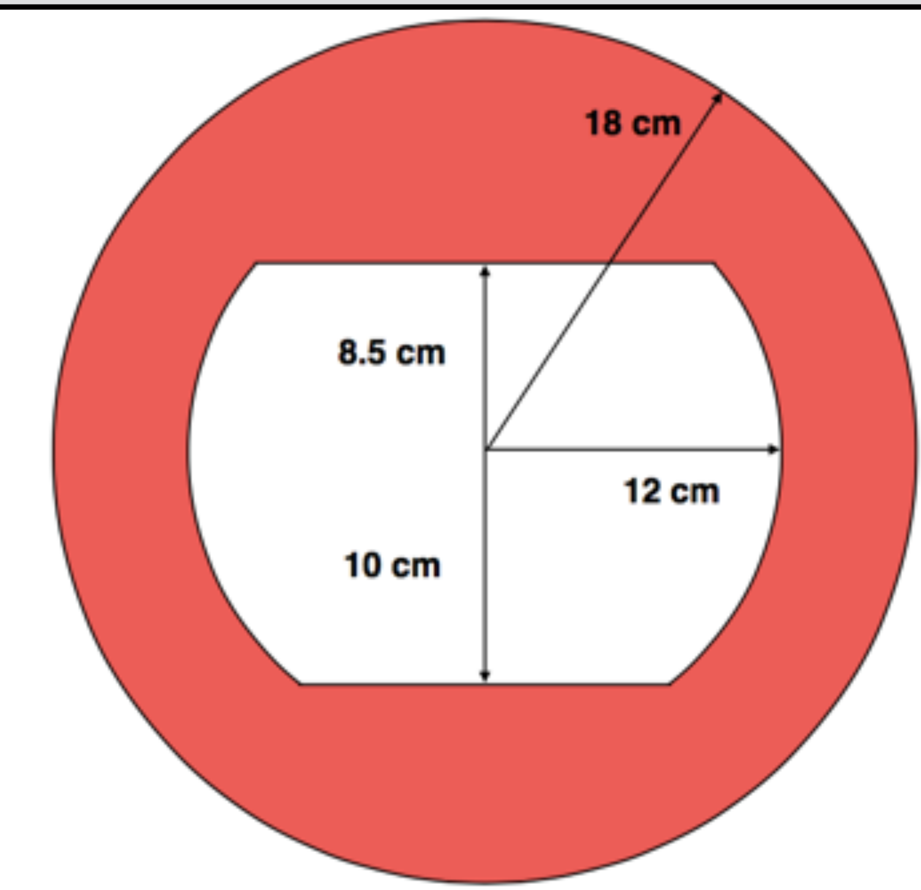

Figure 8.6: *Muon collimator plate size.*

Schematic of Detector Section in Phase-II

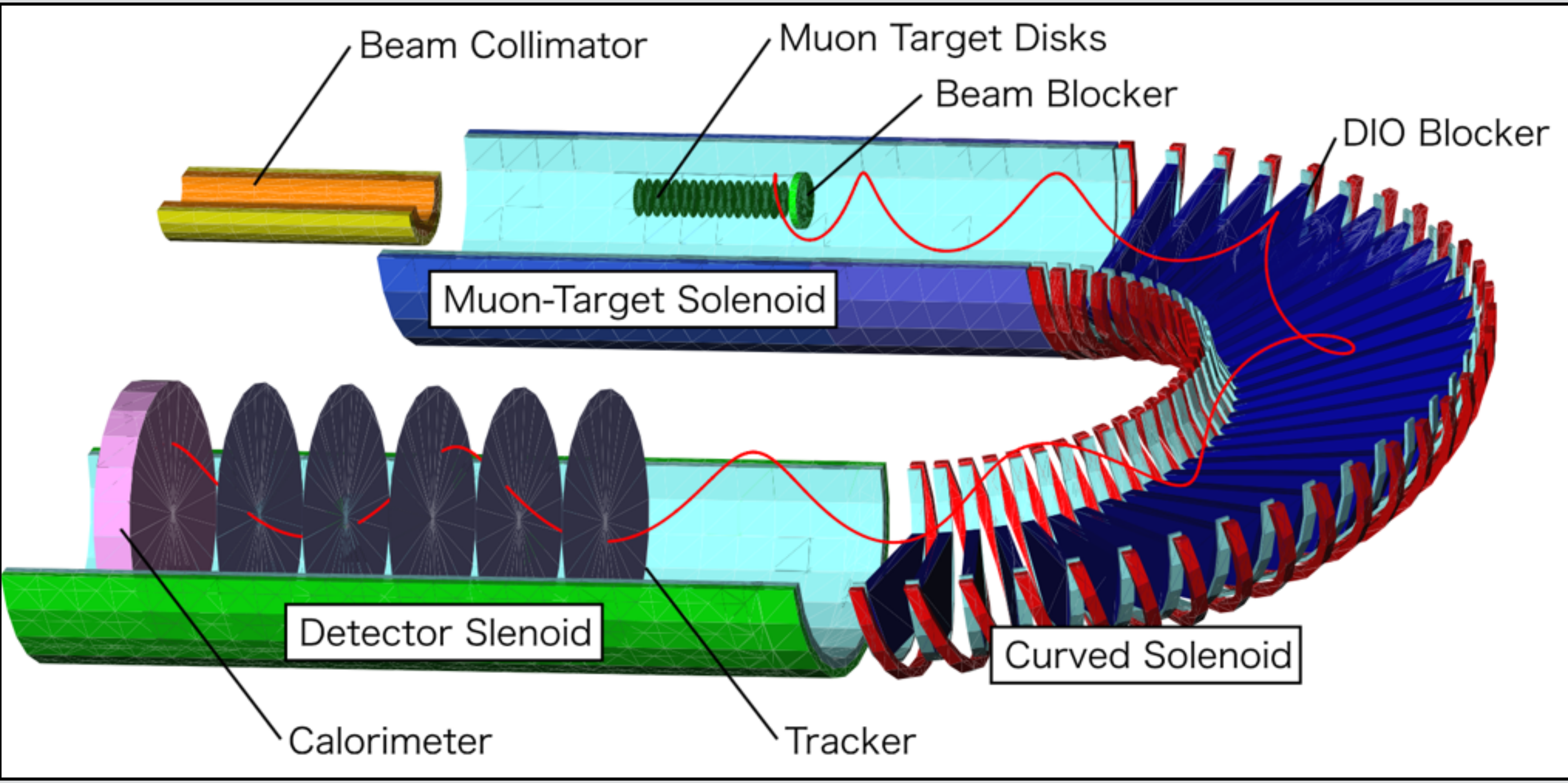

Optimisation of the field map along beam line

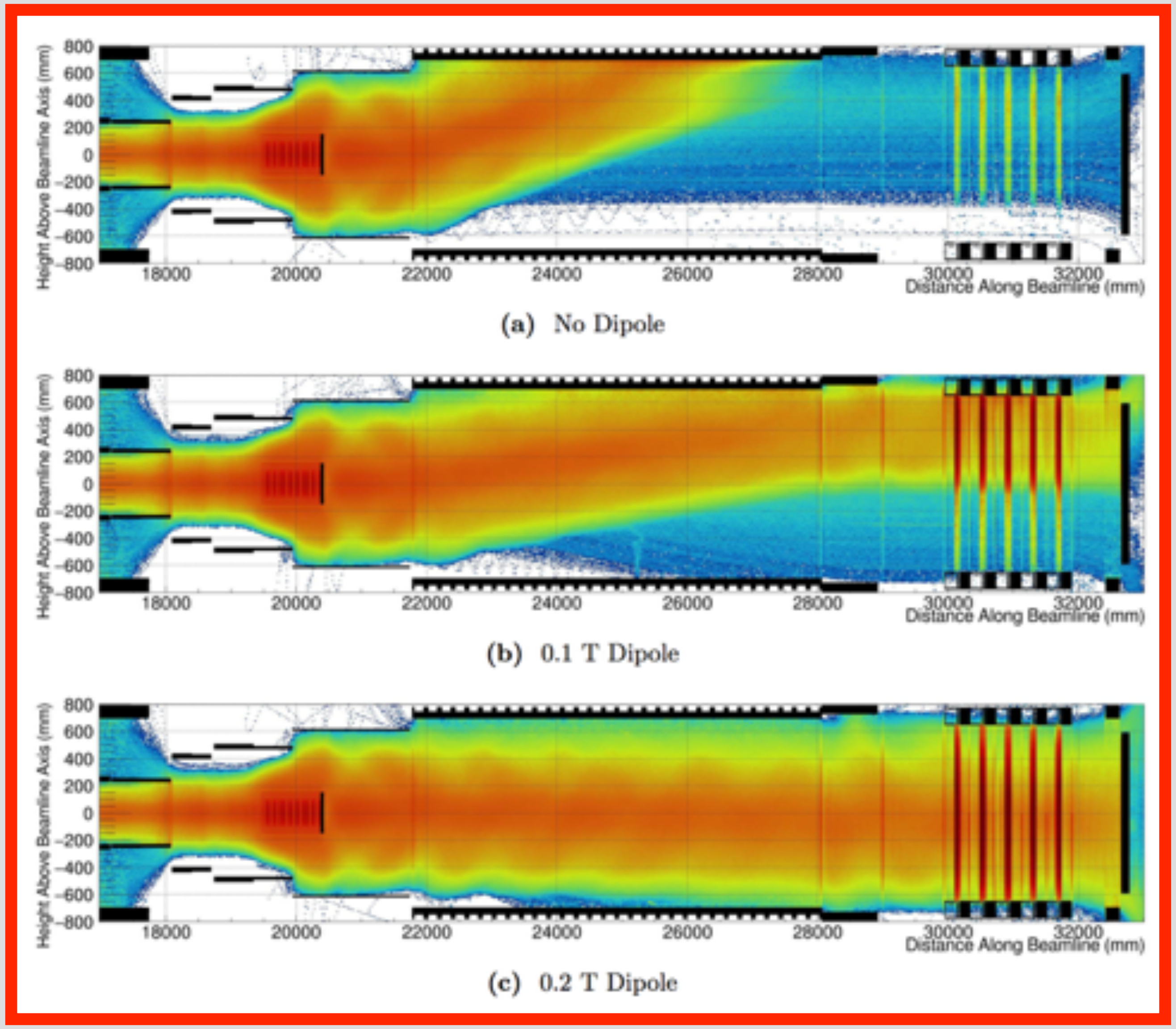

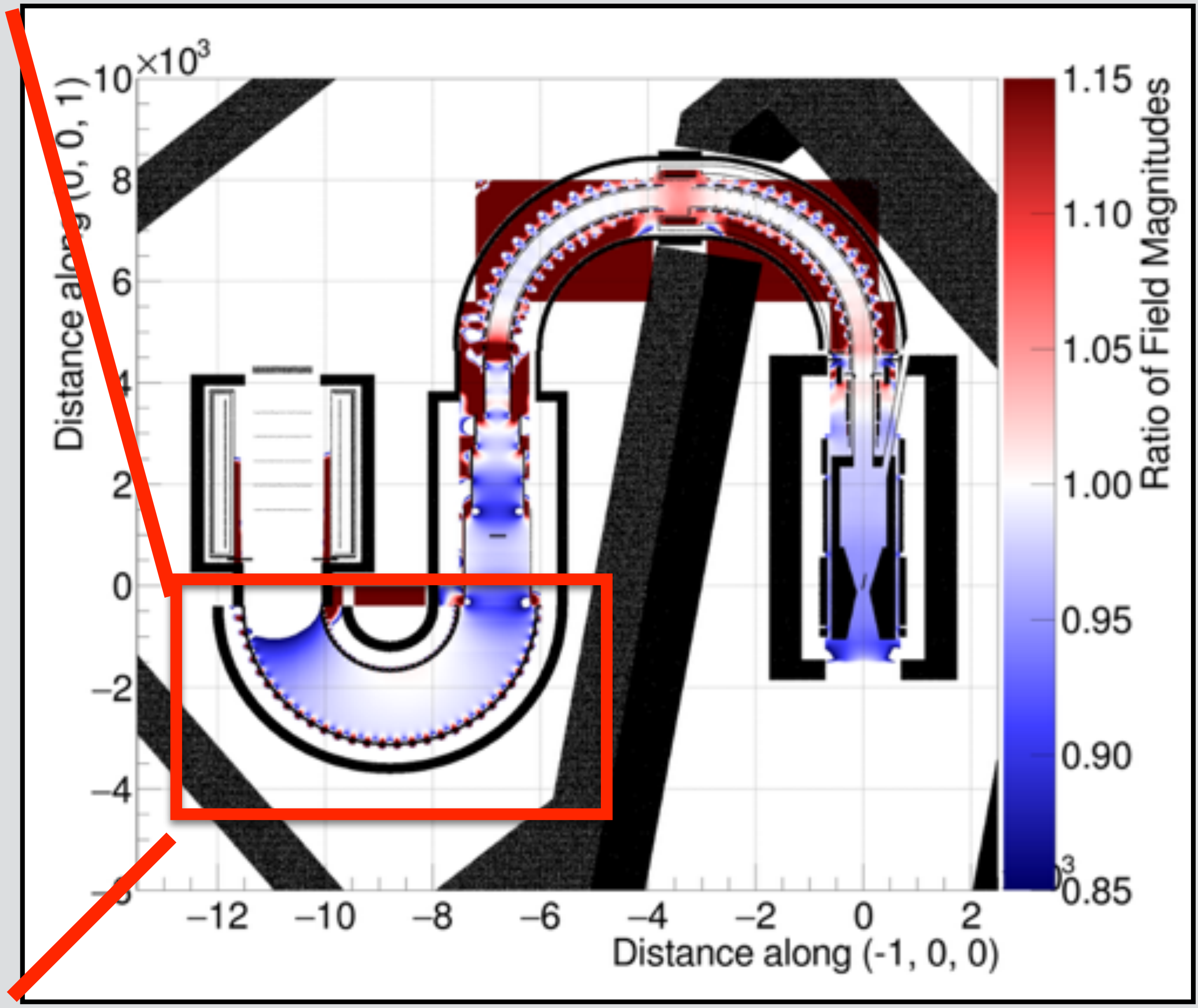

Caution: x axis start from 17000 [mm] ~ Stopping target

- **Optimised results for 105MeV electrons:**
  - **T1: -0.18 T**

Design of Muon Stopping Target

- **Consideration**
  - **Life time**
  - **End-point energy of decay-in-orbit**
- **COMET**
  - **Beam Flash: 200s after POT event →**

    NO Atomic number > 26

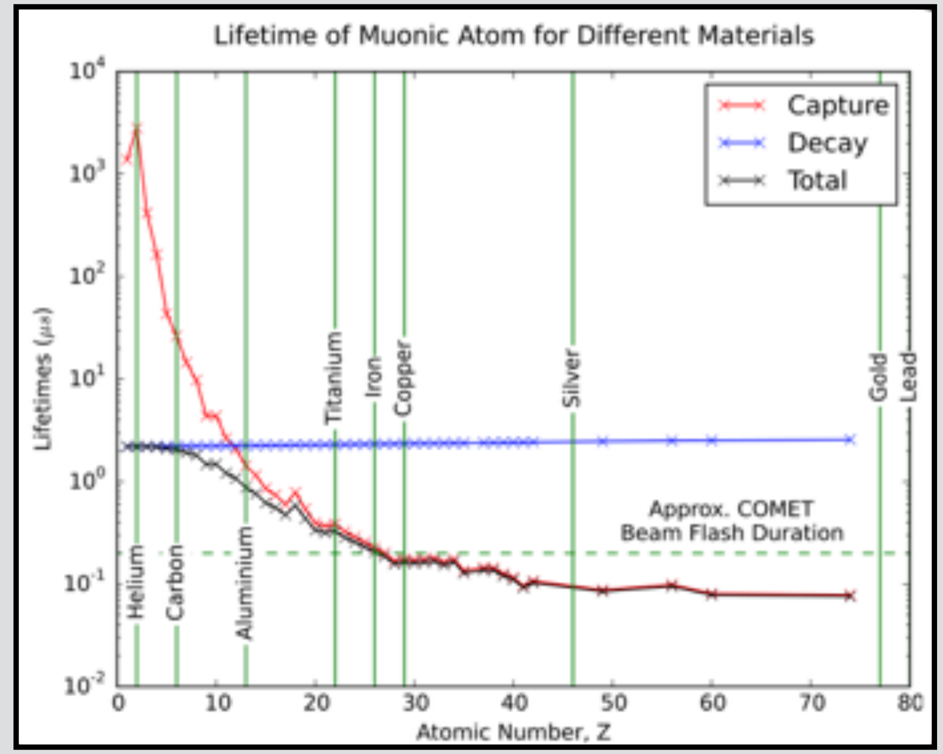

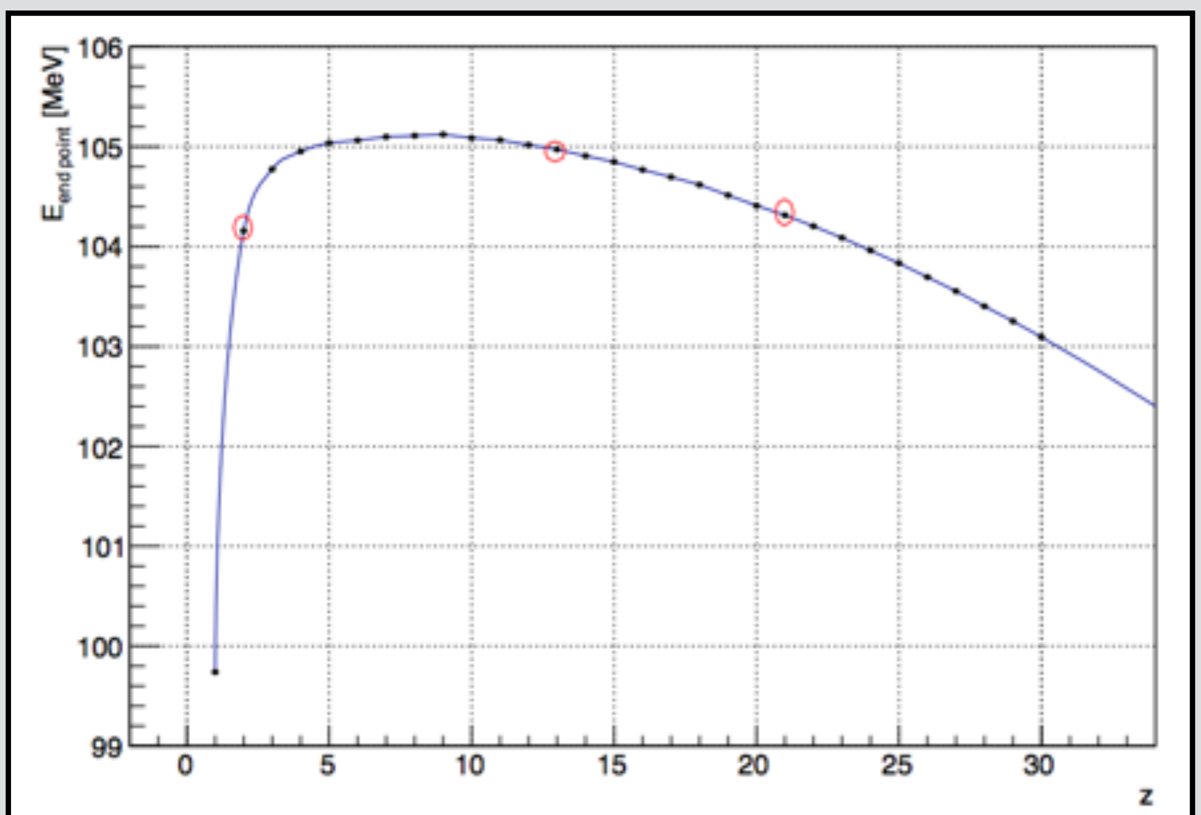

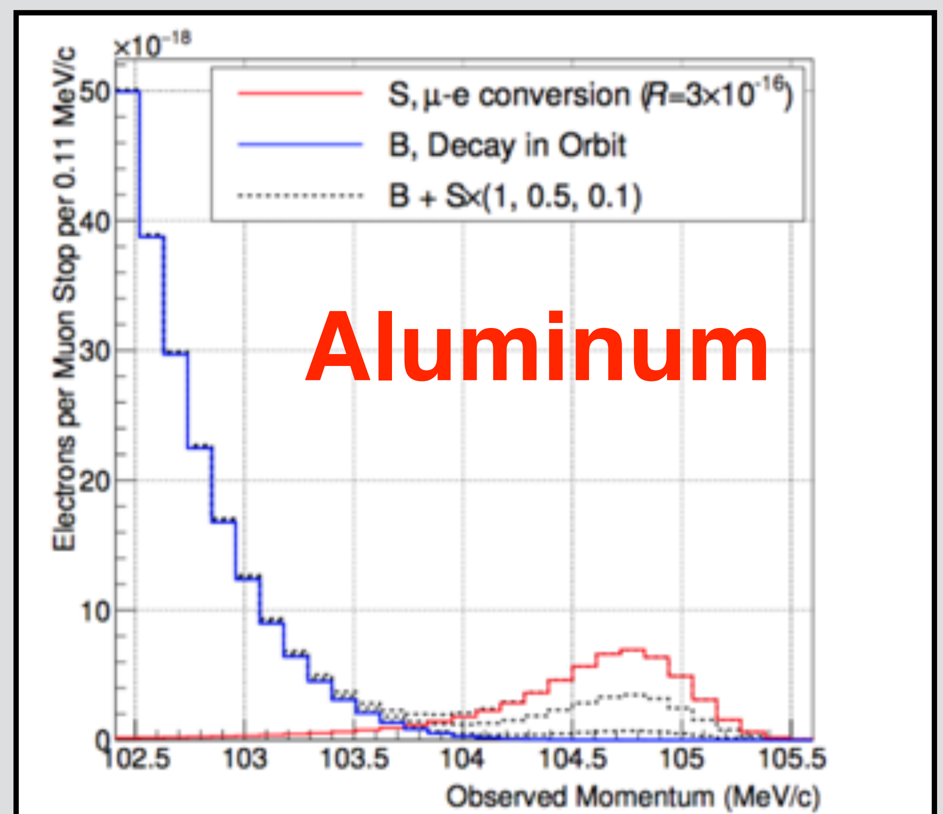

Design of Muon Stopping Target

COMET Phase-I

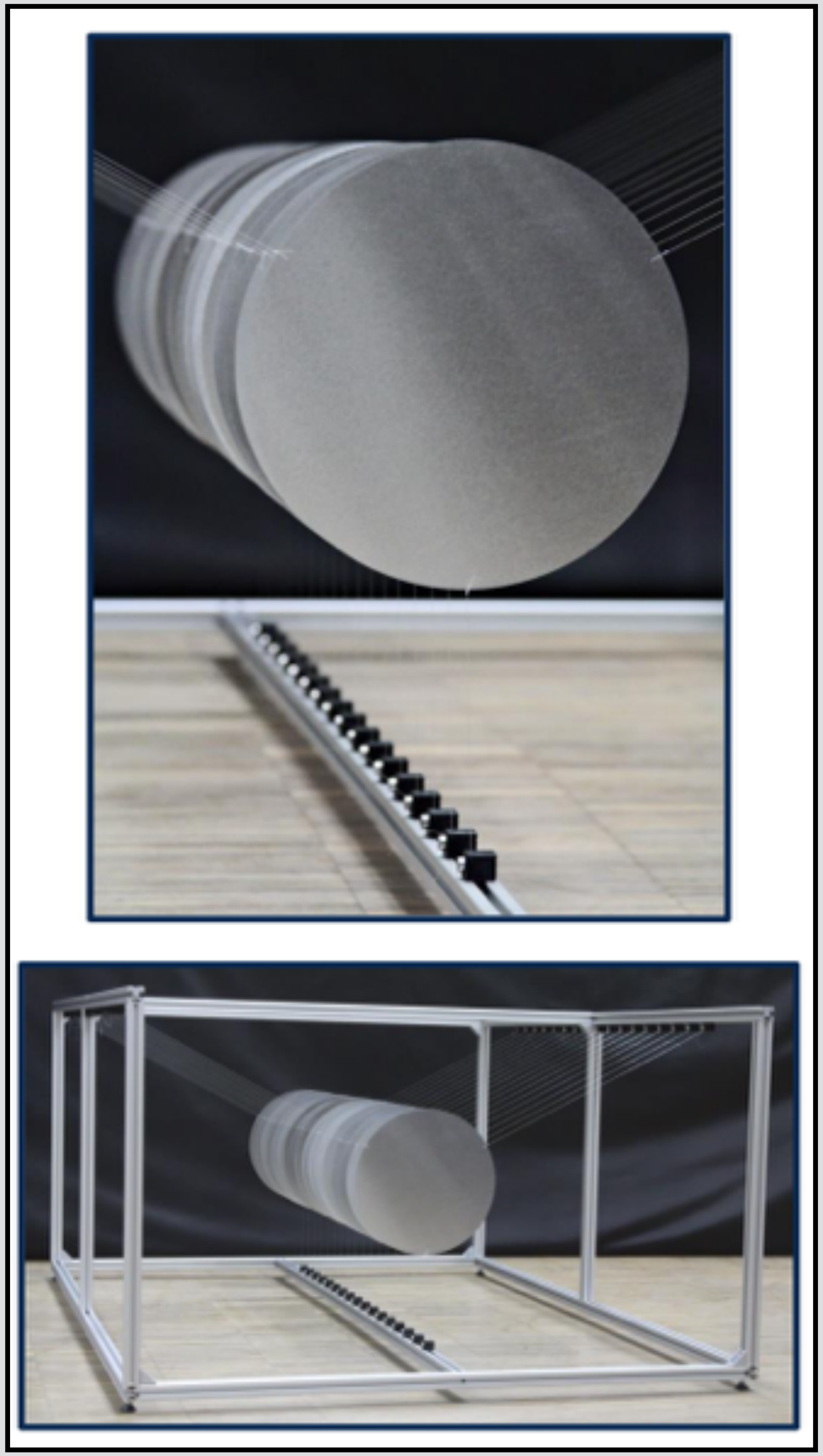

Item	Specification
Material	Aluminum
Life time of muon	864 ns
Shape	Flat disk
Radius	100 mm
Thickness	200µm
Number of disks	17
Disk spacing	50 mm

- **Beam Blocker Right after Muon Stopping target**

Stopping rate and efficiency

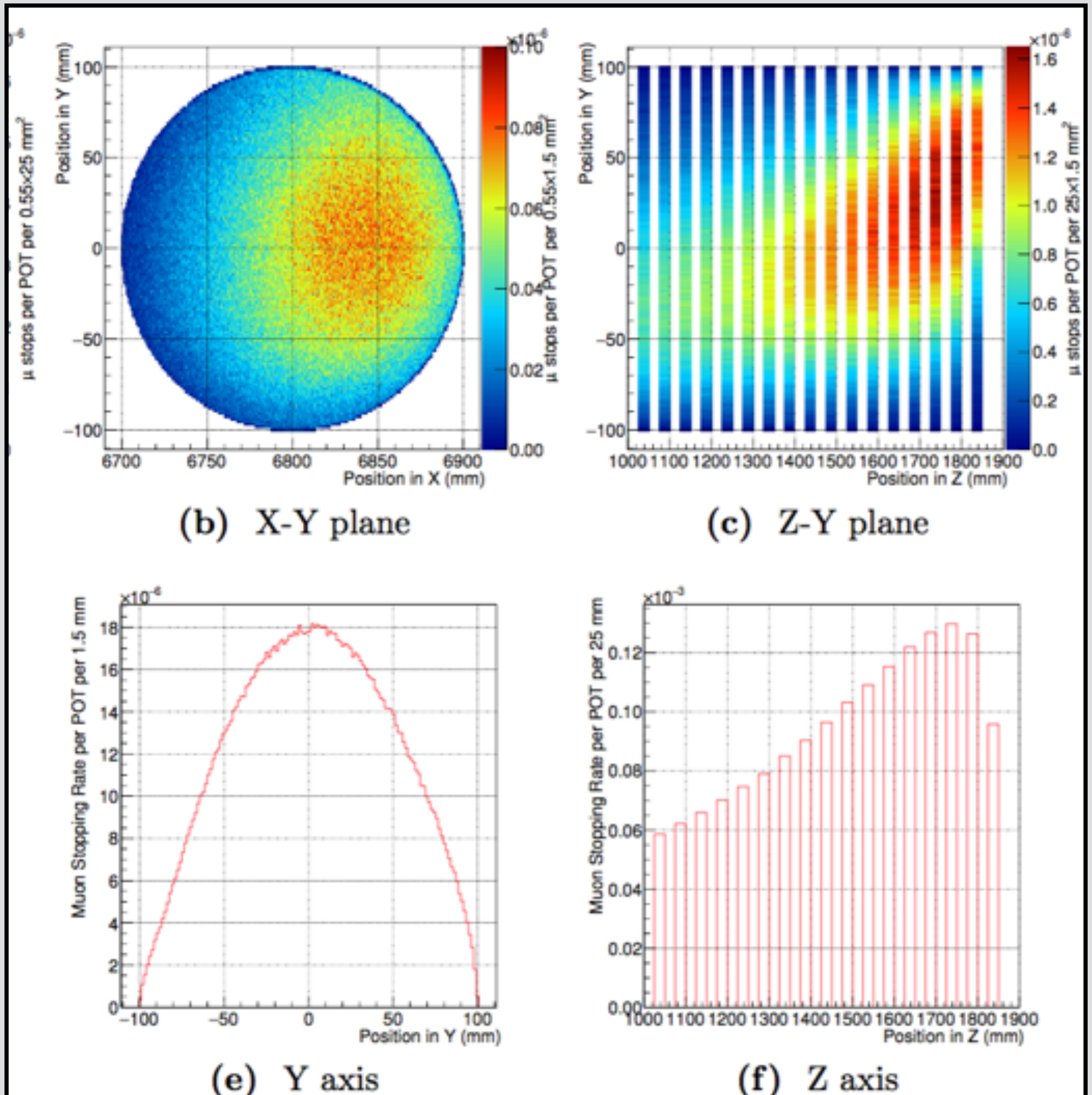

(b) X-Y plane (c) Z-Y plane (e) Y axis (f) Z axis

Beam direction

- High momentum muons at lower Y
- Low momentum muons at higher Y
- With 8.81 x 108 POT,
  - Stopping rate = 1.61e-3
    - Signal acceptance = 0.22
    - Timing window cut efficiency
      - >
    - Momentum cut efficiency
      - >104.2MeV/c : 0.7

Summary of Total acceptance

Overall Acceptance	2009 CDR [45]	This Study
Geometric acceptance	0.20	0.22
Solid angle with mirroring	*(0.73)*	
Beam blocker acceptance	*(0.57)*	
Spectrometer acceptance	*(0.47)*	
Timing window efficiency	0.39	0.53
Momentum cut efficiency	0.72	0.70
TDAQ acceptance and efficiency	0.90	N/A
Reconstruction aspects	0.78	N/A
Recon. efficiency	*(0.88)*	
Track quality cut efficiency	*(0.89)*	
Additional analysis cuts	0.81	N/A
Transverse momentum cut efficiency	*(0.83)*	
E/p cut efficiency	*(0.99)*	
Pitch angle cut efficiency	*(0.99)*	
Total acceptance at 'truth level'	0.056	0.091
Total (with CDR recon. and TDAQ efficiencies)	0.039	0.057

Table 6.1: Numbers that go into estimating the total signal acceptance from this study compared to the previous evaluation in the 2009 CDR. Since this study has not estimated reconstruction issues, we include the previous values in the final estimate on the expectation that with the improvements in reconstruction techniques and with the benefit of Phase-I final reconstruction efficiency will be improved compared to the 2009 CDR values.

Single event sensitivity

Equation for SES:

$$S.E.S \times t_{run} = \frac{1}{(I_p/e)R_{\mu/p}B_{capture}A_{\mu\to e}} = 4.08 \times 10^{-10}$$

I_p/e: Number of protons per seconds = 7μA/1.6×10^{-19}

$R_{\mu/p}$: Stopping rate per POT = 1.61×10^{-3}

$A_{\mu\to e}$: Acceptance 5.7%

$B_{capture}$: 61% (Branching ratio for muon **nuclear capture** in Aluminium

	Single event sensitivity	Total POT ($\times 10^{19}$)	Beam time t_{run} (s)	SES in one year of continuous beam
COMET Phase-II (this study)	2.6×10^{-17}	68.3	1.57×10^{7}	1.29×10^{-17}
COMET Phase-II (CDR 2009 [45])	2.6×10^{-17}	85	2.00×10^{7}	1.65×10^{-17}
Mu2e [42]	2.4×10^{-17}	36	6.00×10^{7}	4.57×10^{-17}
COMET Phase-I [44]	3.0×10^{-15}	3.2	1.26×10^{7}	1.19×10^{-15}

Background studies

Main Background : Muon decay in orbit

Best Measurement SINDRUM-II

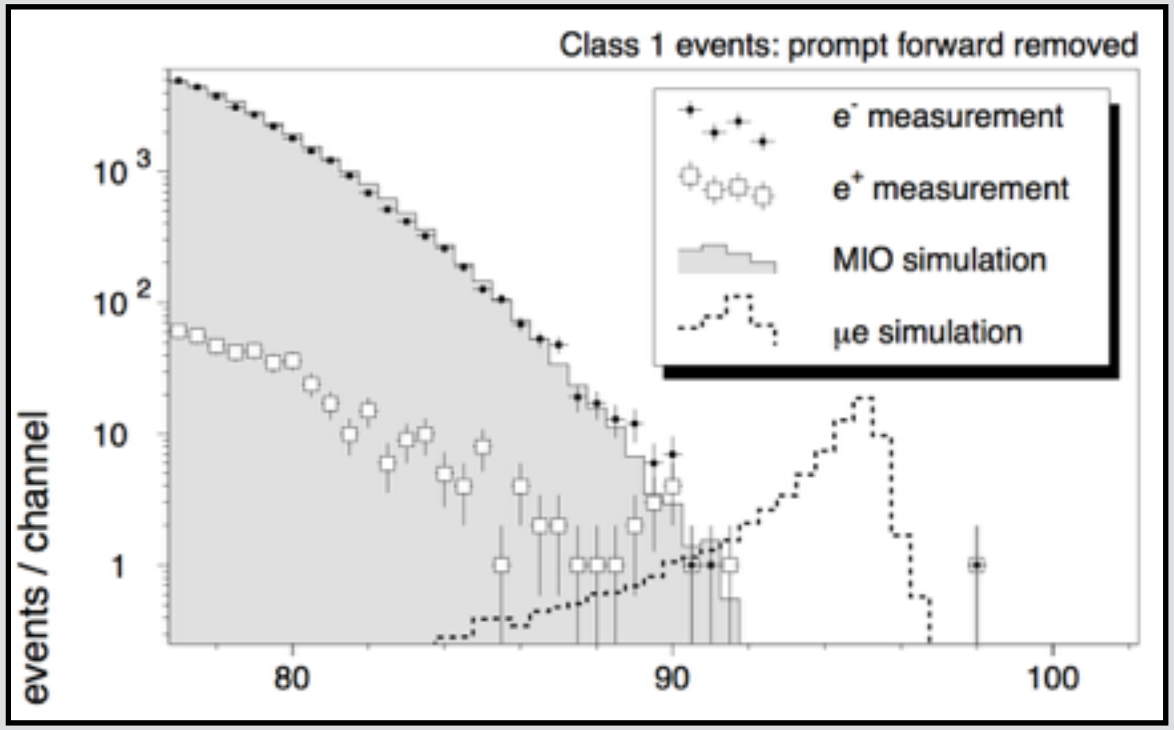

Conservative guess (2011) from theorists

- 104.2MeV/c (2% survive)

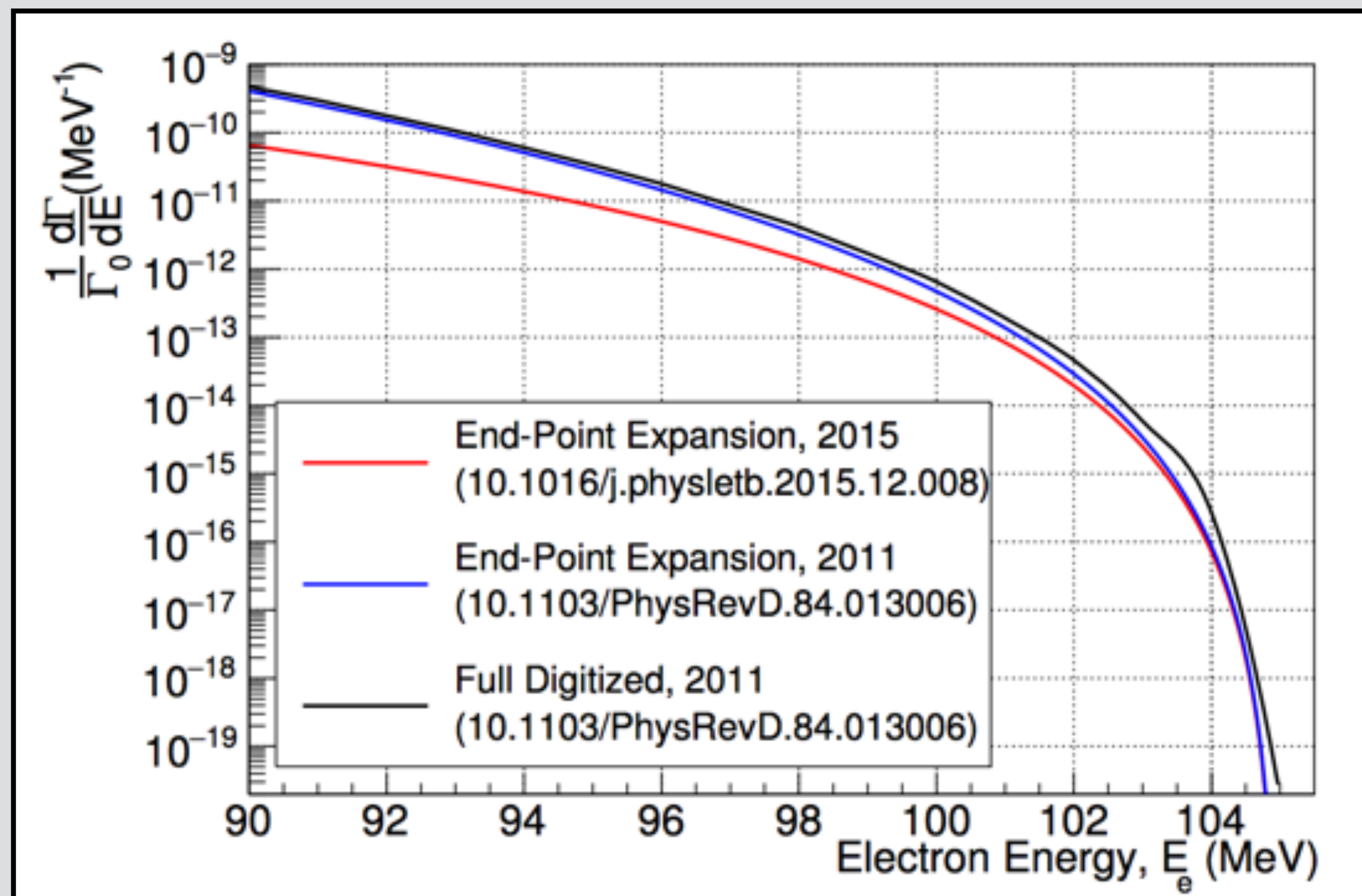

Others backgrounds

Type	Source	Background Rate per μ^- stop	per POT	per second	Total Events	Comment
Intrinsic	DIO	6.20×10^{-20}	9.92×10^{-23}	4.31×10^{-9}	0.068	
	RMC	3.73×10^{-31}	6.01×10^{-34}	2.61×10^{-20}	4.10×10^{-13}	
Delayed	RPC	–	1.73×10^{-27}	7.51×10^{-14}	1.18×10^{-6}	
	Beam	–	1.47×10^{-24}	6.39×10^{-11}	1.00×10^{-3}	Beam includes high-energy electrons from π, μ, and n capture. See Section 7.5 for discussion.
	Stopped $\bar{p}$	–	4.34×10^{-22}	1.89×10^{-8}	0.296	Based on conservative interpolation and extrapolation of limited experimental $\bar{p}$ data. See Section 7.4
	π^- from $\bar{p}$	–	1.95×10^{-30}	8.49×10^{-17}	1.33×10^{-9}	
Prompt	RPC	–	1.82×10^{-24}	7.91×10^{-11}	1.24×10^{-3}	
	Beam	–	2.80×10^{-24}	1.22×10^{-10}	1.91×10^{-3}	See comment for delayed background.
	π^- from $\bar{p}$	–	3.56×10^{-29}	1.55×10^{-15}	2.43×10^{-8}	See comment for delayed background.
Cosmics		–	–	1.87×10^{-8}	0.294	Dominated by conservative miss-rate. See Section 7.6.
Total		–	–	4.22×10^{-8}	0.662	

Further optimisation and R&D Detector system

New design of Muon stopping targets for only COMET Phase-II

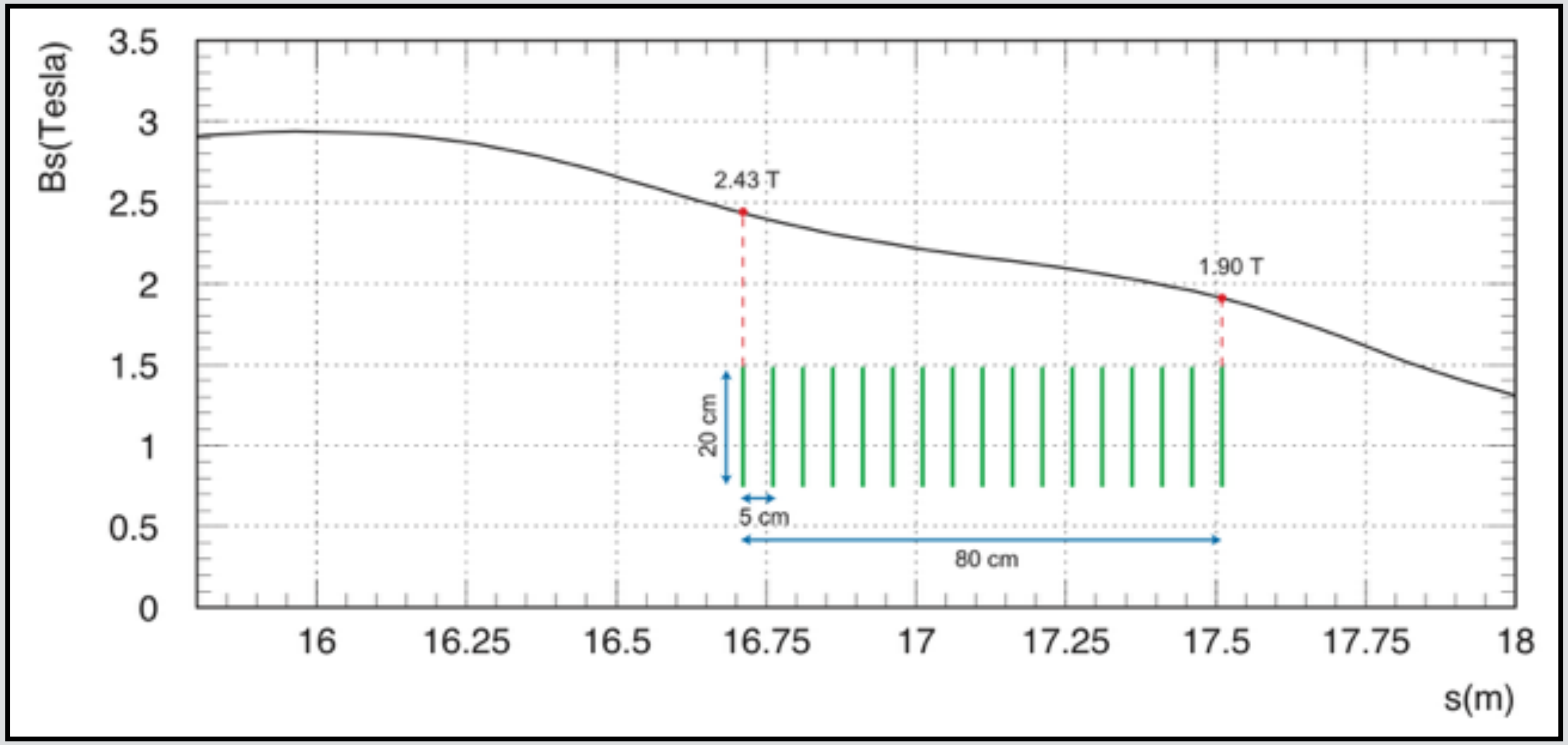

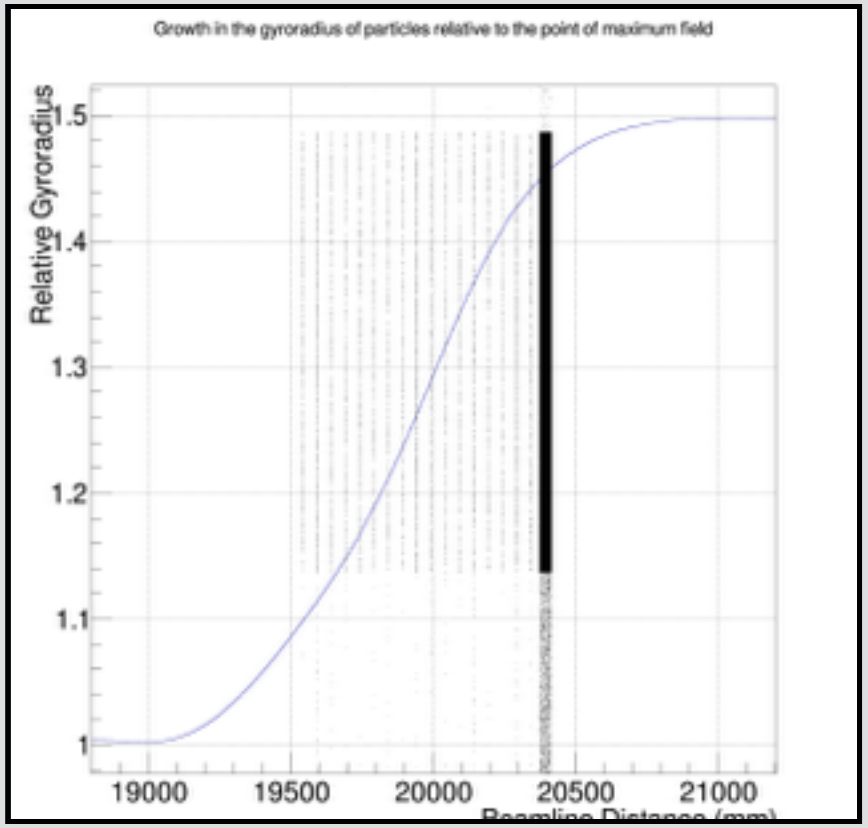

Gradually <u>increasing radius</u> of muon stopping target

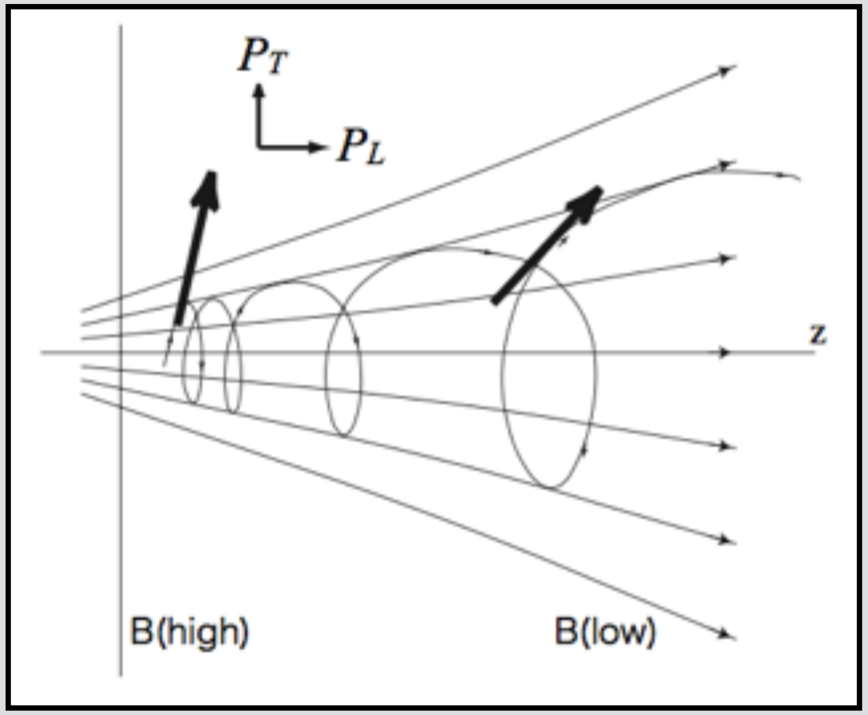

New design of Muon stopping targets

- New target design grows with the magnetic field to improve the stopping efficiency
- Allows beam blocker to be removed so improves signal acceptance

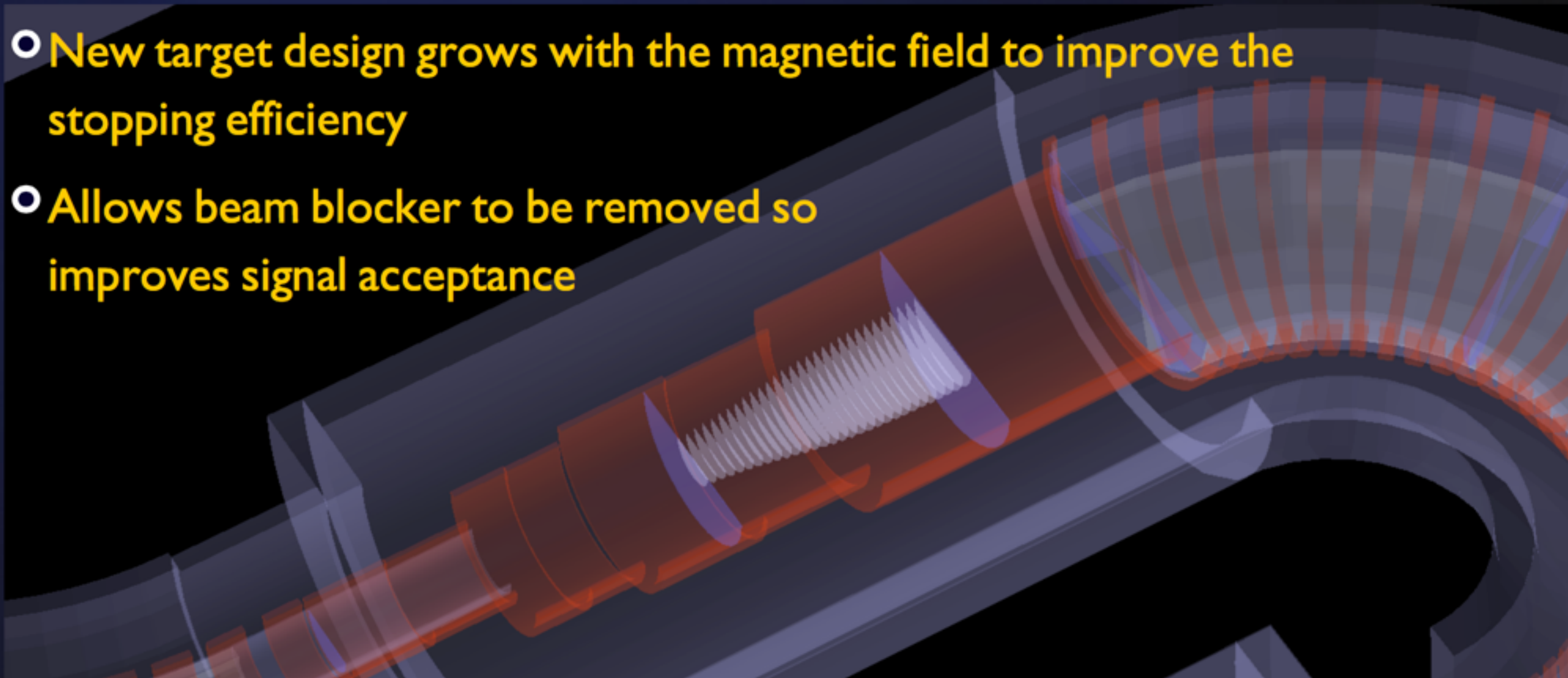

Simulation:

- Ran 75M POT events (limited by computer power at the time)
- Switch off stopped muon decay and capture:
  - All muons stopping in aluminium will undergo conversion

Design of Muon stopping targets

- Number of muon stopping targets
  - 30 disks
- Stopping rate
  - muon stopped : 1.75 times better (2.8×10^{-3}/POT)
  - Signal acceptance : 1.55 times better (48% e^- @ det)
  - This will be pushing the sensitivity higher
- This is GOOD but further optimisation should be carried out

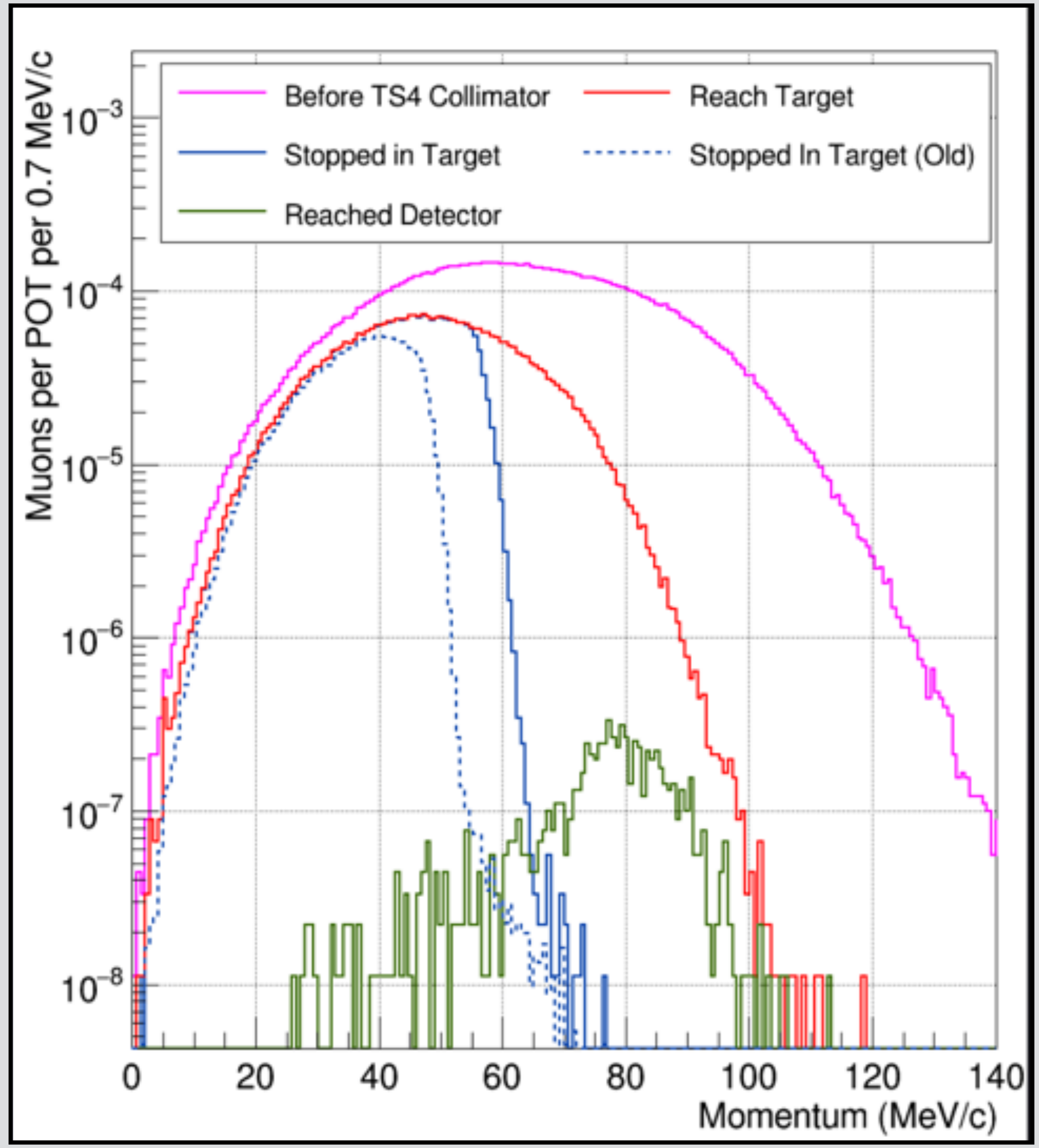

R&D of StrECAL — Straw tracker

- Many tests carried out using full-scale prototype
  - Establish the construction procedure
  - Evaluate out-gas rate of straw tubes
    - No leak, no significant out-gas
  - Beam test w/ 105MeV/c electron was done
    - **σ_x~150um obtained → σ_p~180keV/c**
  - **Operation in vacuum performed in success**
- **All Phase-I straw tubes have been built already**

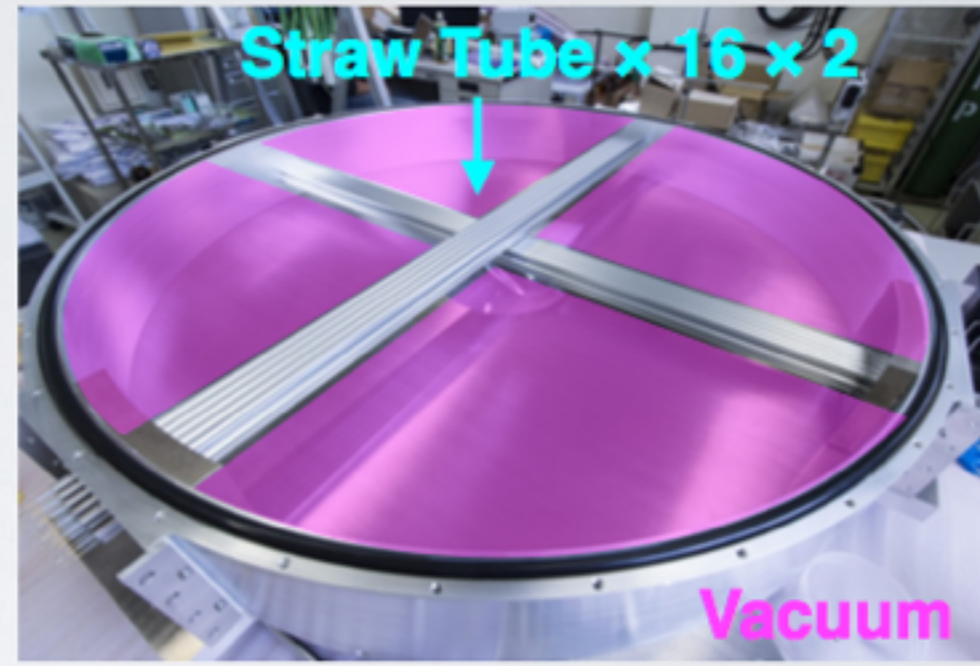

Less than 200um σ_x everywhere

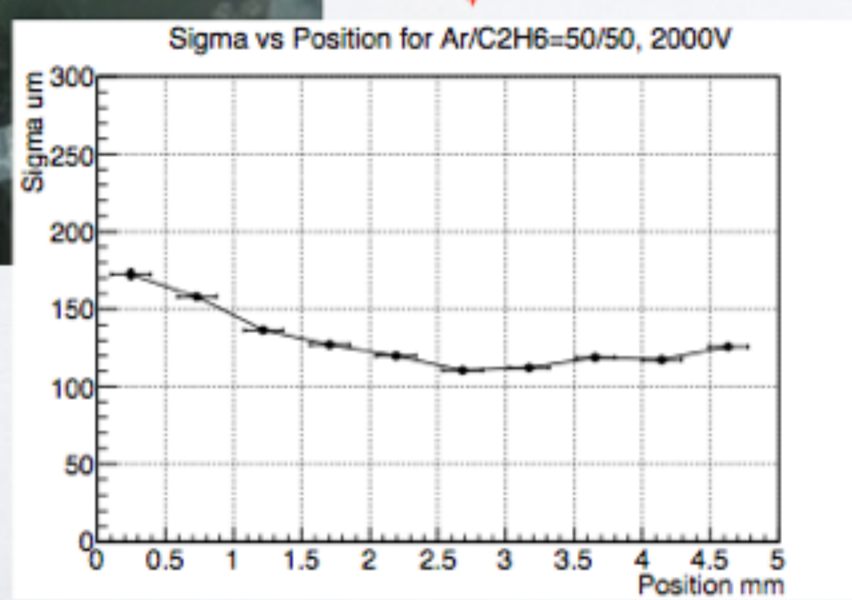

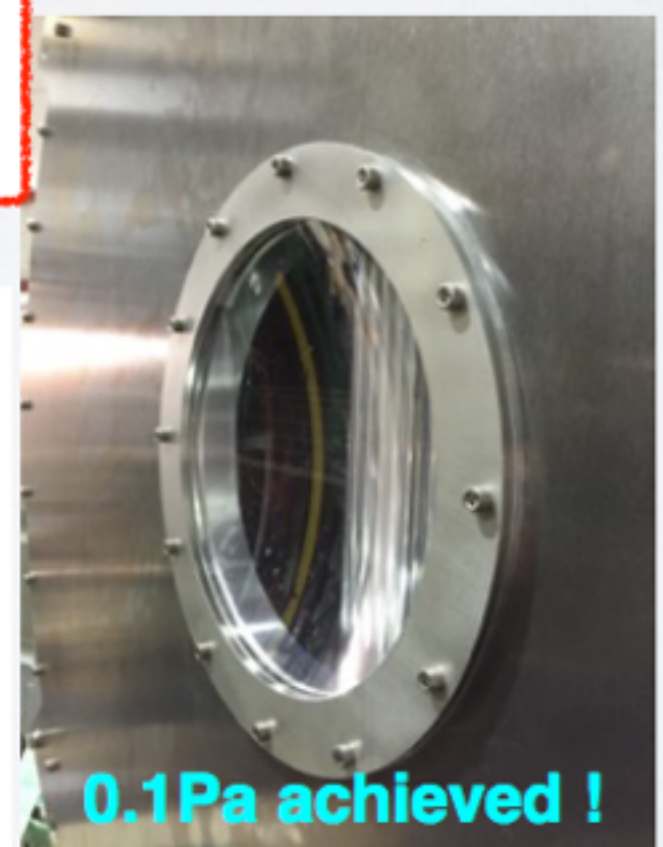

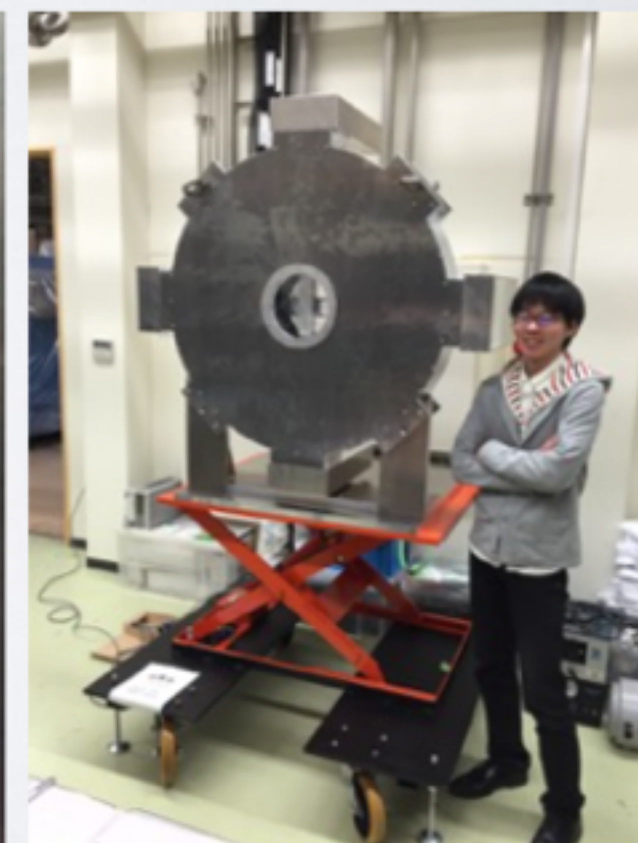

R&D of StrECAL

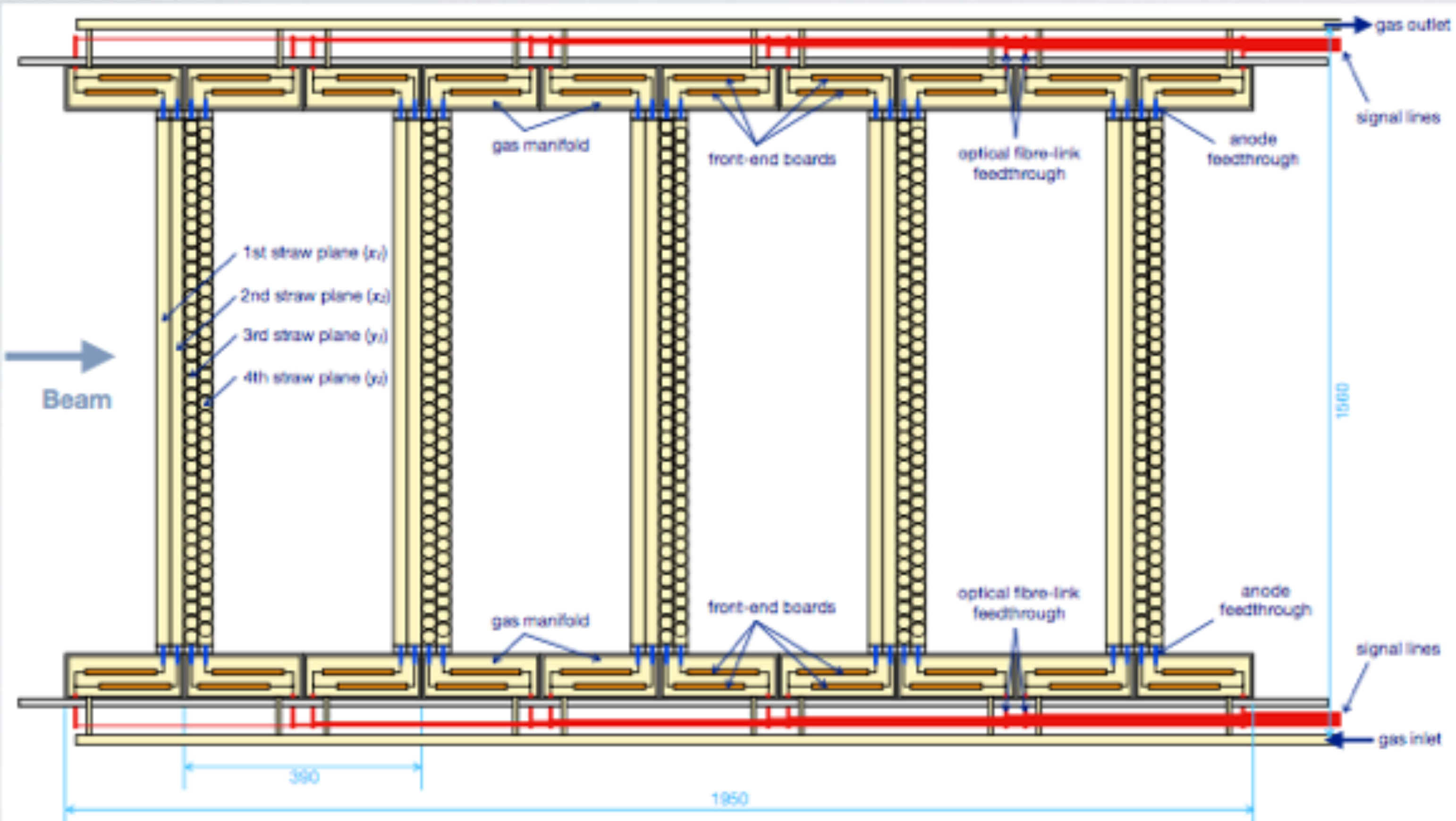

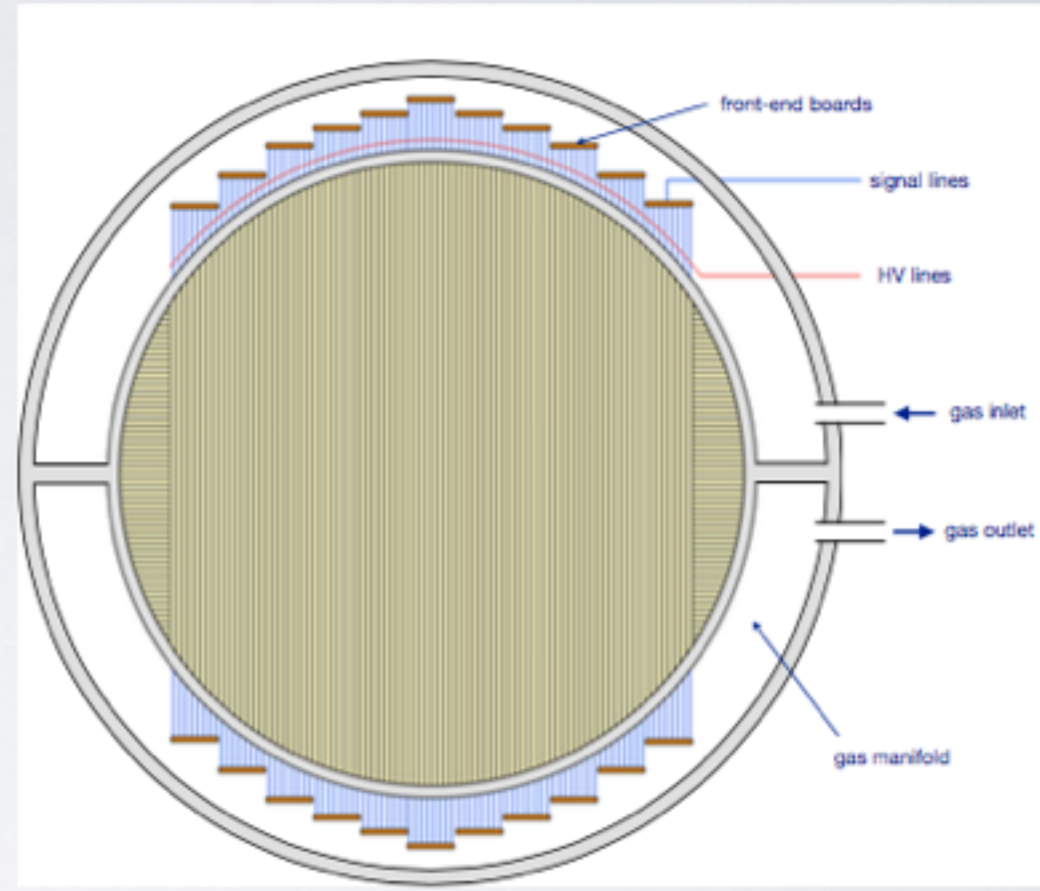

- **Straw** Tube **Tracker** consists of ~2500 straw tubes
  - Main tracker for Phase-I beam measurement / Phase-II physics measurement
  - **Operation in vacuum**
  - 20/12um thick, 9.8/5mmΦ straw tube for Phase-I/Phase-II
  - Gas mixture candidates: Ar:C_2H_6=50:50, Ar:CO_2=70:30
  - **Complete** the mass production of Phase-I straw tube

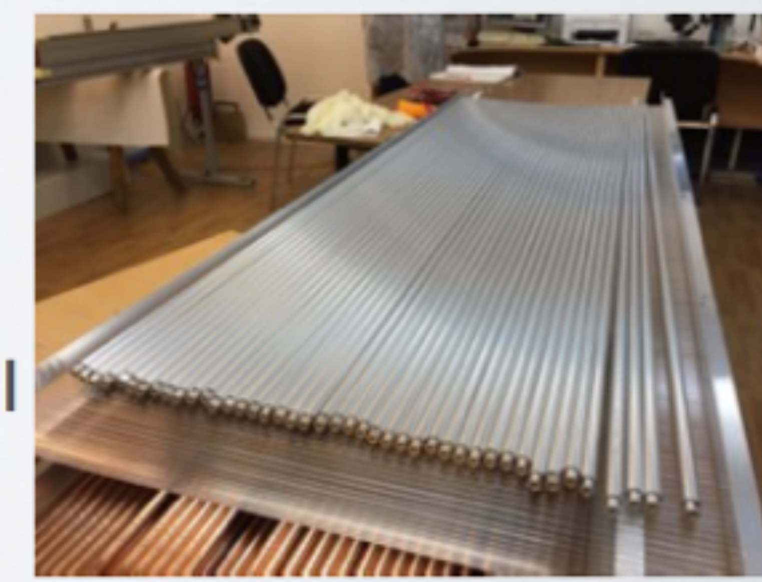

R&D of StrECAL — READOUT

- New waveform digitizer boards being developed based on DRS4
  - **ROESTI**: (**R**ead **O**ut **E**lectronics for **S**traw **T**ube **I**nstruments)
  - **EROS**: (**E**cal **R**ead **O**ut **S**ystem)
  - ROESTI/EROS are almost same except for the analog input
- <1ns σ_T obtained using ROESTI v3 by applying calibration
- **“Real” daisy chain readout developed recently**

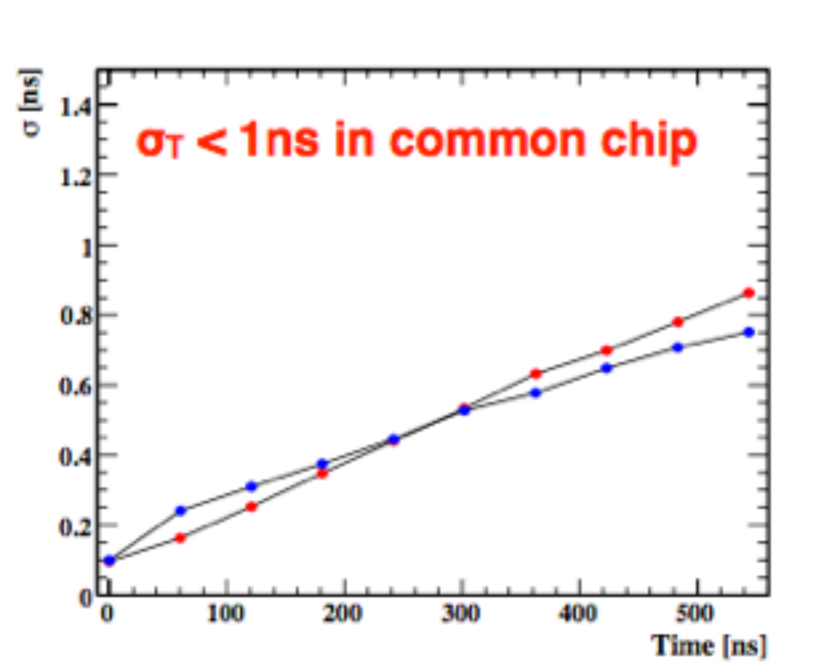

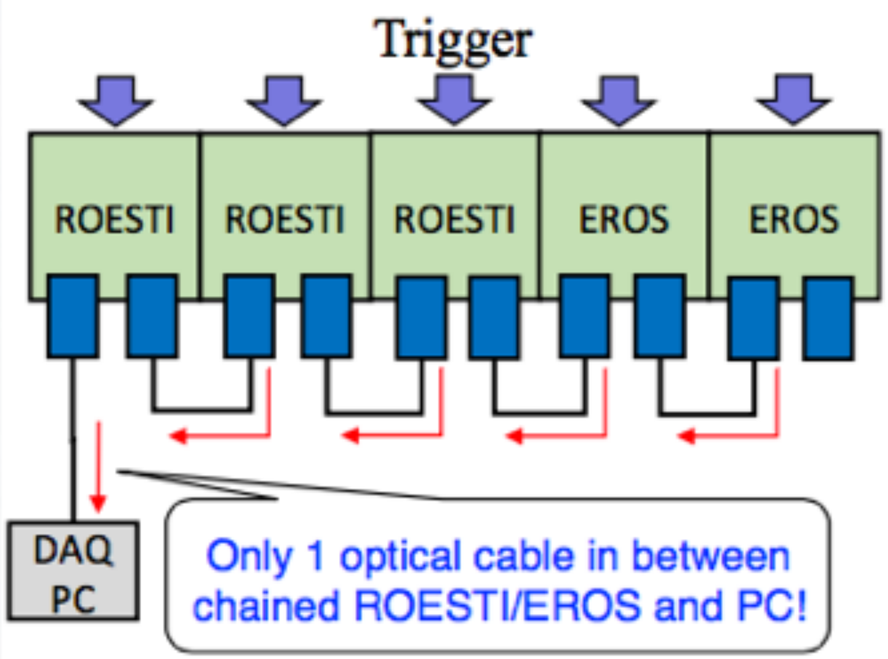

StrECAL in COMET Phase-I

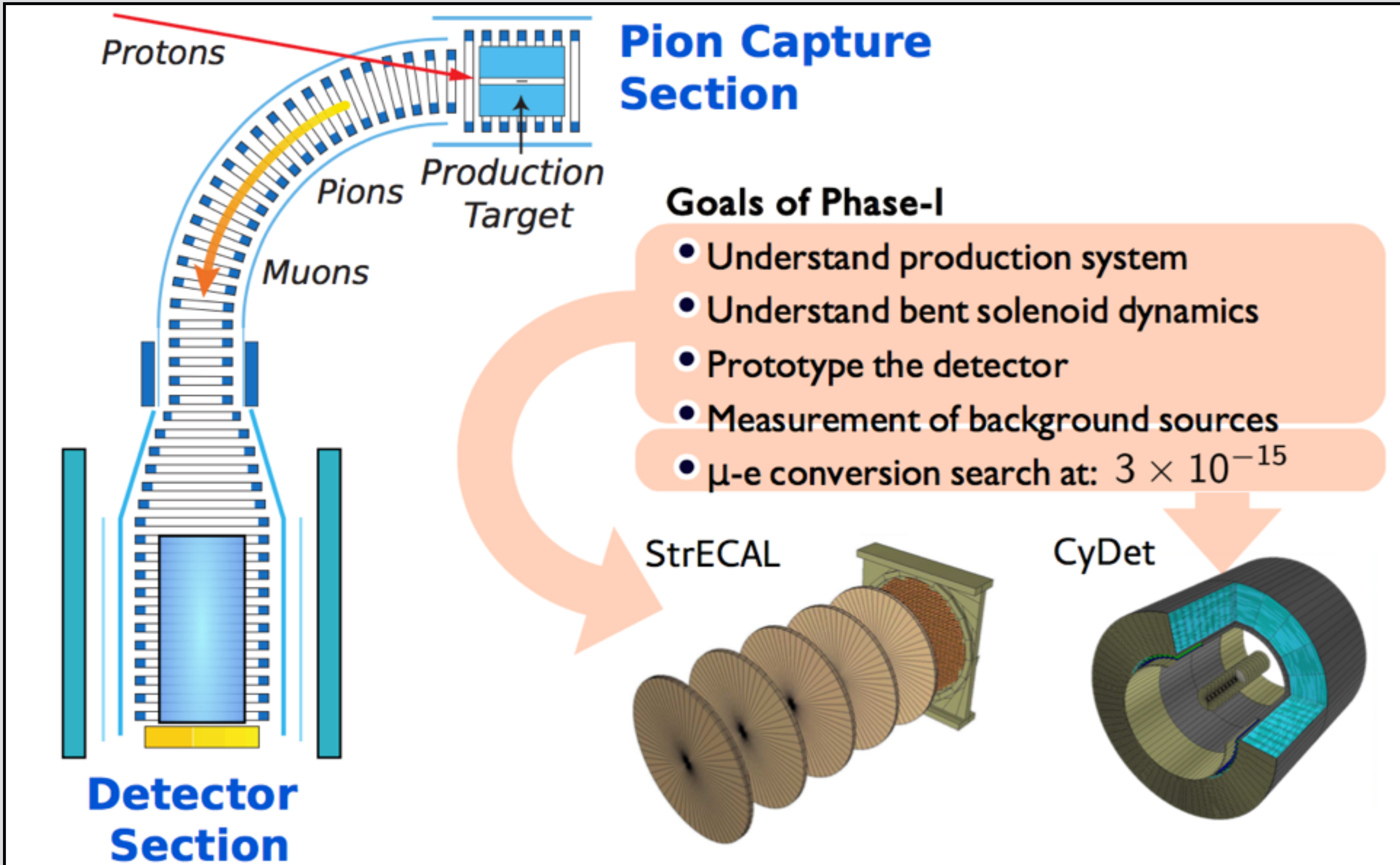

Detector in COMET Phase-II

- StrECAL
  - Straw tube trackers (Station)
    - Momentum measurement
  - Crystal ECAL
    - Particle Identification
  - Low material budget
  - High momentum resolution
    - 5% uncertainty at 105 MeV/c

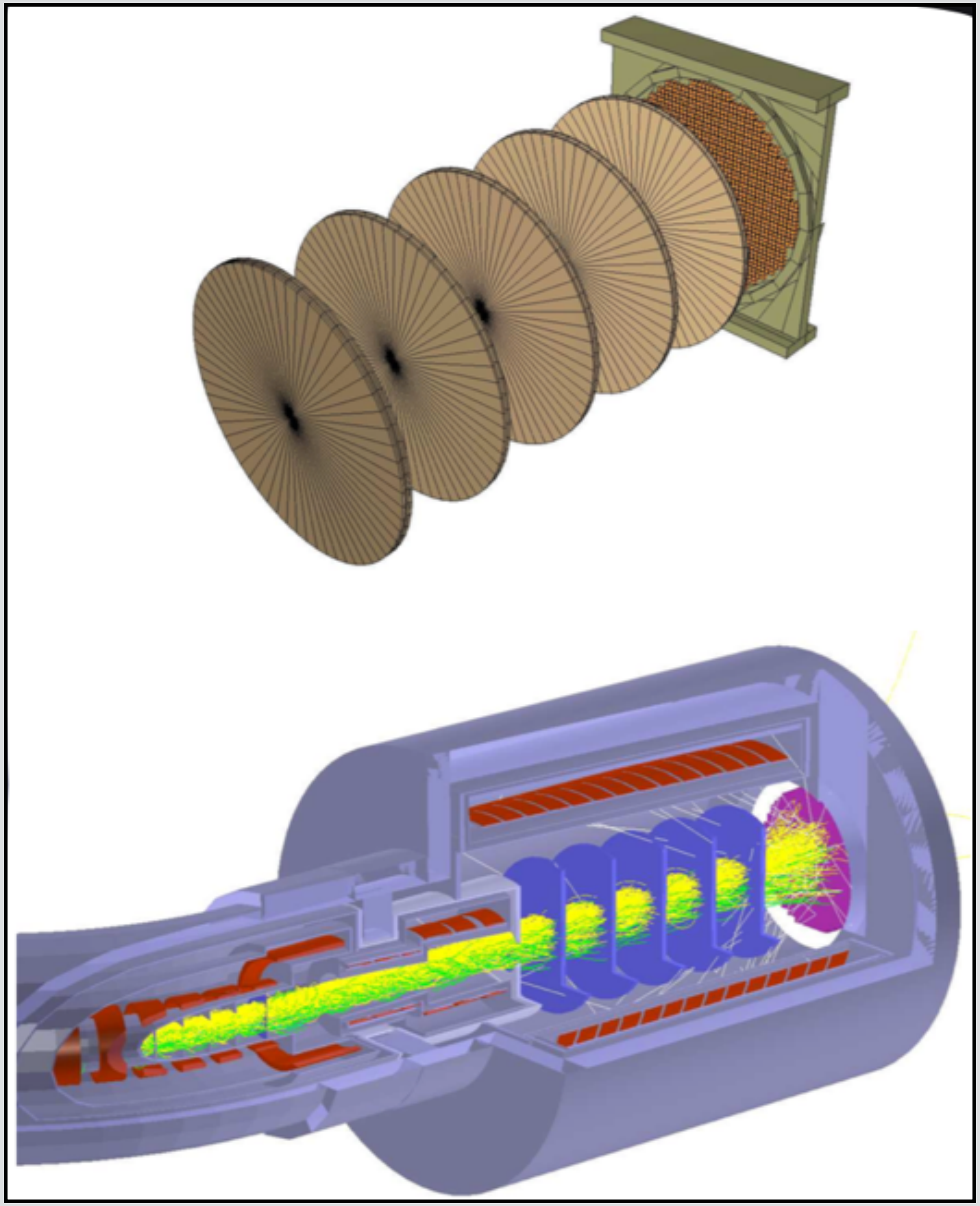

Summary

- Beam power 56kW, 8GeV
- Physics Run : 1 year → Single event sensitivity
  - 2.10^{-17} , which is 10,000 times better than the current limit
  - 2×10^{18} muons stopped
  - 0.2 % muons stopped per proton on target (POT)
  - 10^{21} POT
- Development and construction are ongoing well
- Detector system will be used in Phase-I for prototype testing for Phase-II

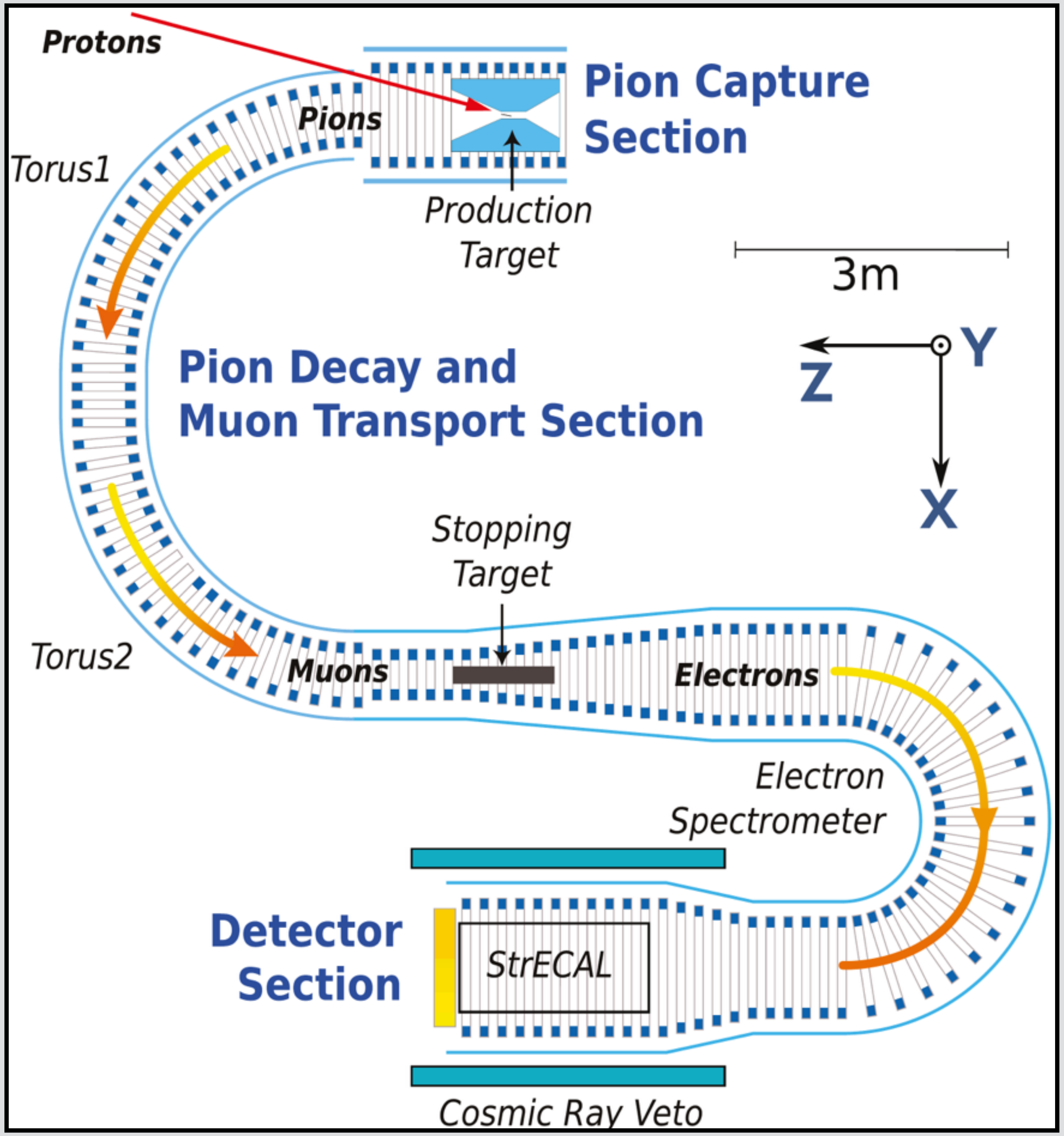

Thank you

Acknowledge

Thanks Dr. B. Krikler for helping

Backup

R&D of StrECAL — ECAL

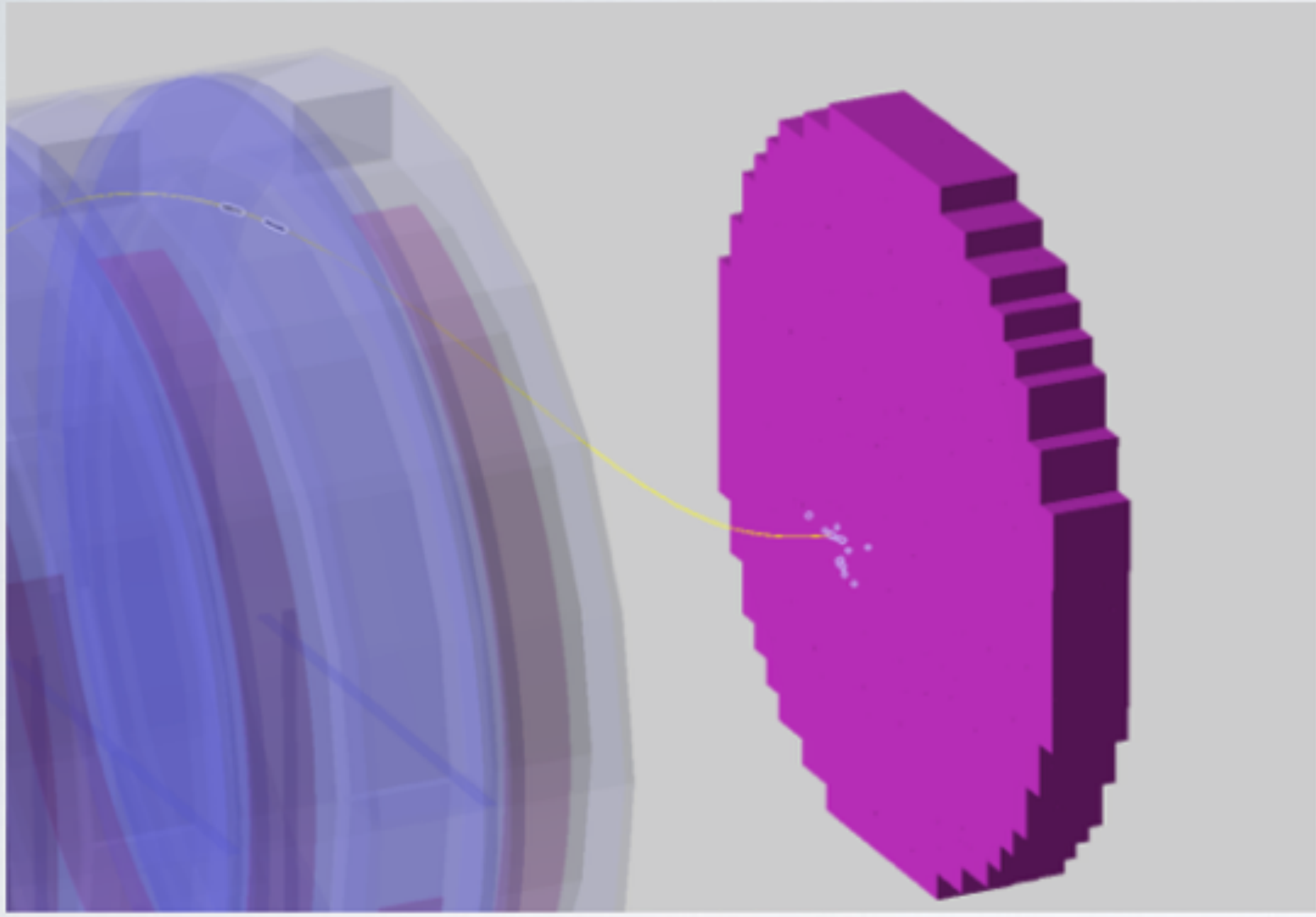

	NaI(Tl)	GSO	LYSO
Density, g/cm^3	3.67	6.71	7.1
Att. length, cm	2.6	1.38	1.12
Decay const., ns	230	30-60	41
Max emission, nm	415	430	420
Relative LY	100	20	70-80

Comparisons of scintillator characteristics

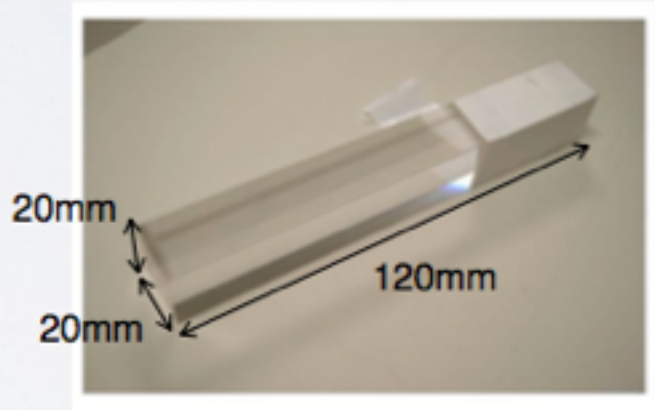

- ECAL is an array of ~2,000 scintillator crystals to cover ~1m of radius
  - Choose **LYSO** because of the higher light yield and faster time response than GSO
  - Use in both Phase-I & Phase-II
  - **Measure the energy deposit** and **trigger the event**
  - 10mm×10mm APD sensor attached to the back of each LYSO crystal
  - Crystals and APDs inside vacuum

Optimisation of Muon Stopping Target

- **Consideration**
  - **Muon stopping rate**
  - **Energy deposition of electron**
- **Parameters**
  - **Location**
  - **Disk shape**
  - **disk spacing**

Improvement of Sensitivity is only 2 % for location scanning

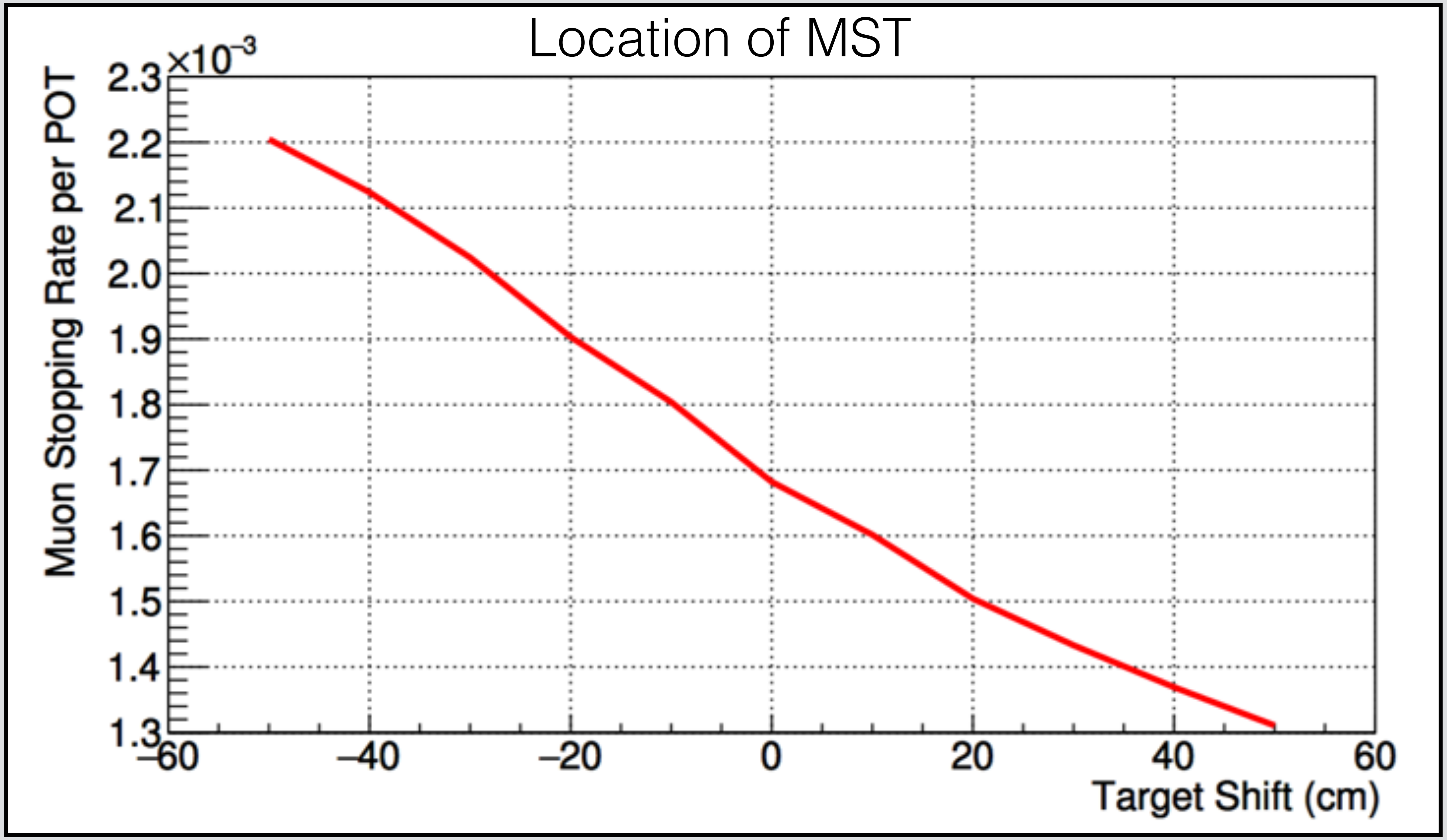

Optimisation of Muon Stopping Target

Improvement of Sensitivity is only 2 % for location scanning

- **Consideration**
  - **Muon stopping rate**
  - **Energy deposition of electron**
- **Parameters**
  - **Location**
  - **Disk shape**
  - **disk spacing**

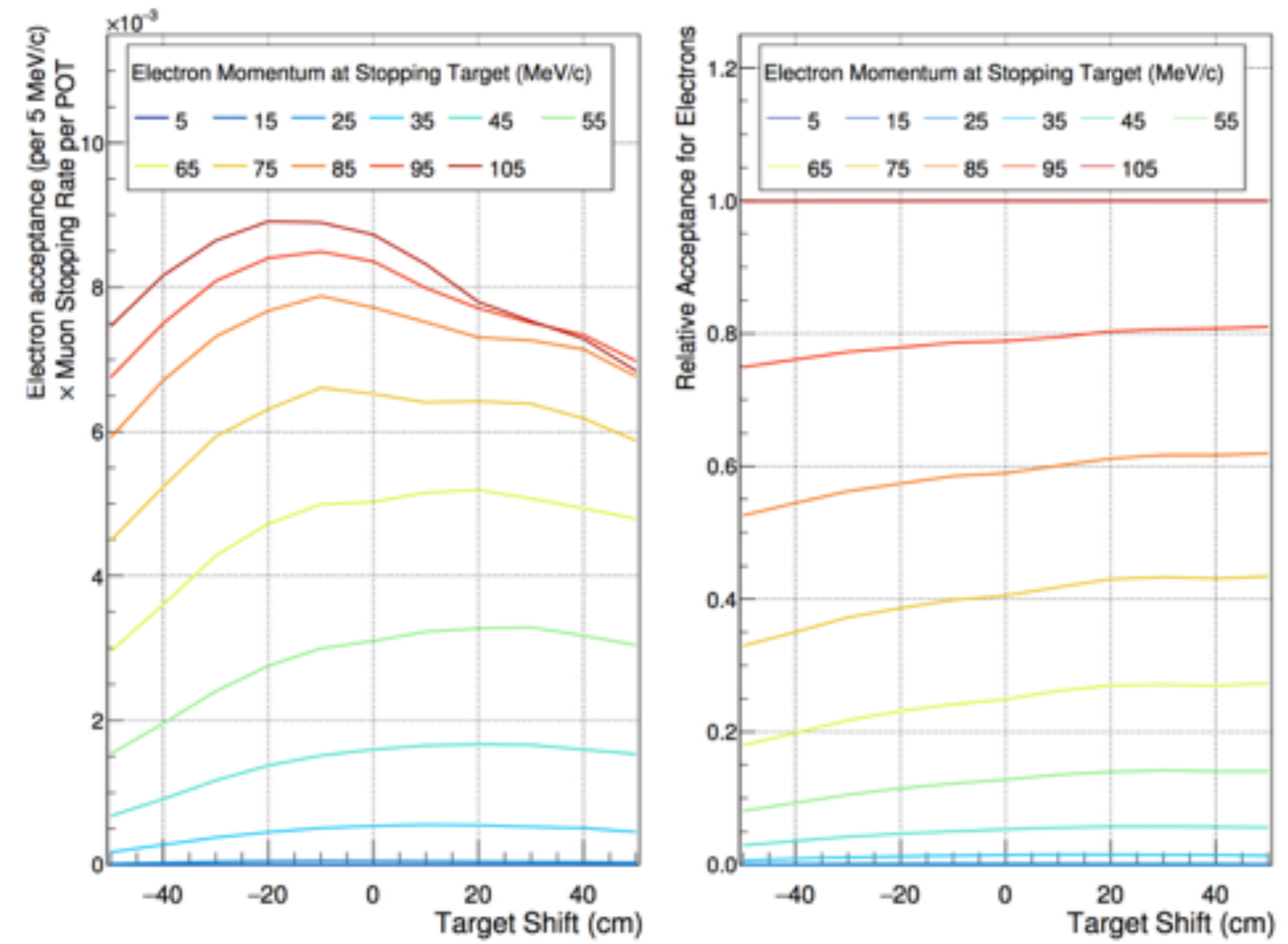

(a) Sensitivity (b) Change in Shape

Figure 5.17: (a) The variation in sensitivity (acceptance × stopping rate) to electrons with different momenta as a function of the target position with respect to the nominal location. The darkest red line towards the top of the plot represents the sensitivity to signal, and it is that line that should therefore be maximised. (b) The change in the shape of the acceptance vs. momentum spectrum as a function of the stopping target location.

Optimisation of Muon Stopping Target

Improvement of Sensitivity is only 2 % for location scanning

- **Consideration**
  - **Muon stopping rate**
  - **Energy deposition of electron**
- **Parameters**
  - **Location**
  - **Disk shape**
  - **disk spacing**

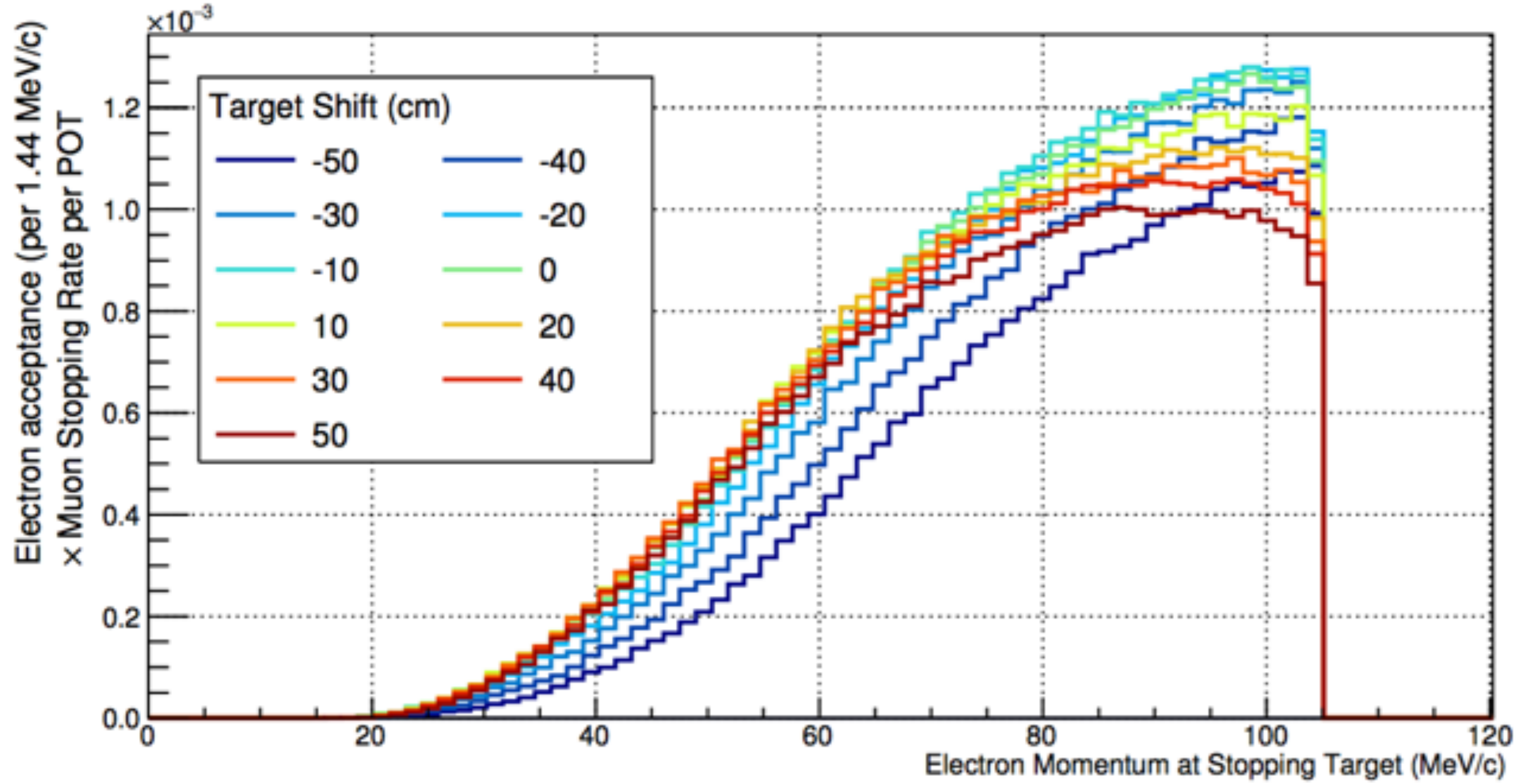

Figure 5.16: The momentum dependence of the electron acceptance into the detector for different target positions. The spectrum for each target position is normalised to the muon stopping rate for that position, such that each curve shows the sensitivity to electrons of that momentum.

Extinction factor

Experimental apparatus installed at the end of K1.8 beam line in the J-PARC Hadron Hall

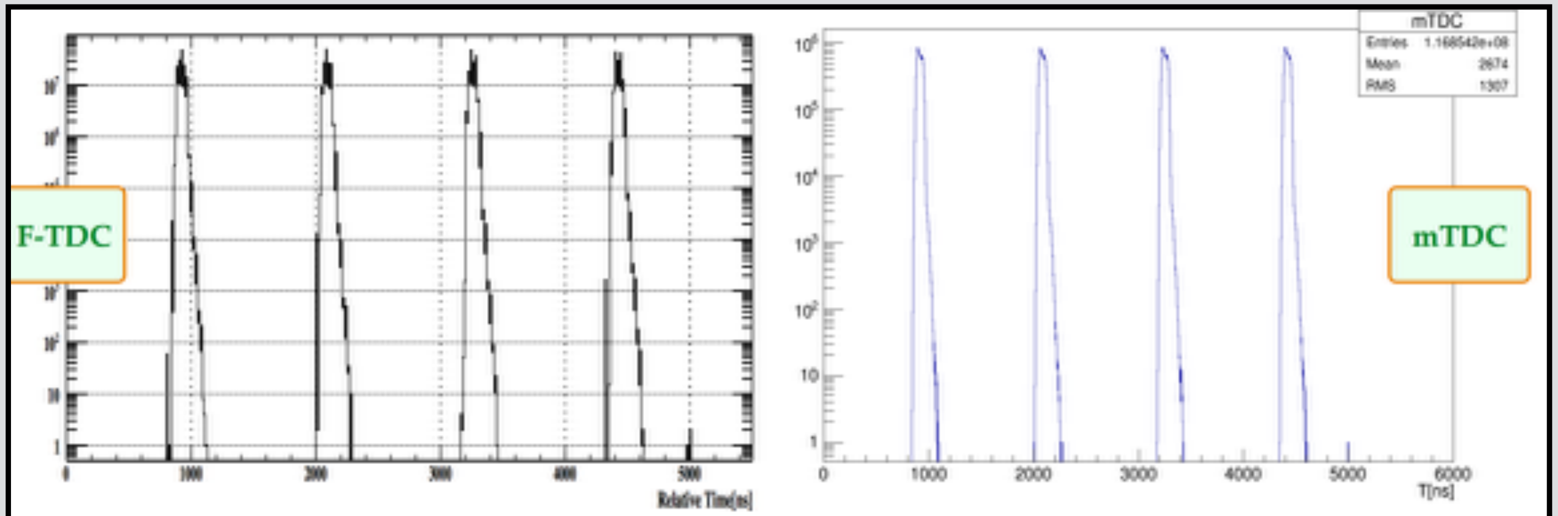

- 4 bunches filled into front buckets, and bunched-SX keeping RF with 180 kV
- Injection-kicker timing is shifted by 598 nsec forward
    - *ie*. residual particles in rear buckets should be swept away
- Measured extinction = **5.6 ~ 9.5 × 10^{-9} @(V_{RF}=180kV)** (Very very preliminary !!)
    - Careful check is ongoing with accelerator group.

Proton beam

Table 4.1: Pulsed proton beam for the COMET experiment.

Beam Power	56 kW
Energy	8 GeV
Average Current	7 μA
Beam Emittance	10 πmm·mrad
Protons per Bunch	$< 10^{11}$
Extinction	10^{-9}
Bunch Separation	1~2 μs
Bunch Length	100 ns

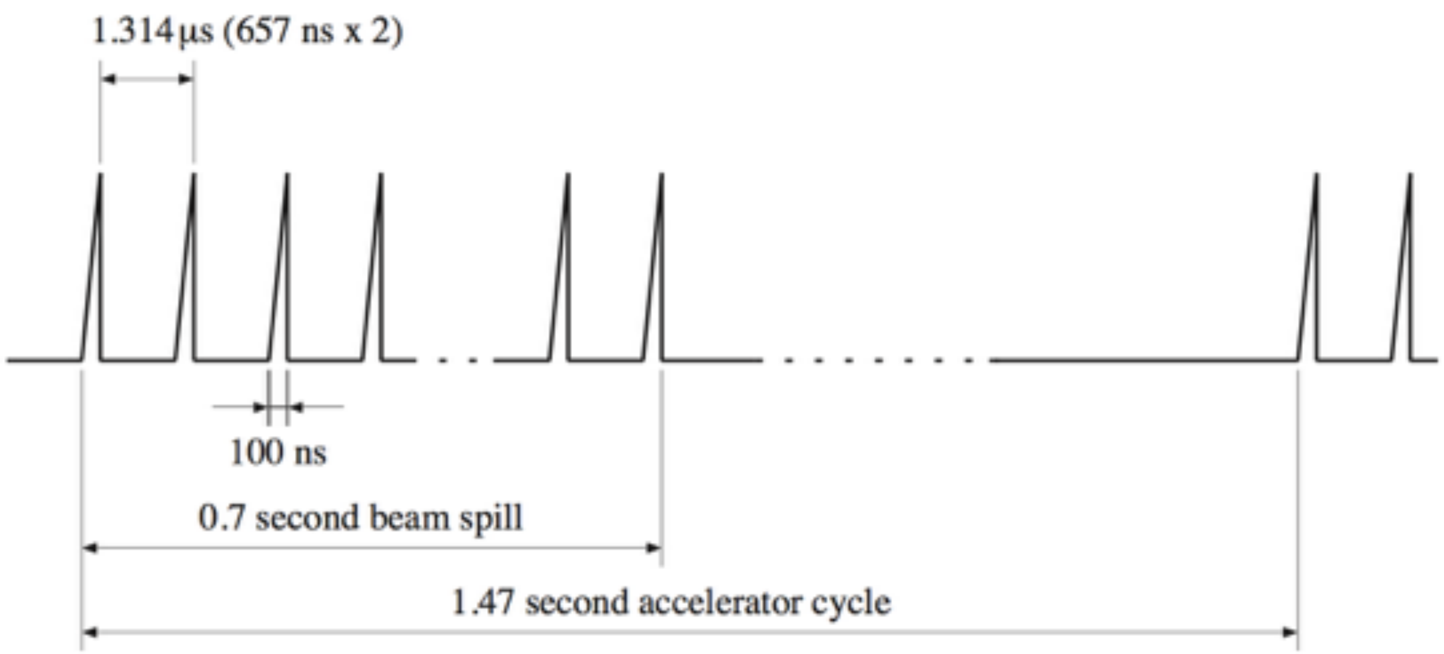

Figure 4.2: Bunched proton beam in a slow extraction mode.

Simulation techniques

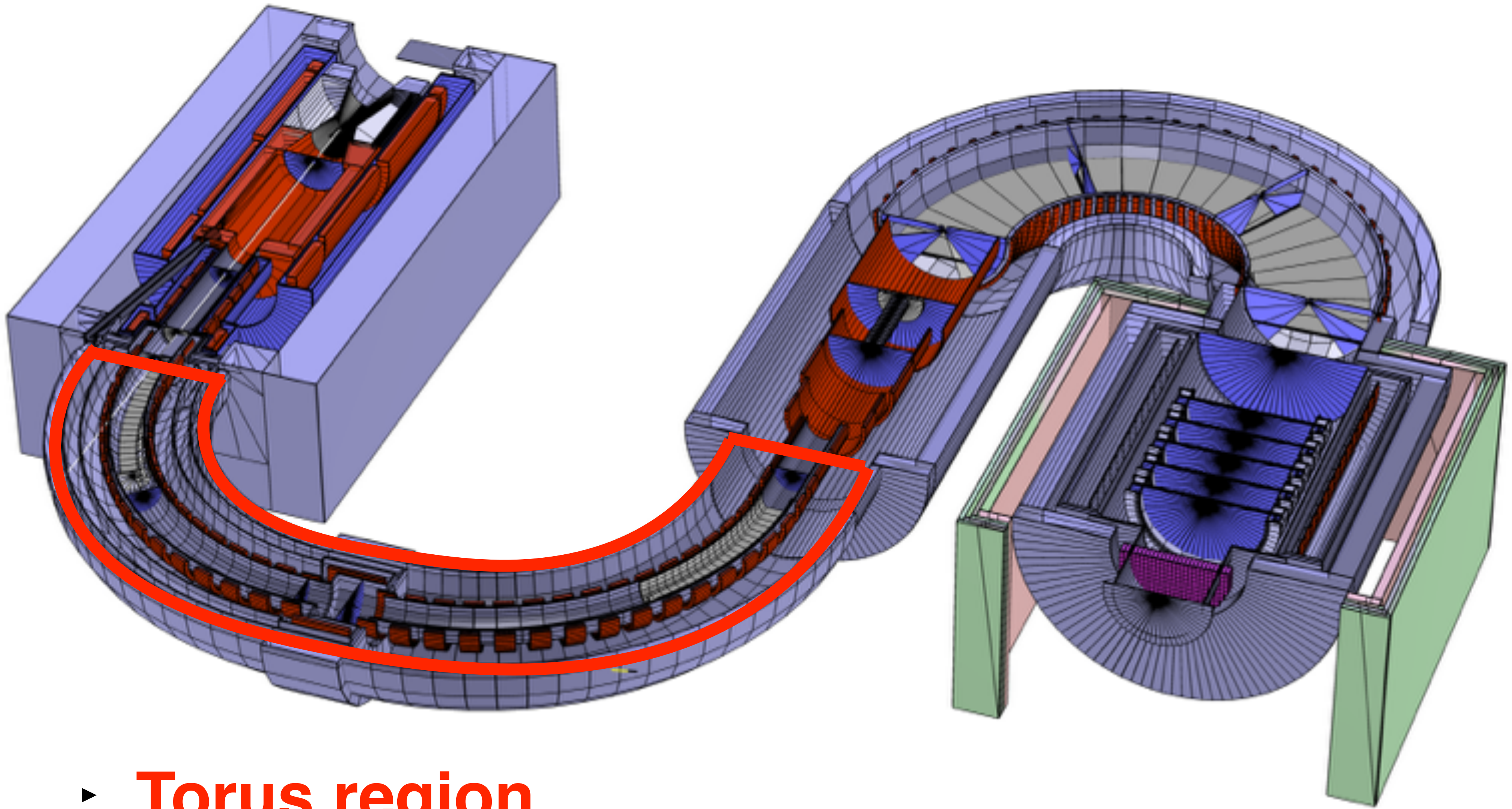

- Torus region

- Simulating lots of muons directly from production target is hard
  - Particles entered Torus will be saved for further simulation

Optimisation of the field map along beam line

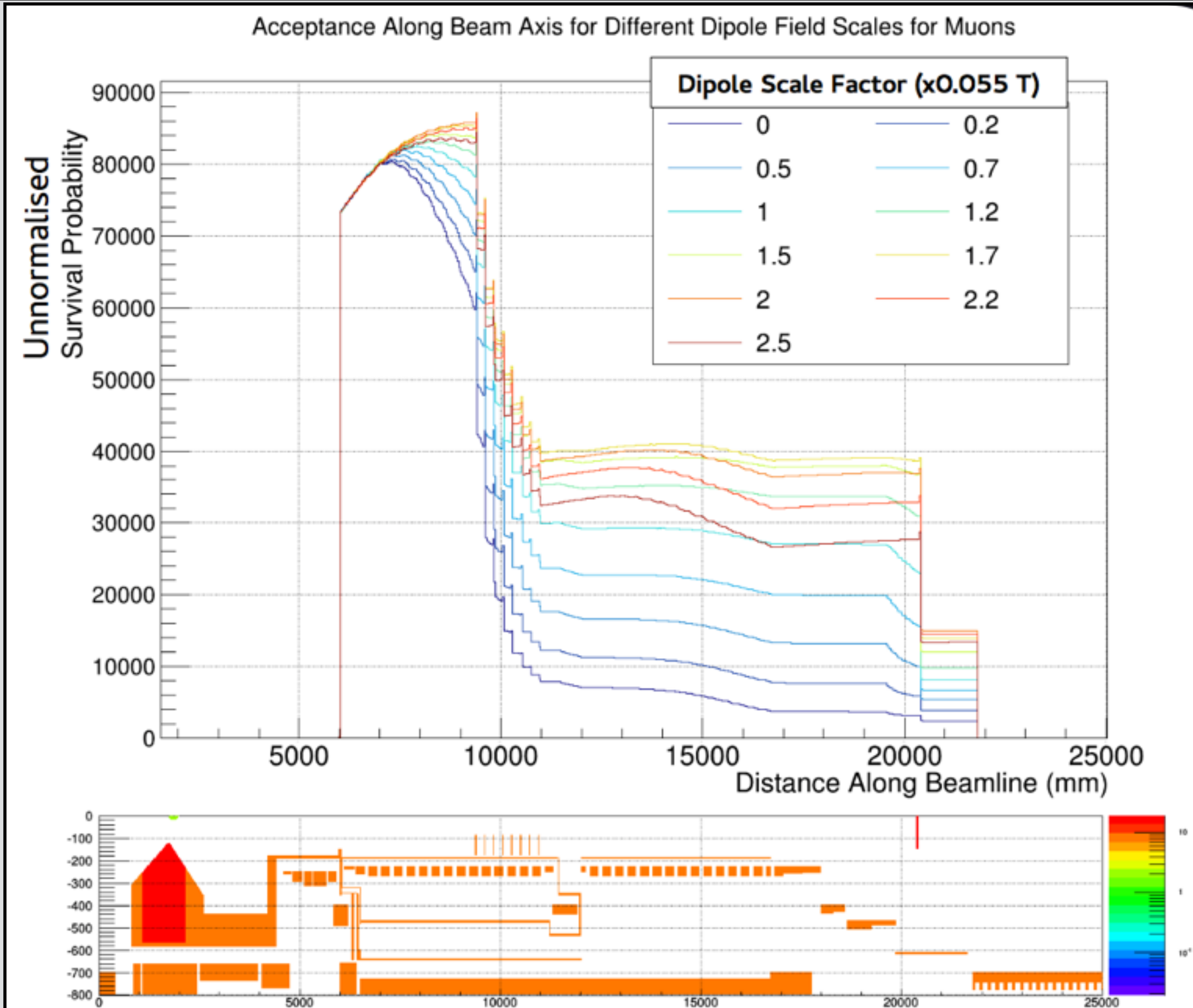

Pion production target system

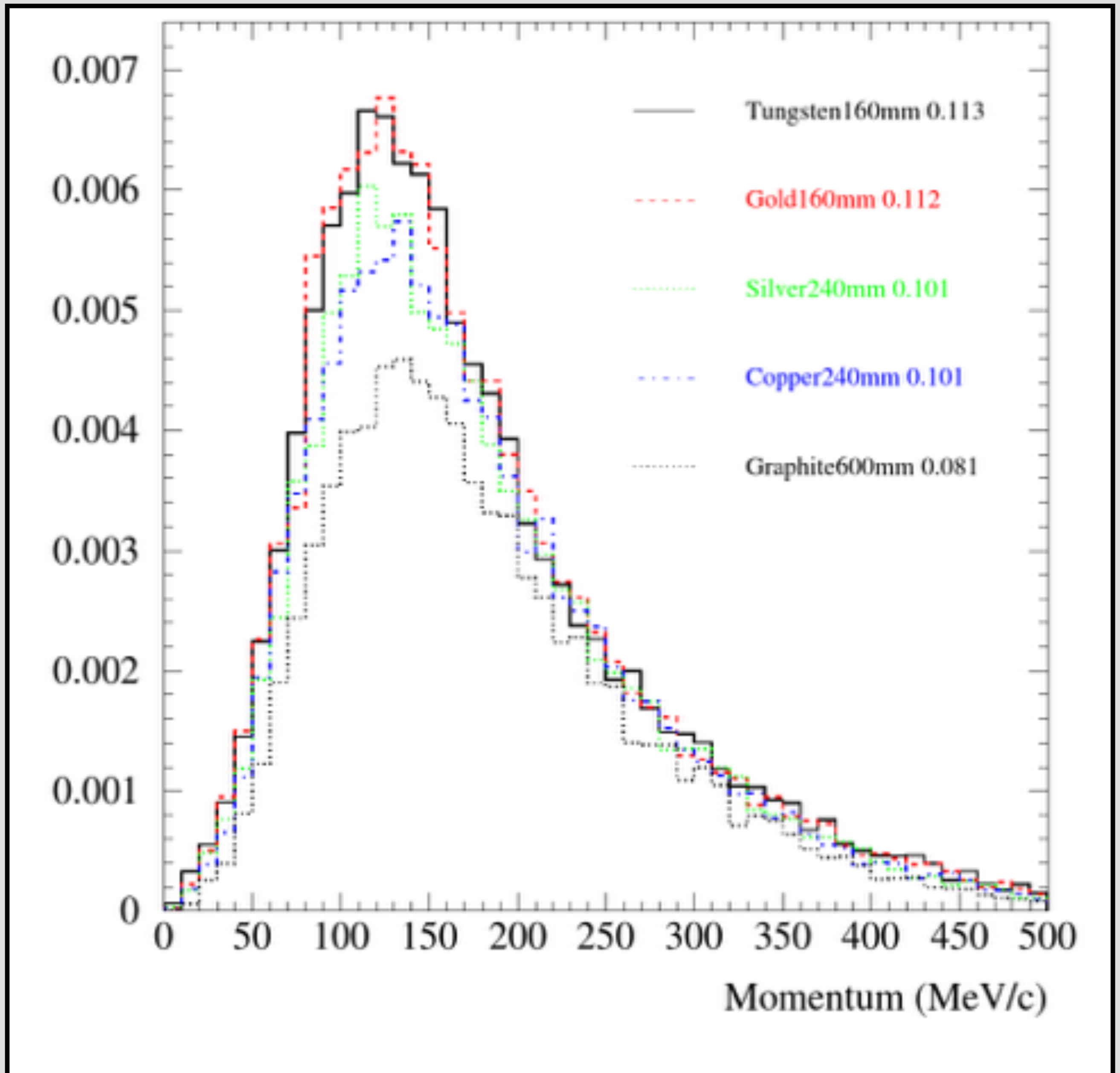

Figure 5.4: Pion yields for various target materials.

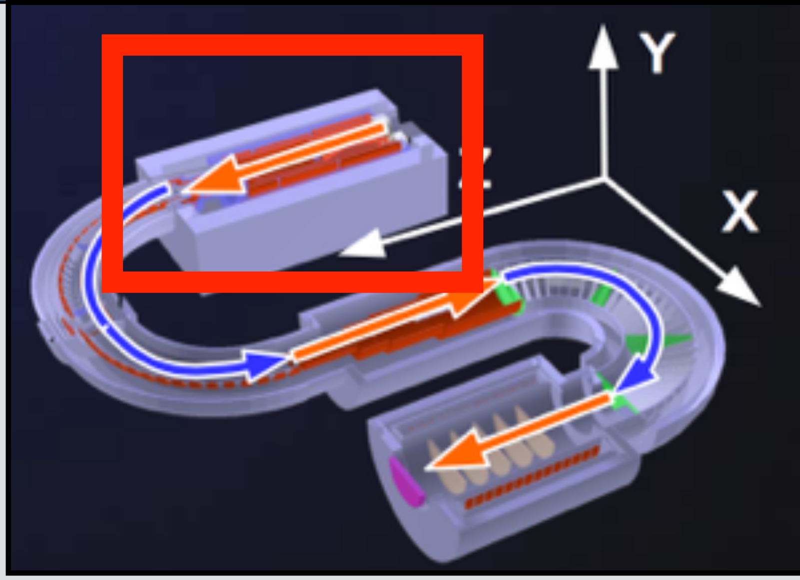

- Production target size :
- Different targets produce pions with similar momentum distribution, but Gold and Tungsten seem to give the best yields

Muon nuclear capture

AlCap: Aluminium Capture of Muons

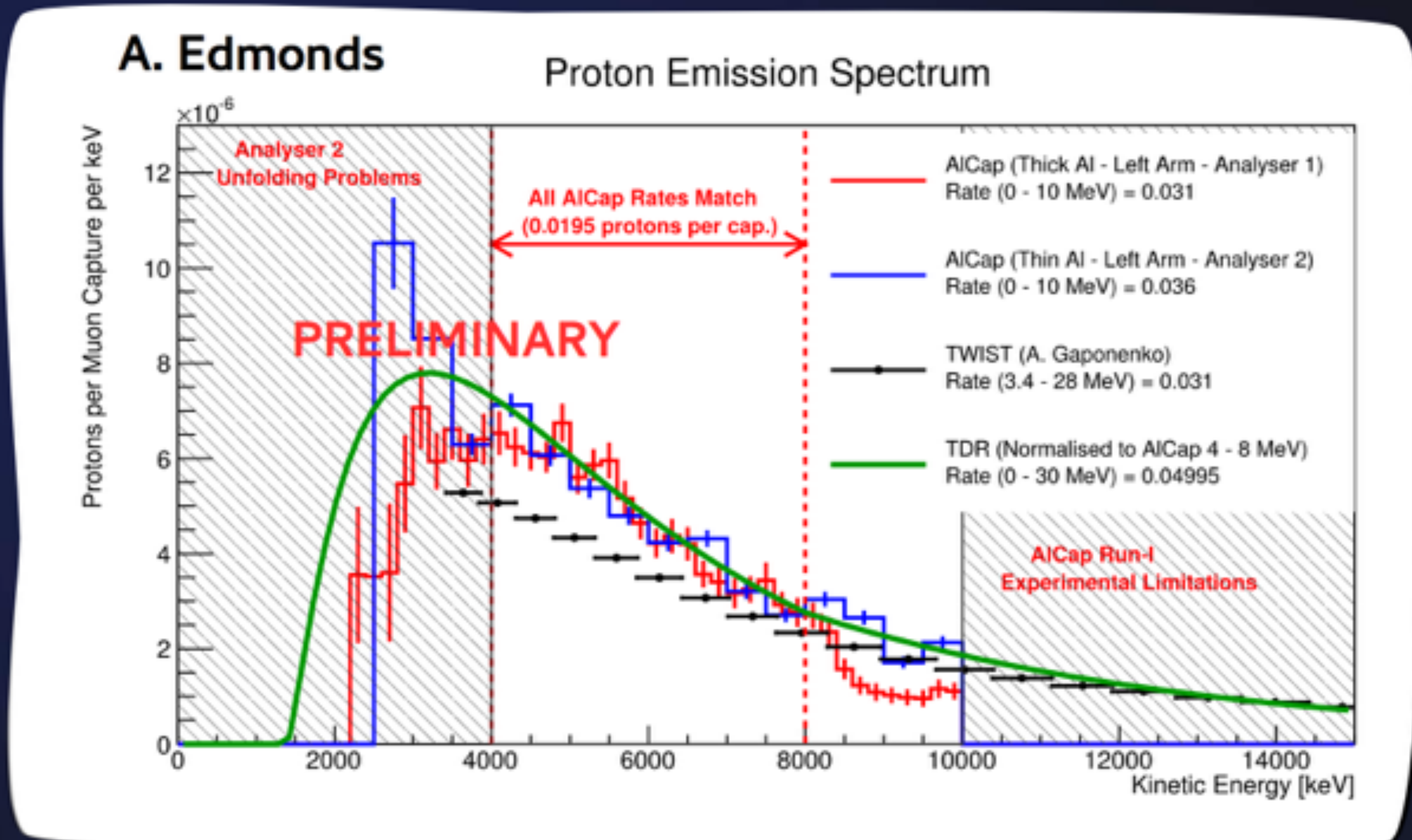

- Joint effort between Mu2e and COMET
- 3 runs at Paul Scherrer Institute from 2013 to 2015
- Studying charged and neutral particles emitted following muon capture on aluminium

Bunch structure of the beam

Bunch Train : 1 bunch ~ 8e6 protons

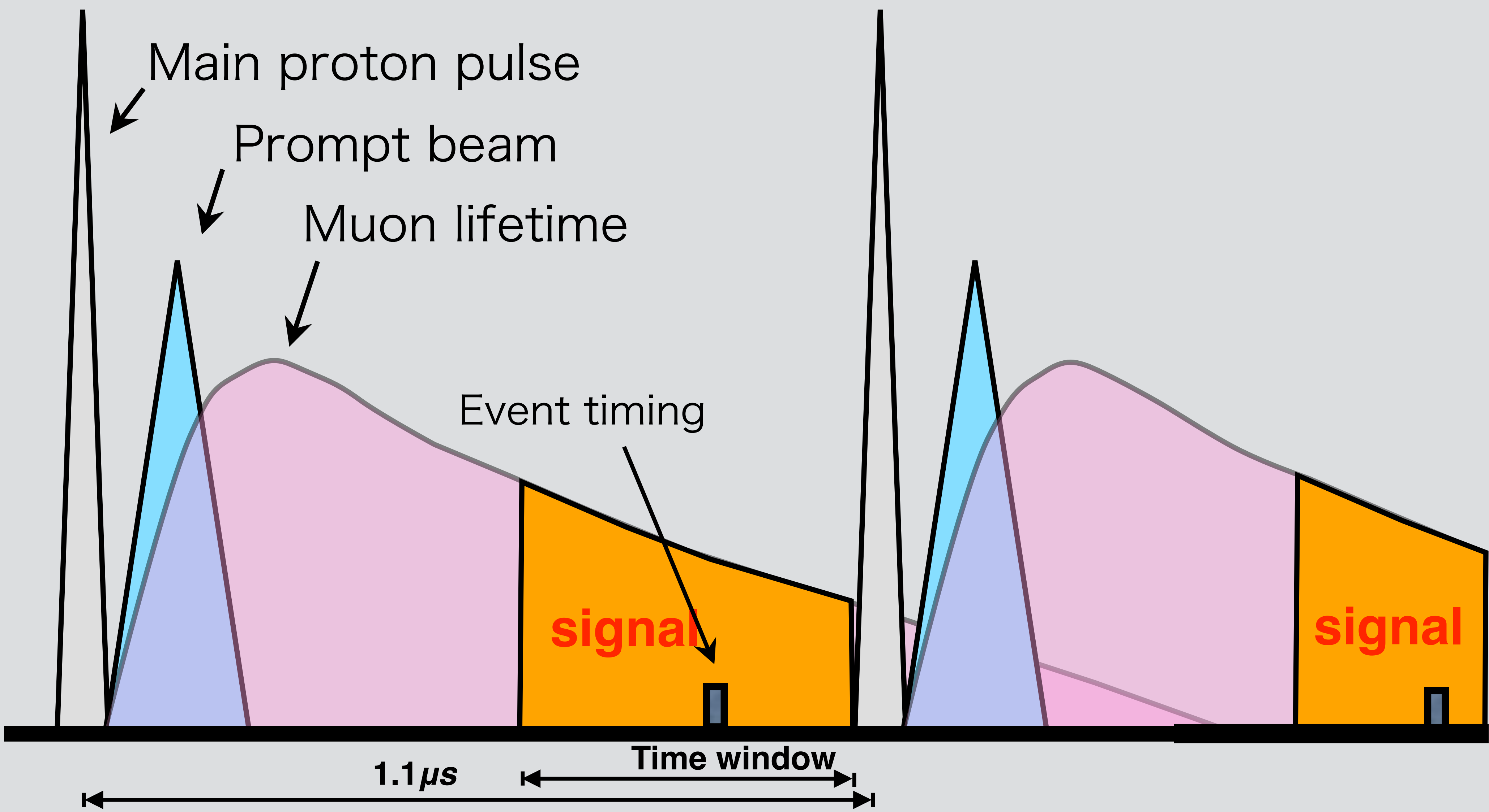

Custom Physics Models

Electrons from Bound Muon Decay

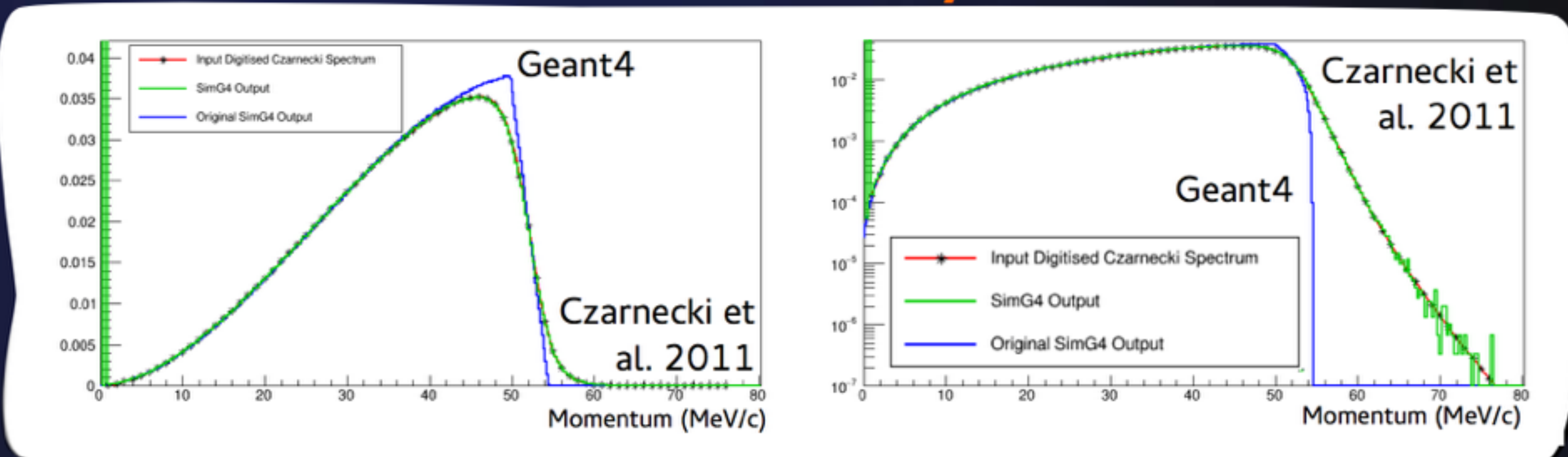

Protons from Muon Nuclear Capture

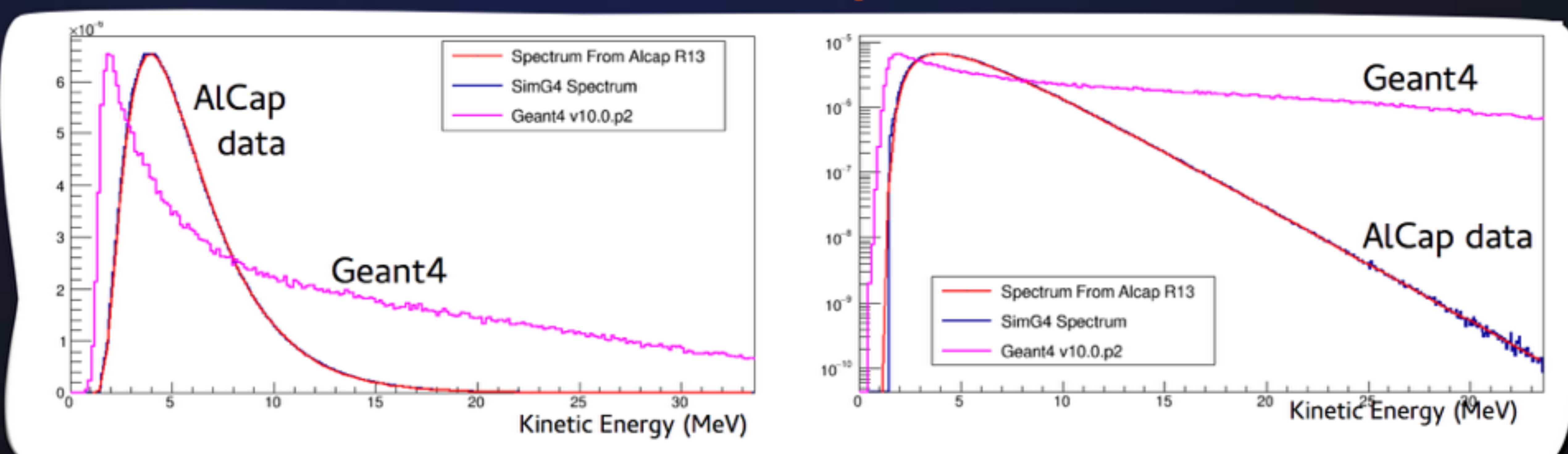

Cascade of muons in orbit

Counting muons with the 2p-1s x-ray

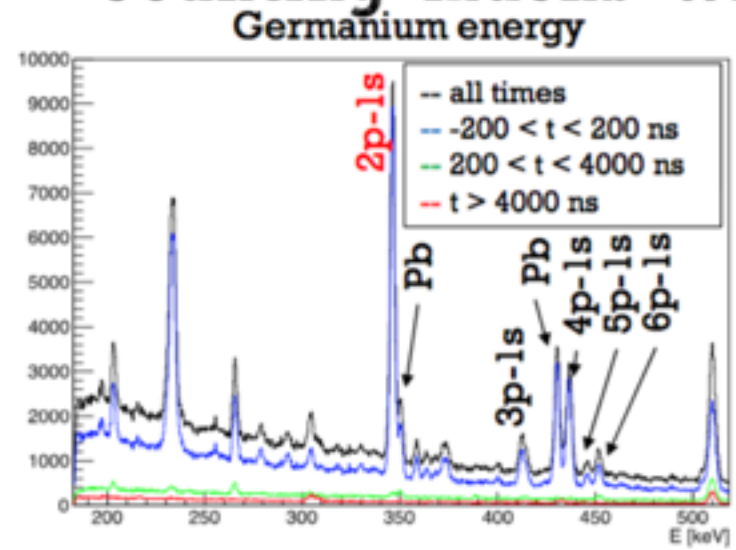

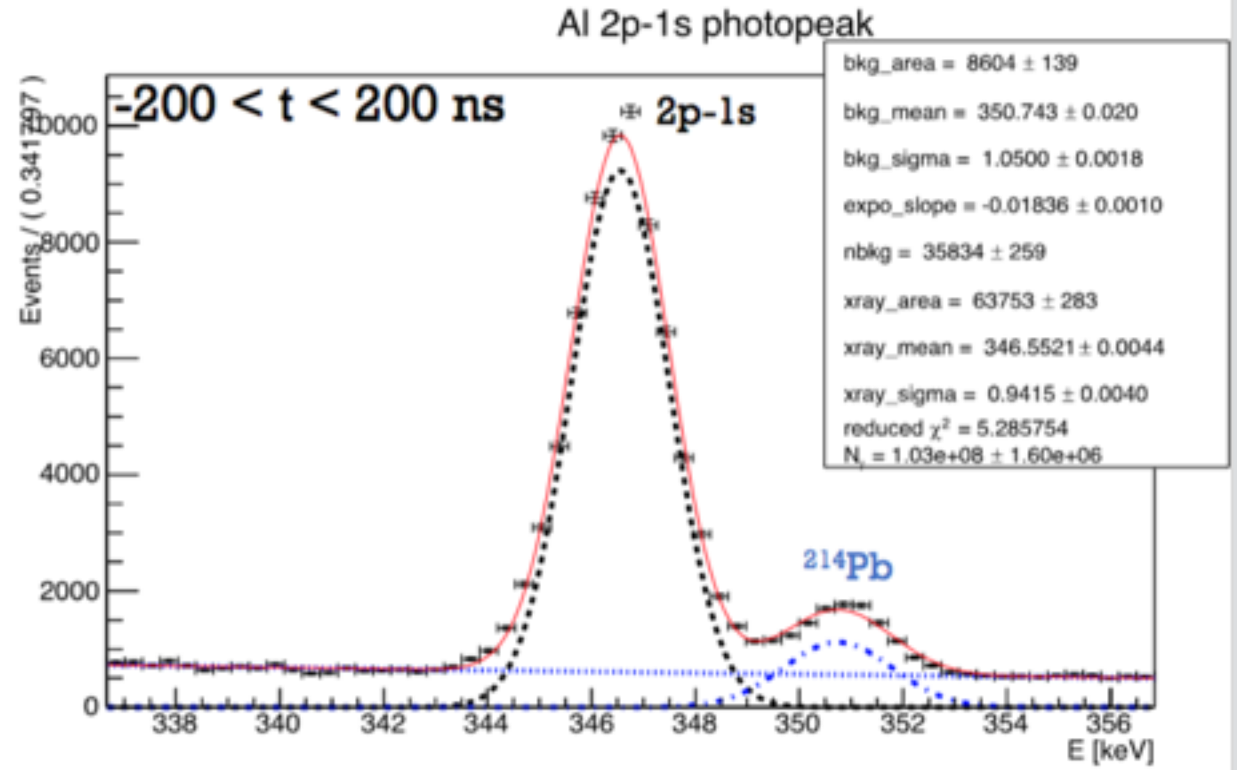

Energy	346 keV
Emission Probability	79.8(8)% per stopped muon *
Acceptance	7.64(9) x 10^{-4}
Counts	63753(283)
Total	1.03(2) x 10^{8}

* Phys Rev C 76, 035504 (2007)

$$\text{Total} = \frac{\text{Counts}}{\text{Acceptance} \times \text{Emission Probability}}$$

- **Being able to know number of muons captured by the atom**
  - **Muonic X-ray**

Production target

- **Differential Cross section of negative pion production on a tantalum[1] target from 10 GeV proton**

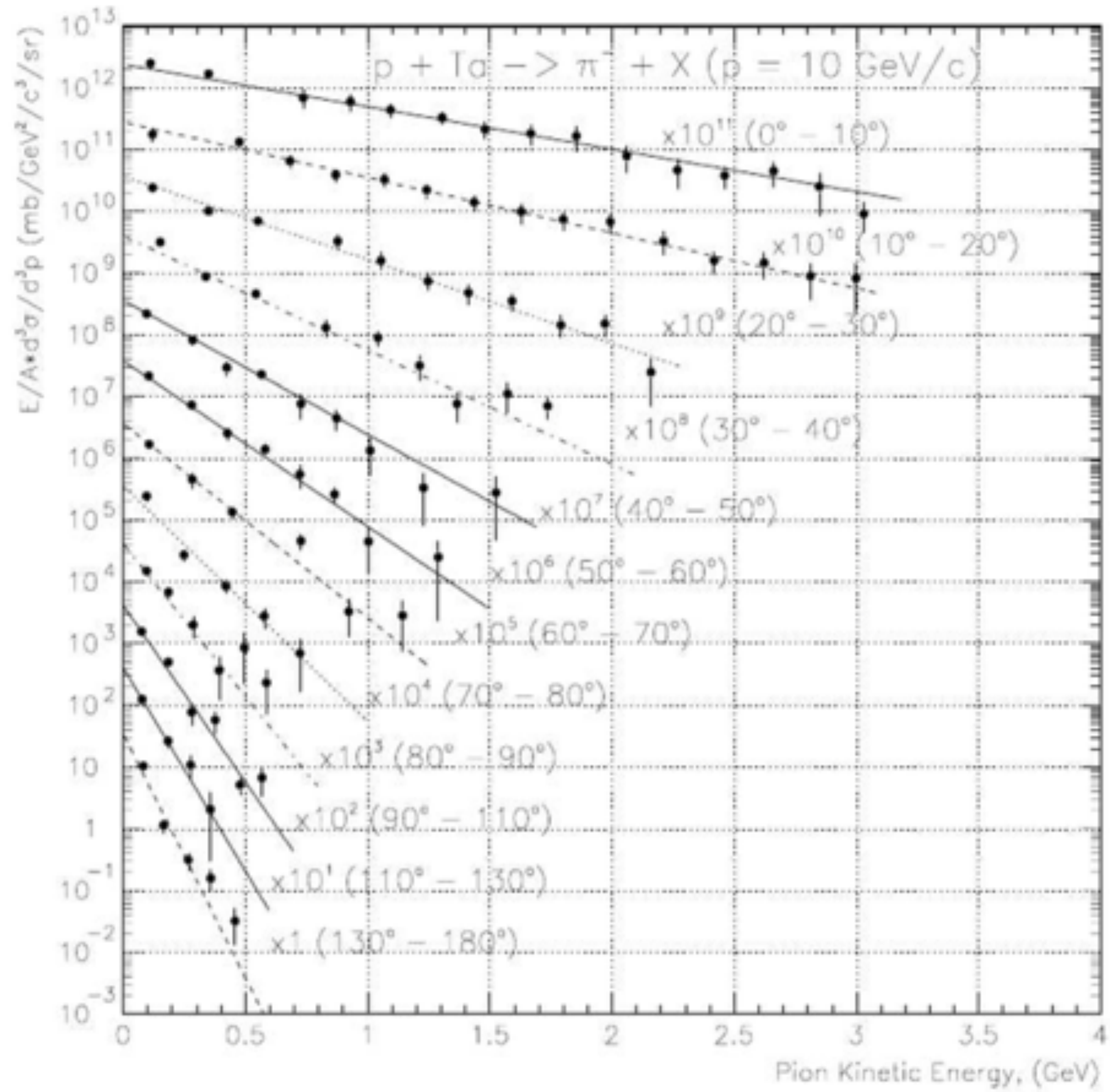

Figure 3.1: Double differential cross section of pion production on a tantalum target from protons with 10 GeV kinetic energy (reproduced from Meco note 23 [46] which itself used [47]). It is clear that the high-energy component of the spectrum is suppressed as you move to higher production angles which is important for reducing background rates. Note that each line is scaled an order of magnitude compared to the line below.

Muon Beam studies — Field map

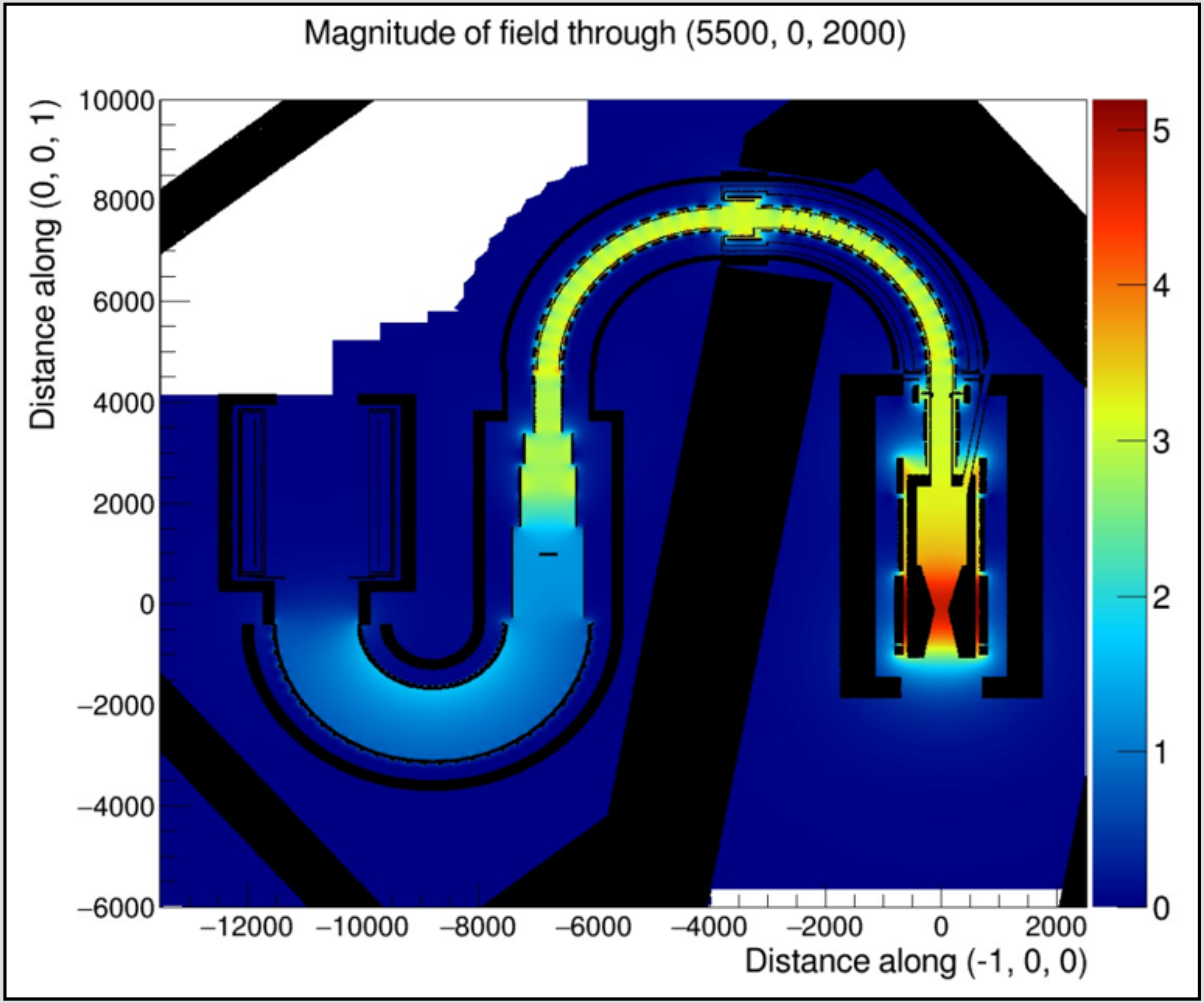

Momentum cut

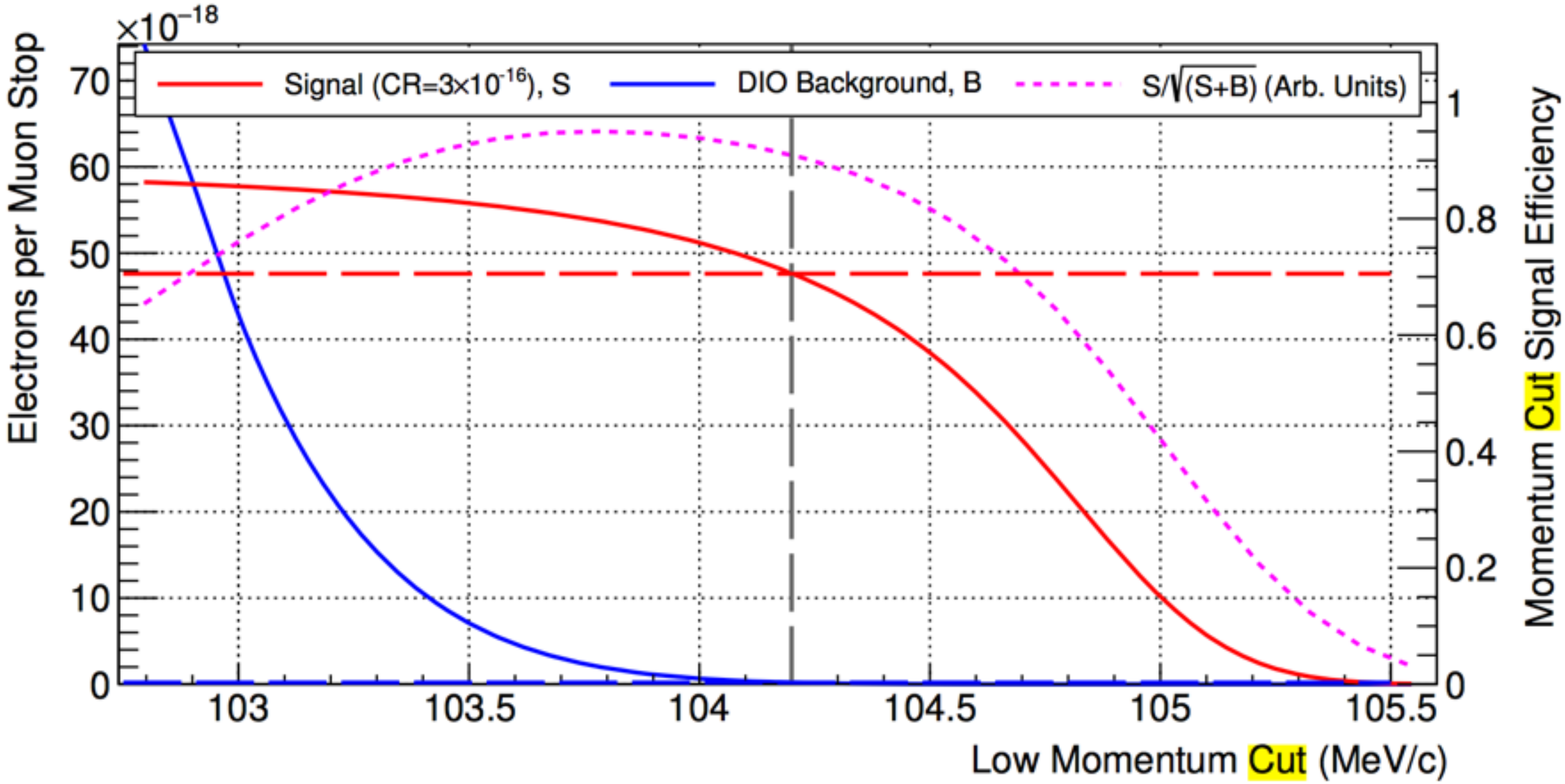

Figure 6.7: Relative signal versus DIO background as a function of the low-momentum cut value assuming a conversion rate of $\mathcal{R} = 3 \times 10^{-16}$ and with a fixed upper threshold of 105.5 MeV/c. The magenta line is the signal over square root of signal plus background for this conversion rate shown as an indicator of the optimum cut value.

Timing window cut

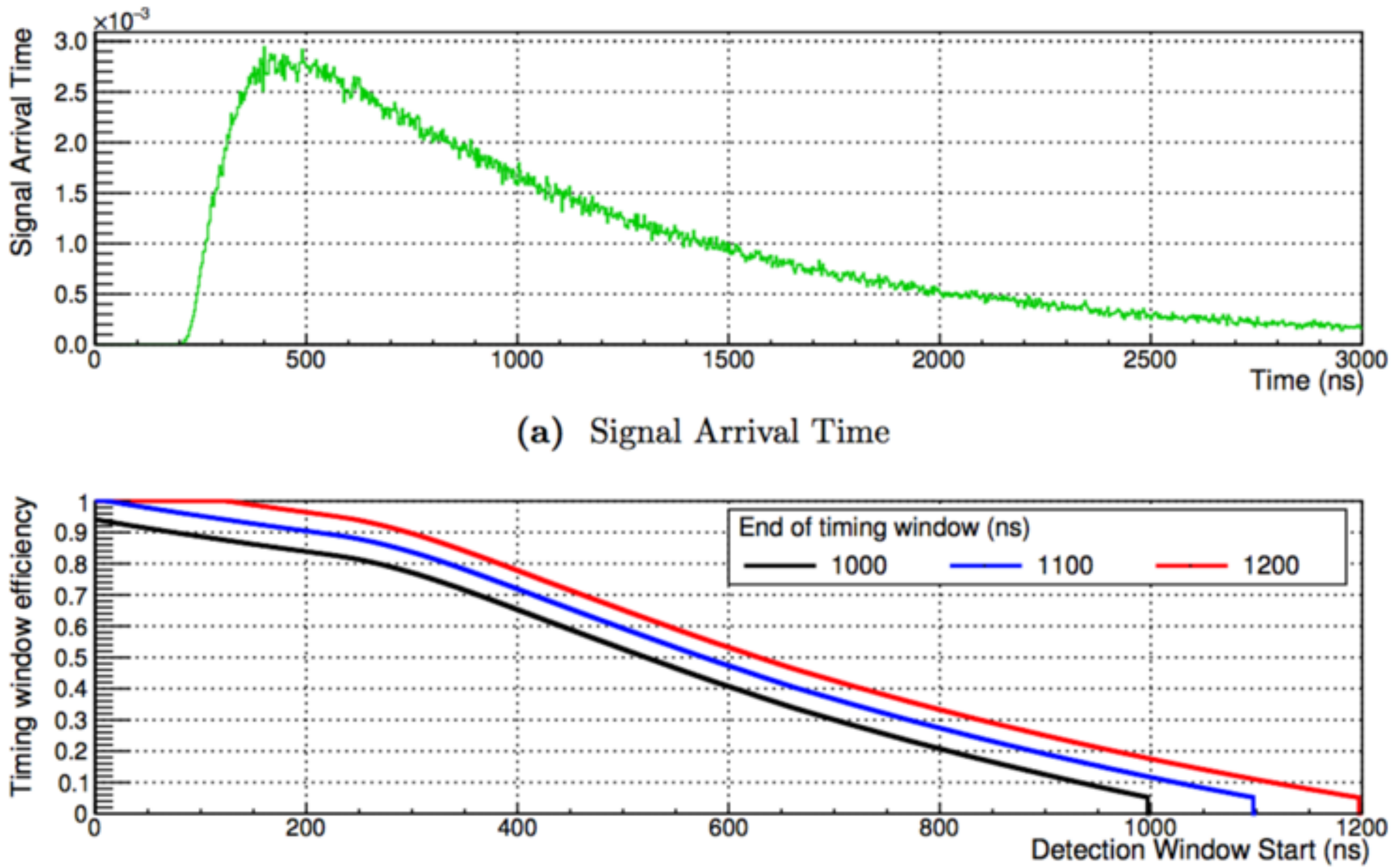

(a) Signal Arrival Time

(b) Timing Cut Efficiency

Figure 6.4: Timing of signal electrons. (a) The arrival time of signal electrons at the detector, including the effect of the proton pulse width, particle transportation, and the muon lifetime. (b) the efficiency of the timing window as a function of the switch-on time. Assumes a pulse separation of 1.17 μs.

Stopped Pions

- Prompt background:
  - Extinction factor = 1e-12
  - Pion stops per POT = 4.3e-7
  - Out-of-time stops = 4.3e-19
- Delayed background:
  - Pion stops per POT = 4.3e-7
  - Assuming same lifetime curve as Muons (which should over-estimate)
    - Fraction stopping from 500 to 1000 ns = 3.9e-2
  - Delayed pion stops << 1.6e-8 per POT

Stopped Pions

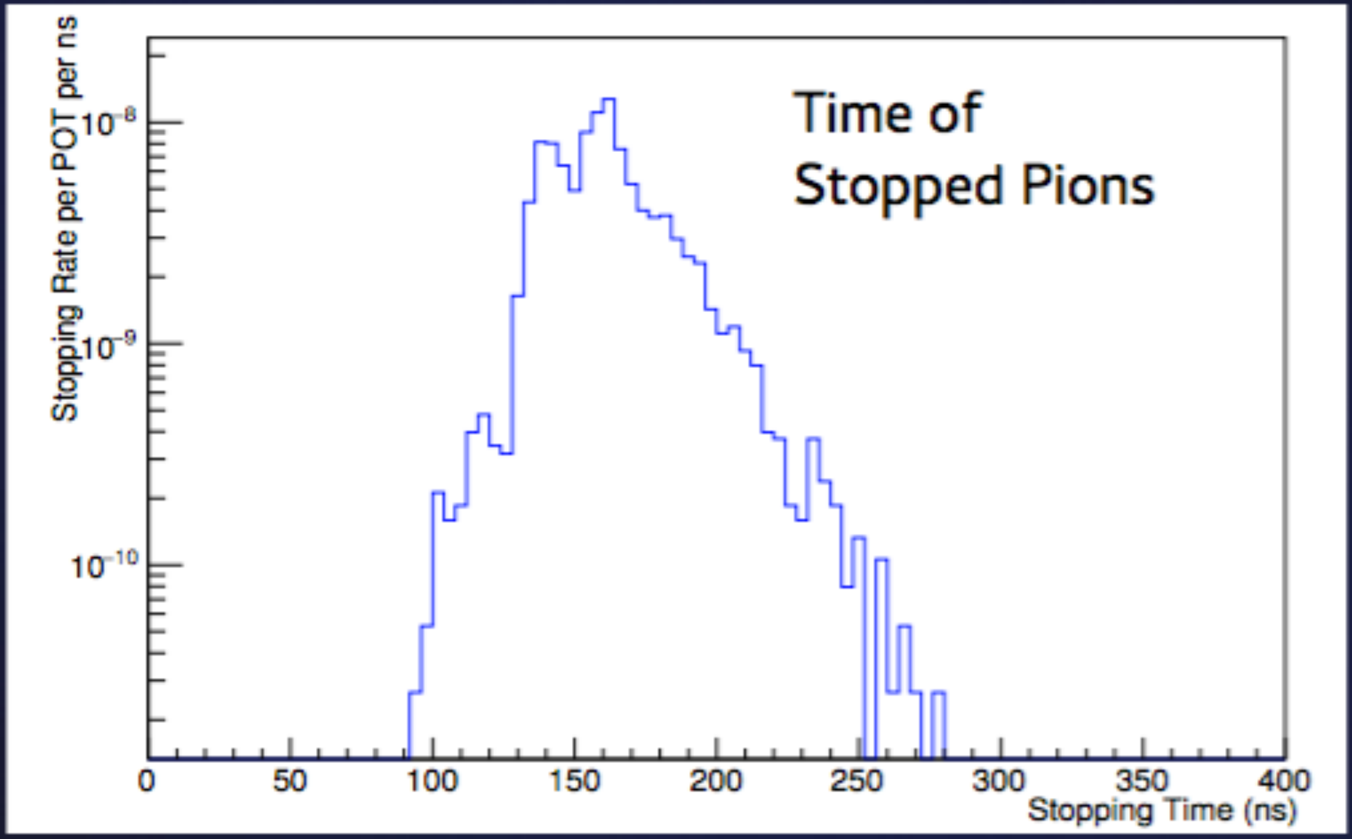

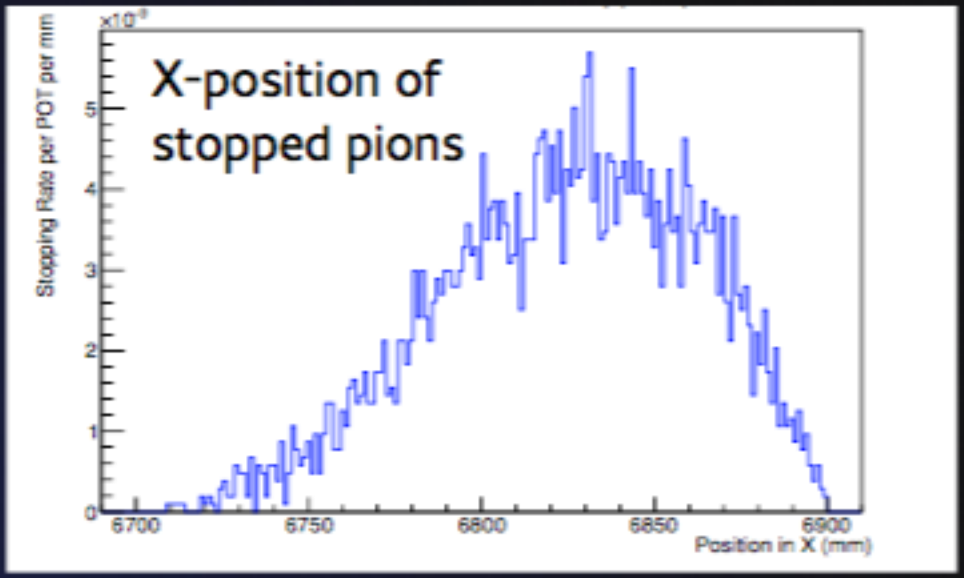

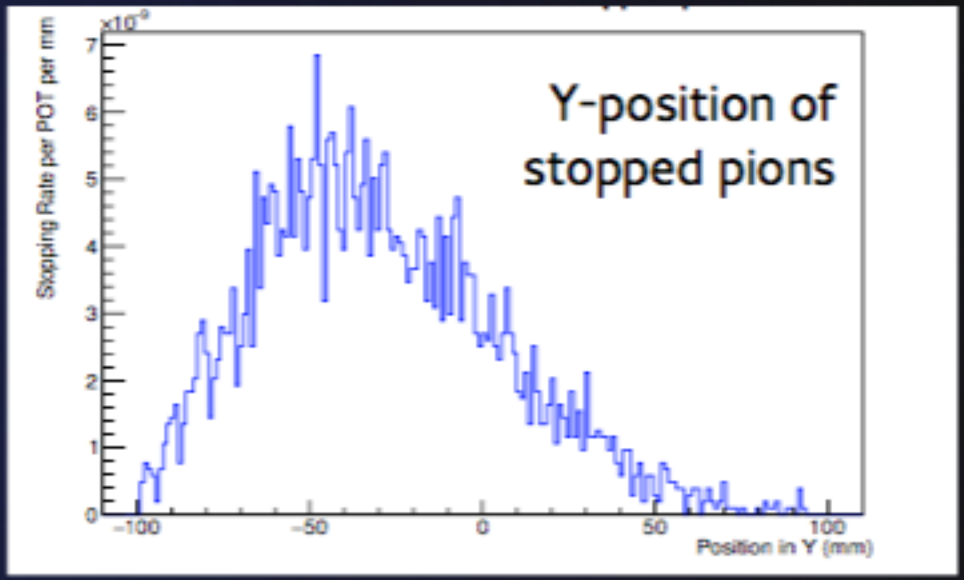

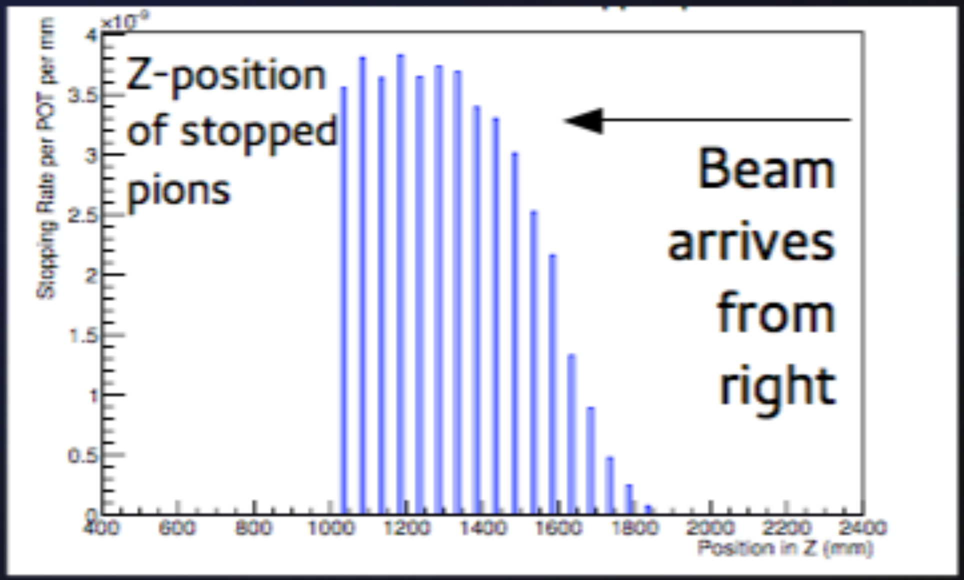

- Stopping rate: 4.33e-07 per POT
- Based on 9.4e9 POT
  - Reseed 2.5e8 POT 40 times
- Skew of stopping distribution in Z
  - Unexpected
  - High momentum muons reaching to back?
  - This is not secondary pions being produced from protons / neutrons etc

Stopped Muons vs. Pions

Stopping Distribution along beam axis

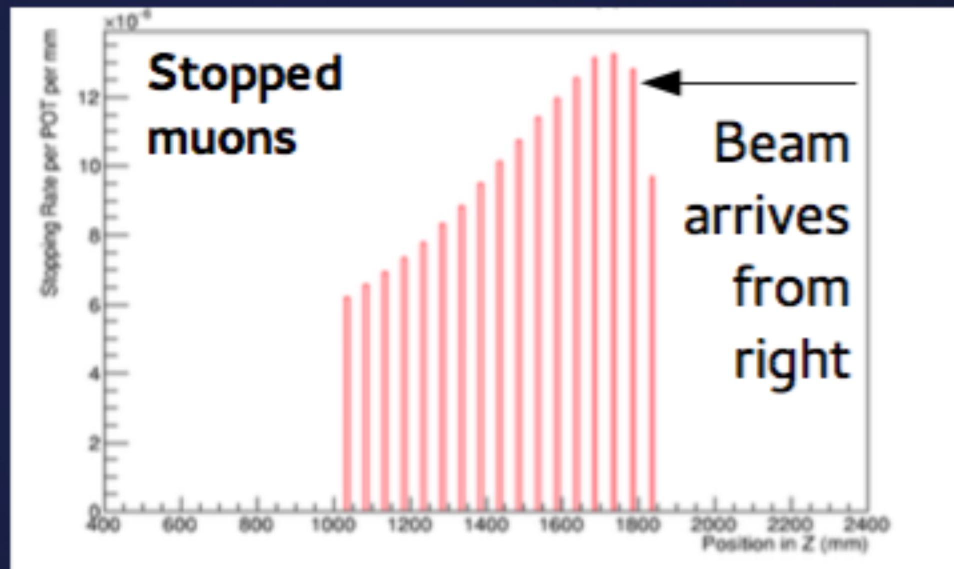

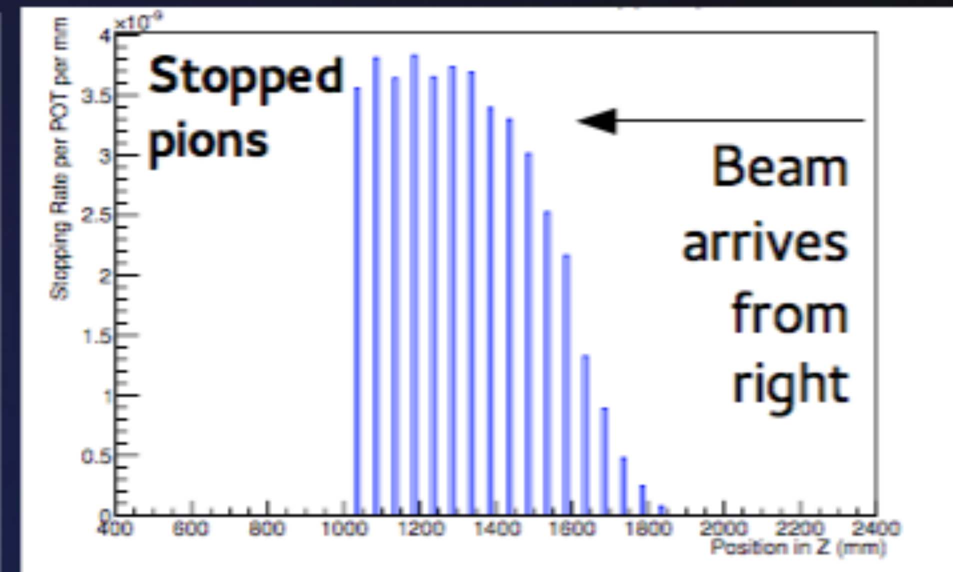

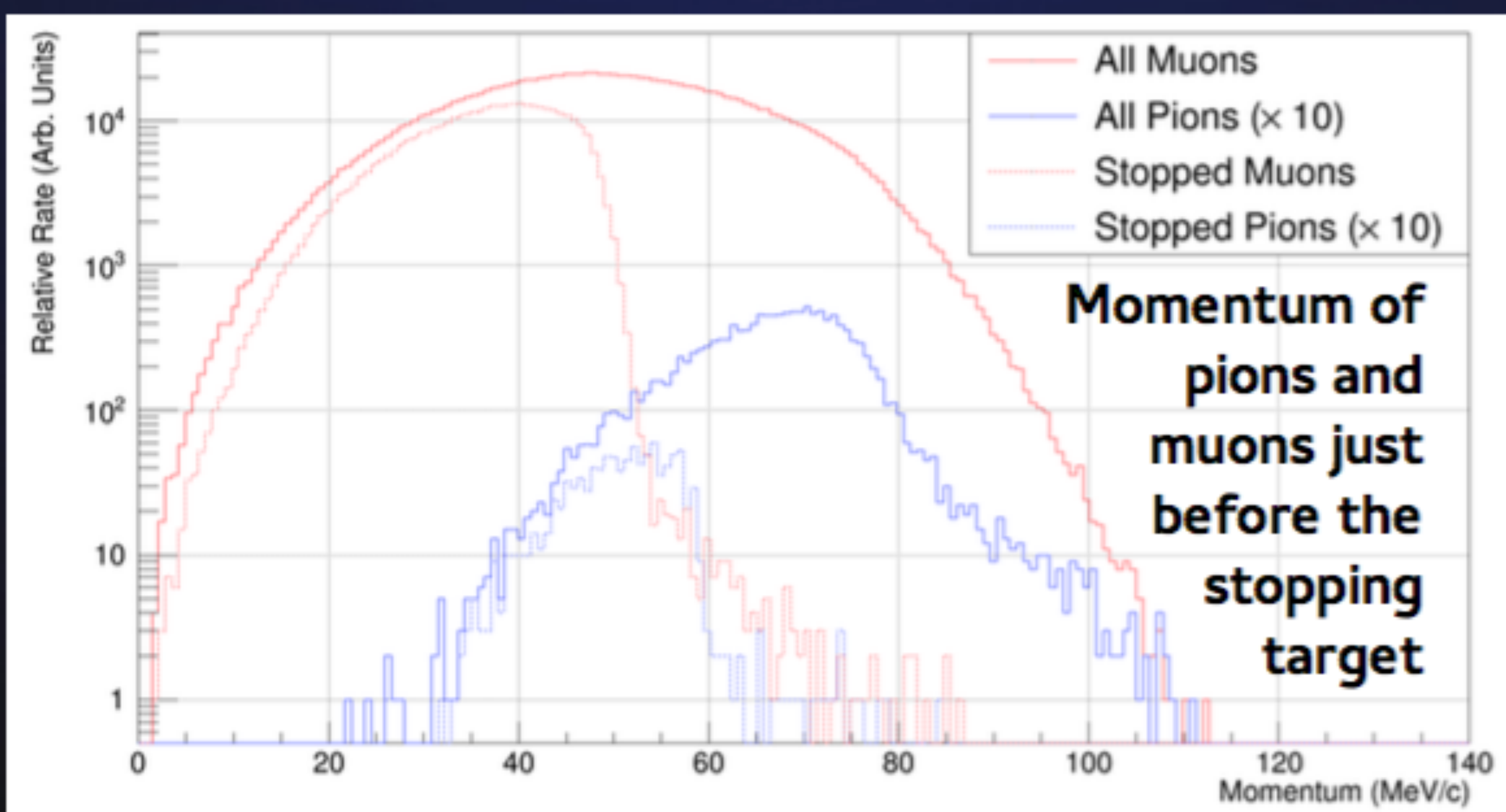

- Mean momentum for stopping particles:
  - Muons: 36 MeV/c
  - Pions: 50 MeV/c
- Maximum momentum is similar

Radiative Mu Capture

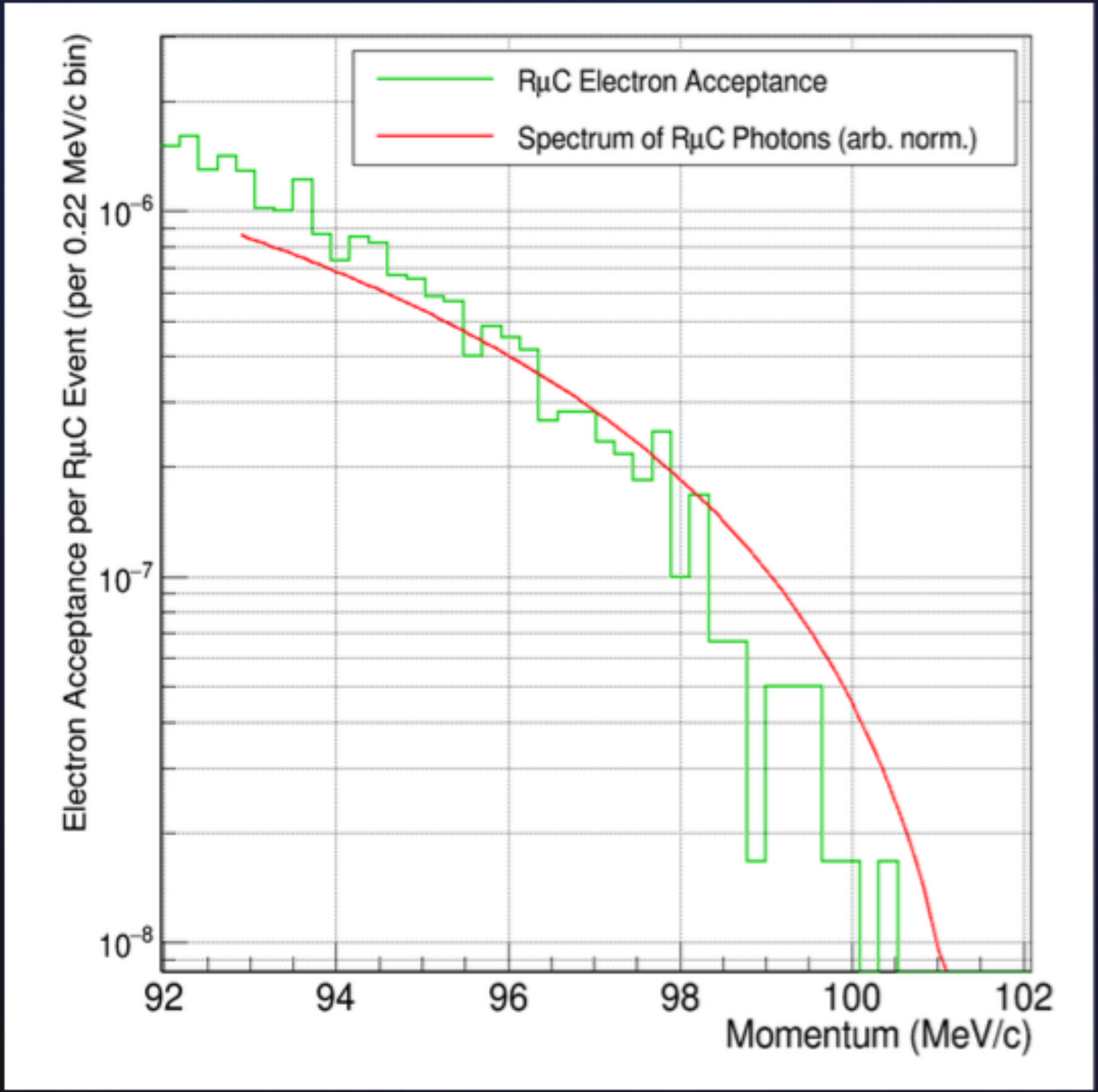

- As per the Phase-I TDR, use end-point expansion for RMC photons:

$$R = C(1 - 2x + 2x^2)(x)(1 - x)^2$$

$$x = \frac{E_\gamma}{E_{\gamma max}}$$

$$E_{\gamma max} = 101.85\ \text{MeV}$$

- No photon can occur above 101.85
  - Doesn't contribute to background rate
  - Only an issue with pile-up or reconstruction errors
- Left plot: Simulation of RMC events
  - 6e7 RMC photons with $E > 90$ MeV at target
  - Observe 36 electrons with $98 < E < 102$ MeV/c
  - Acceptance per RMC photon for electrons in this range: 6e-5 %

Photons from RPC (Radiative Pion Capture)

DOI: 10.1103/PhysRevC.5.1867

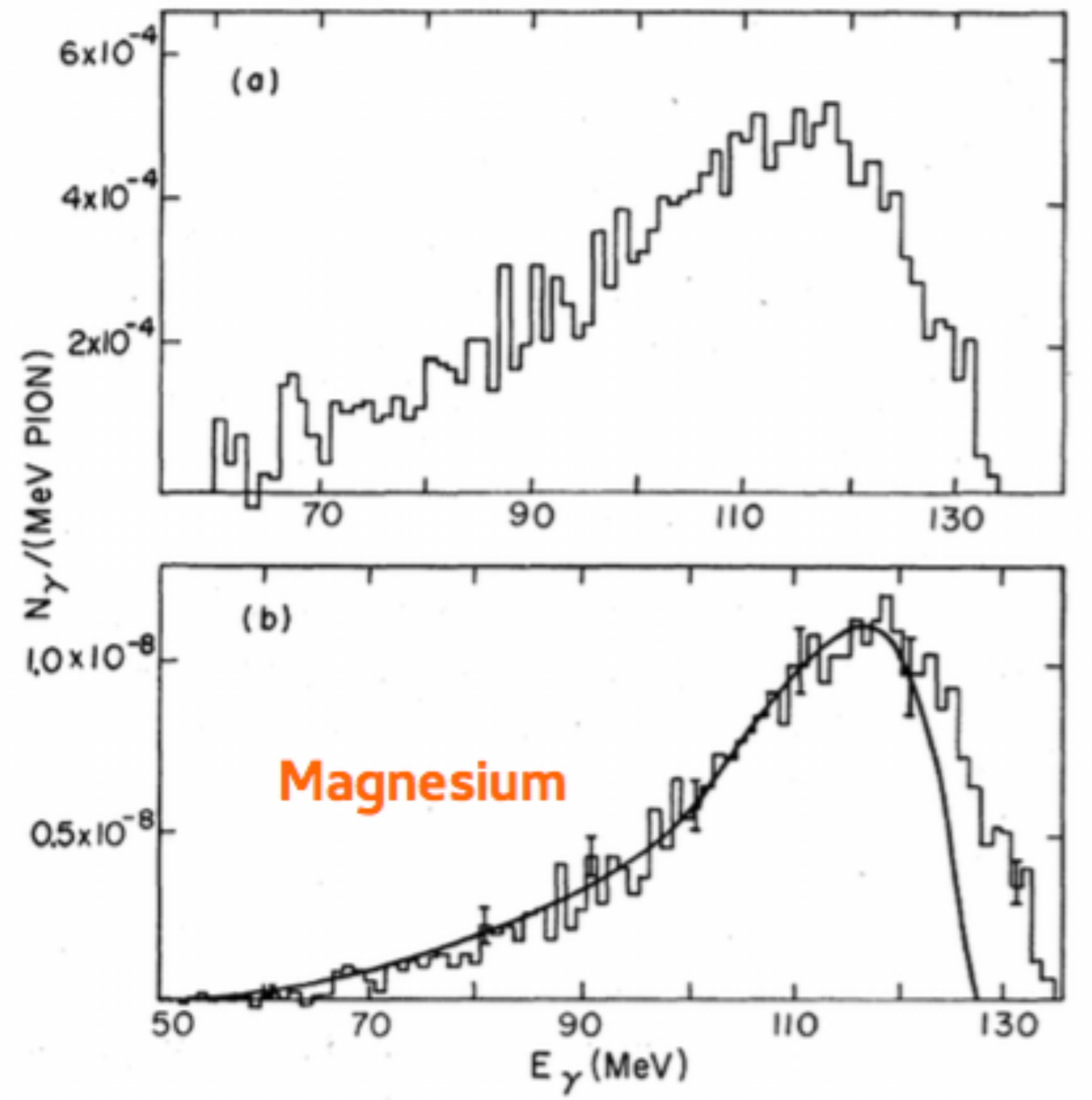

FIG. 7. Energy spectrum of photons from radiative pion capture in magnesium. (a) Spectrum with efficiency divided out (see note, Fig. 4). (b) Measured spectrum with in-flight background subtracted; solid line: pole-model predictions.

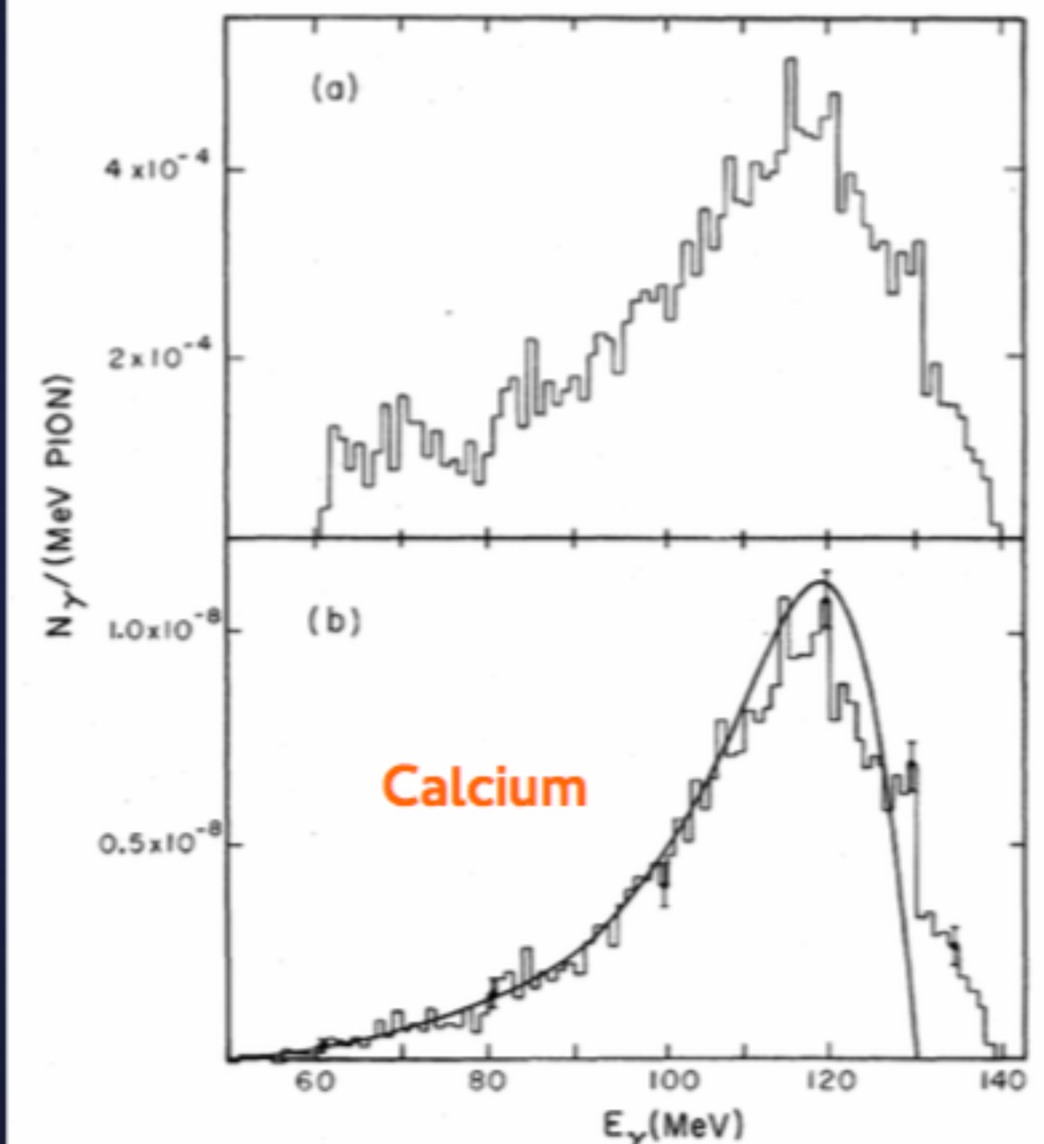

FIG. 8. Energy spectrum of photons from radiative pion capture in calcium. (a) Spectrum with efficiency divided out (see note, Fig. 4). (b) Measured spectrum with in-flight background subtracted; solid line: pole-model predictions.

Photons from RPC

DOI: 10.1016/S0375-9474(97)00187-5

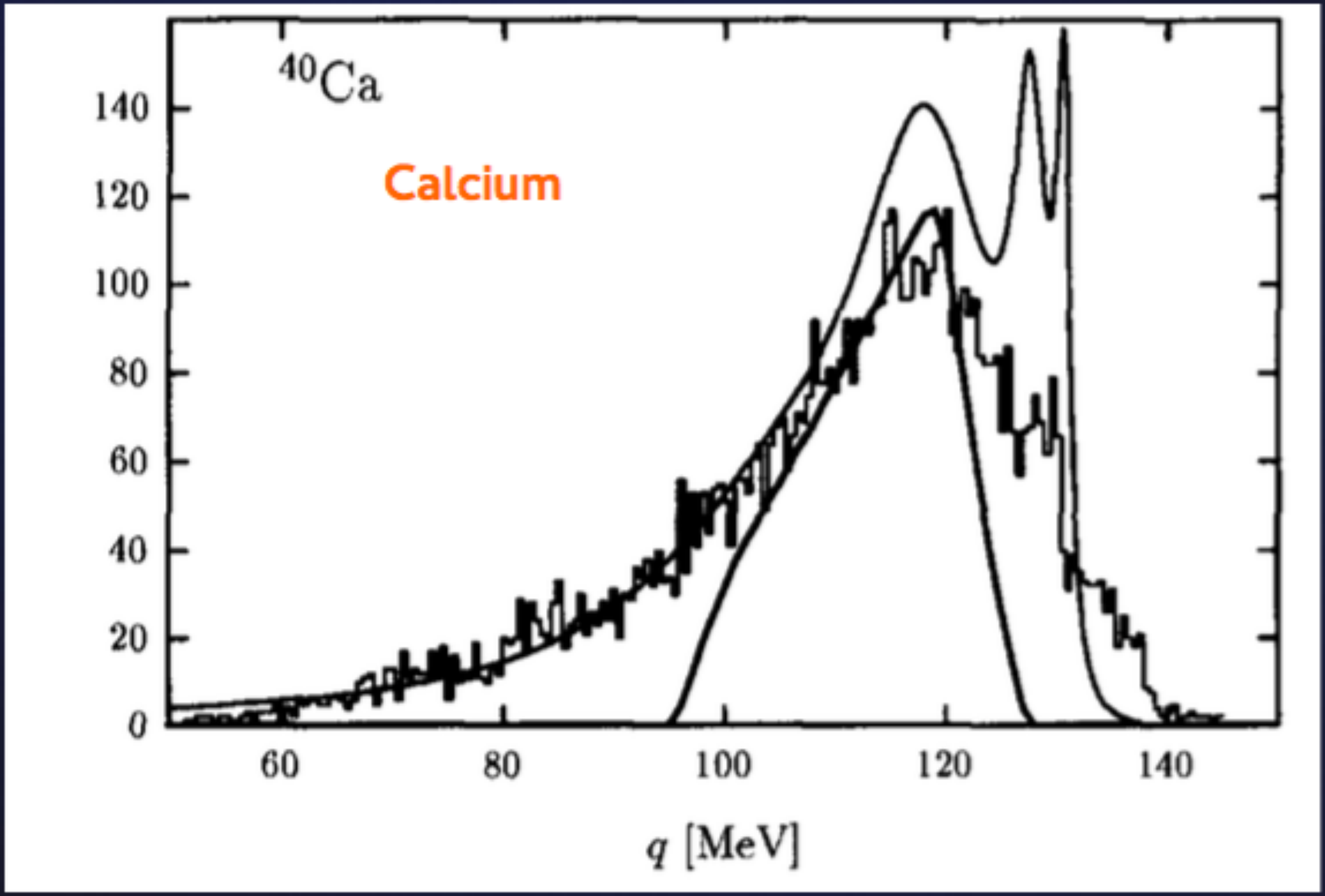

- Phase-I TDR uses this experimental spectrum, which is taken from previous paper

Fig. 4. Results for $dR^{(\gamma)}/dq$ in ^{12}C, ^{16}O and ^{40}Ca. Two-body contributions have now been included. Experimental data, taken from Refs. [2,28], are given in arbitrary units. Our results have been normalized to the data at q = 105 MeV. For comparison, we have in ^{40}Ca also shown the FG results presented in Fig. 3 of Ref. [6] (thick line). The absolute value of the FG distribution around the peak is about a factor two or three greater than the SM one (thin line) and it has been normalized to the peak of the data. Additionally, the FG curve has been shifted 10 MeV to the left.

Simulating RPC Background

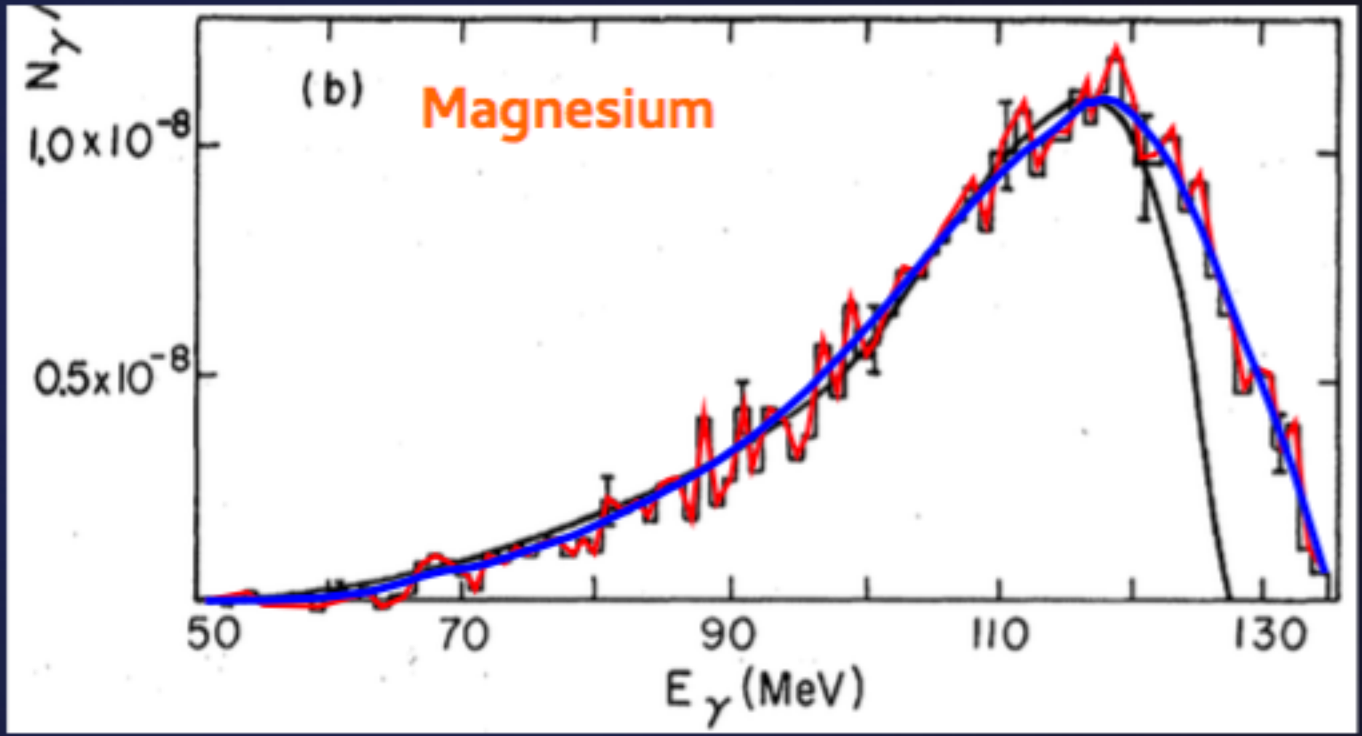

DOI: 10.1103/PhysRevC.5.1867

- Digitize spectrum for pion-capture on magnesium (red line)
- Smooth the spectrum (blue line)
  - Use TGraphSmooth::SmoothSuper()
- Input 4e6 RPC photons with realistic stopping distributions into simulation
- Geant4 performs photo-conversion

Radiative Pion Capture

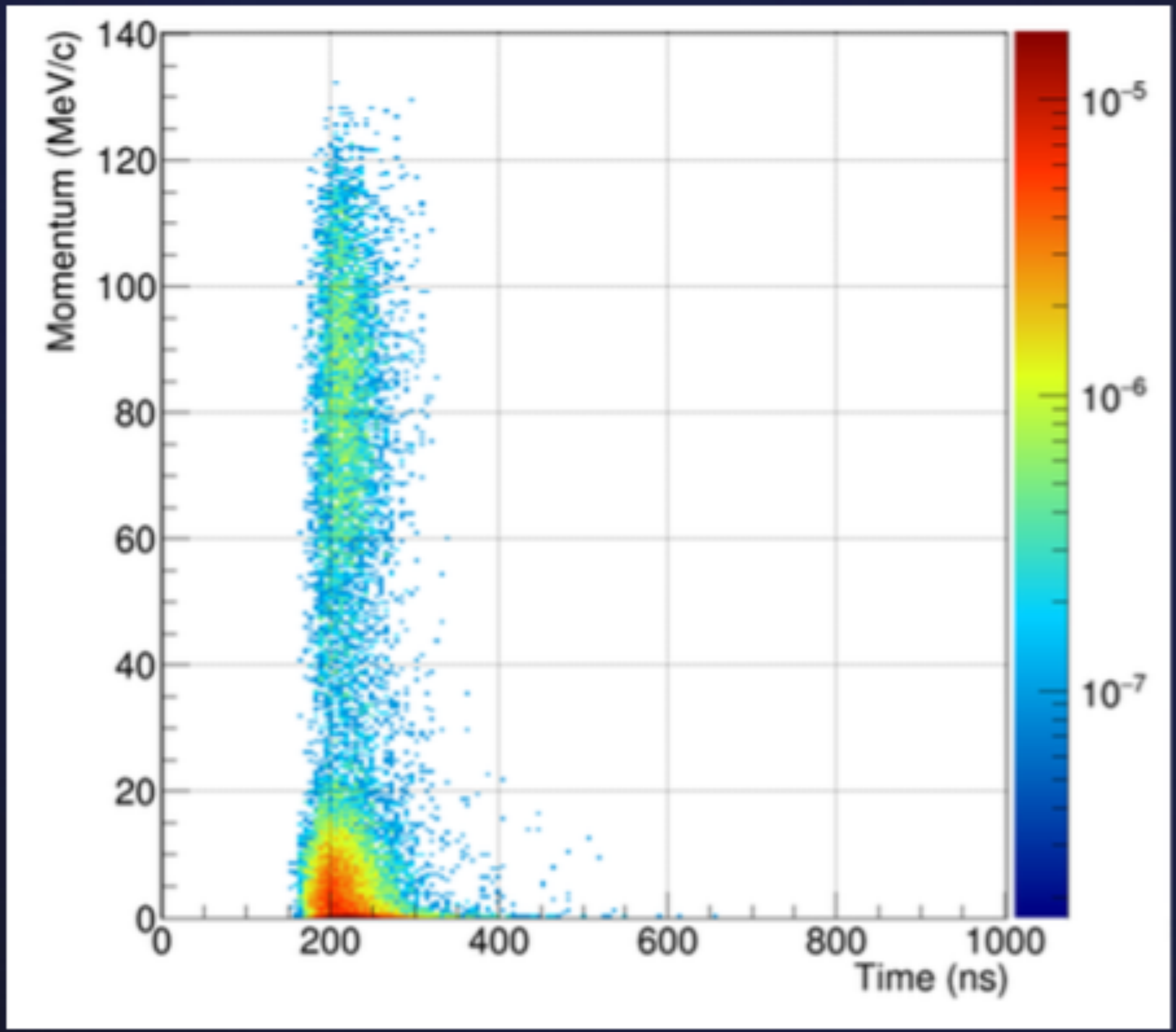

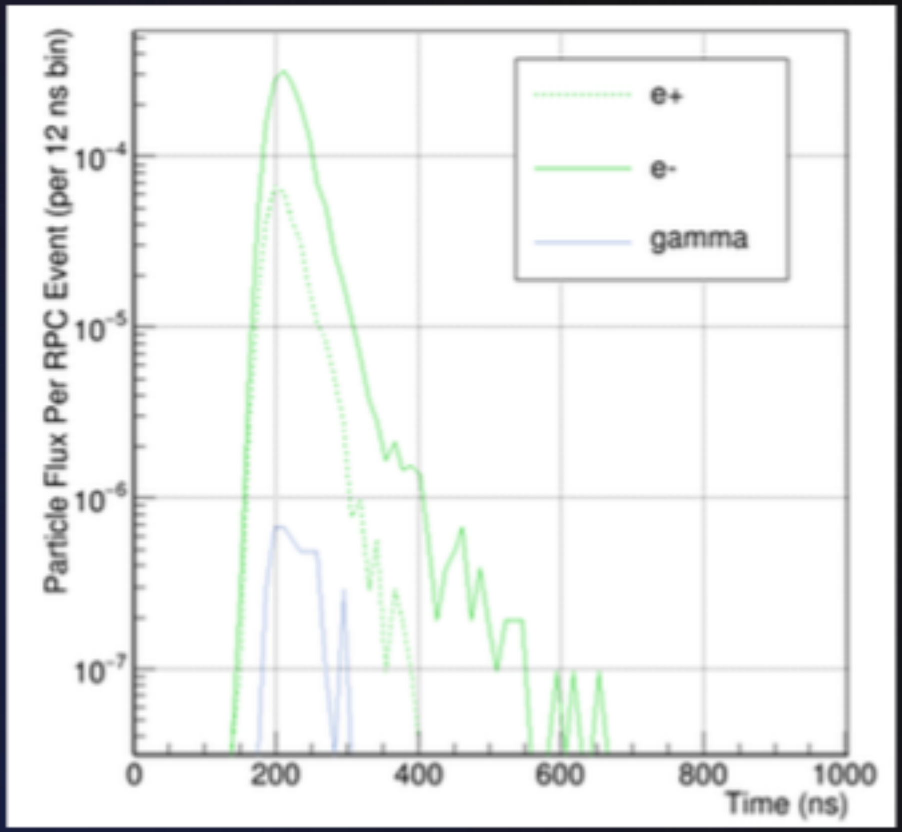

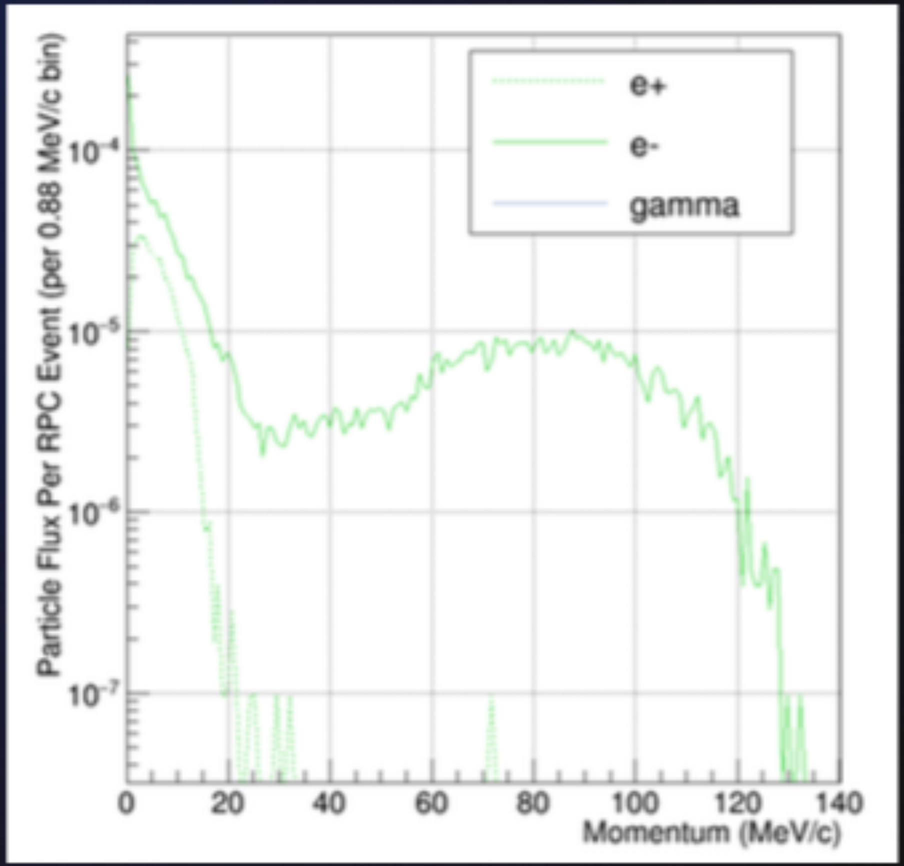

- Between 103.6 and 104.97 MeV/c:
  - 1.05e-5 electrons per RPC event
- All of these arrive before 360 ns

Radiative Pion Capture

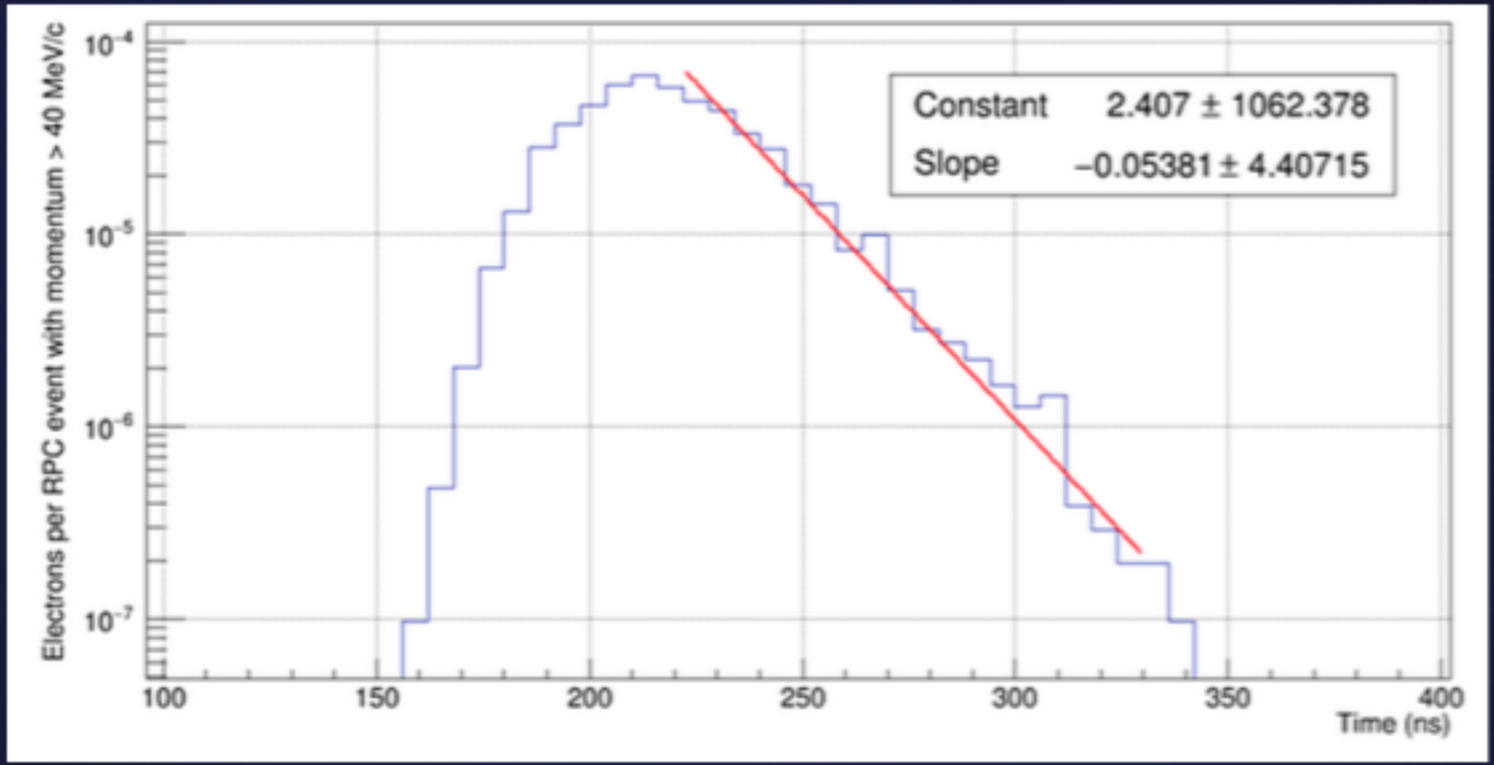

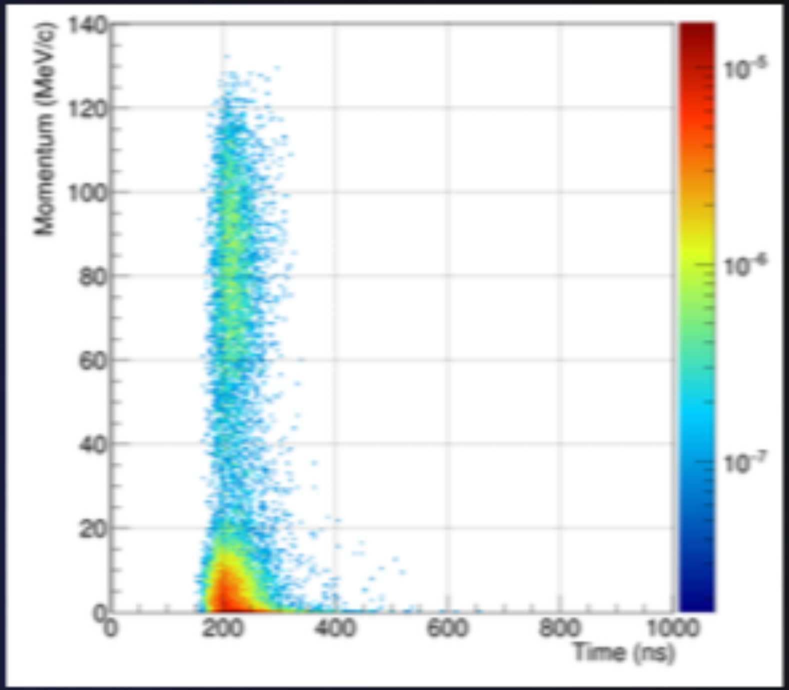

- Arrival time of RPC electrons with momentum > 40 MeV/c:
  - Decay constant = 18.6 ns
- By extrapolation, acceptance of RPC electrons:
  - From 600 to 1200 ns = 2.0e-12 electrons per delayed RPC event
  - From 700 to 1200 ns = 9.0e-15 electrons per delayed RPC event
- RPC Background rate:
  - Delayed = 4.3e-7 (pi stops per POT) x 1.05e-5 (RPC per pi stop) x 2.0e-12 (time acceptance of RPC e-)
    = 9.0e-24 per POT
  - Prompt = 4.3e-7 (pi stops per POT) x 1.05e-5 (RPC per pi stop) x 1.0e-12 (extinction factor)
    = 4.5e-24 per POT

Anti-proton background

- Literature
- http://dx.doi.org/10.1088/0954-3899/30/7/008
- Anti-proton production cross section at 8 GeV is about 0.01 mb on Carbon

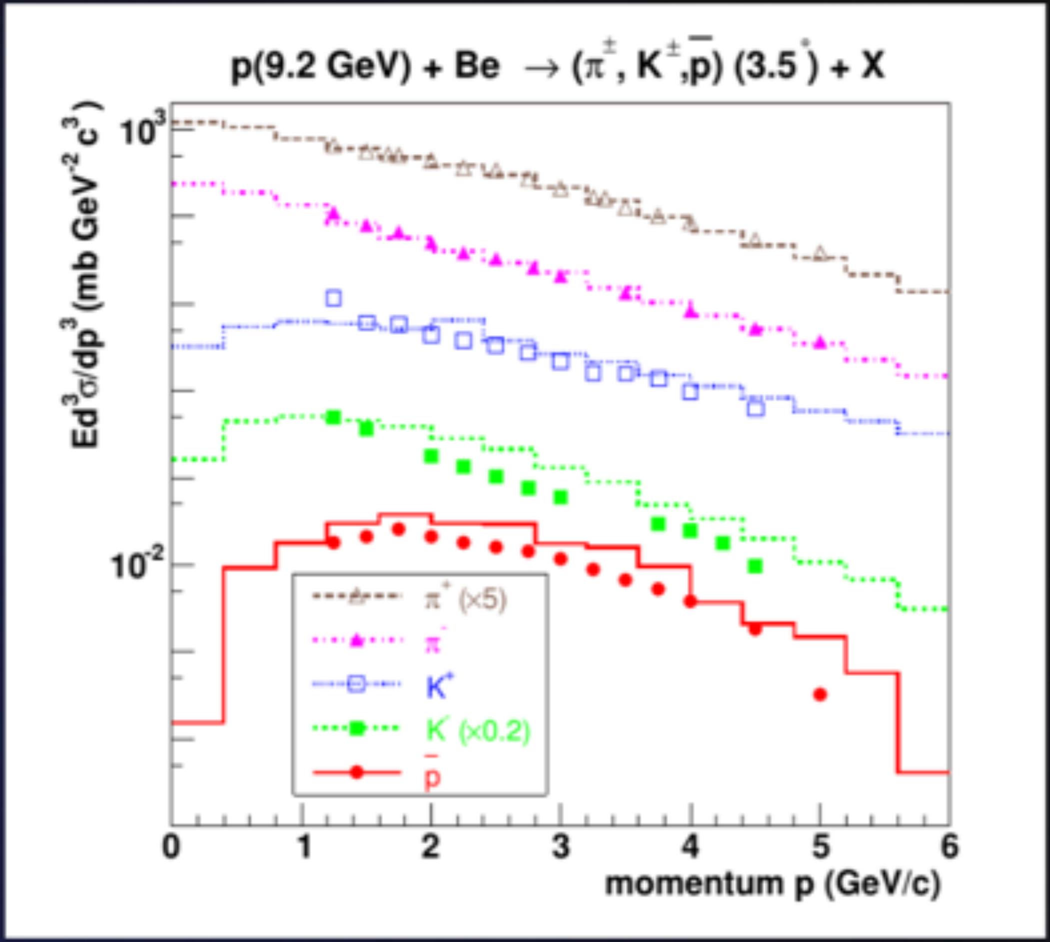

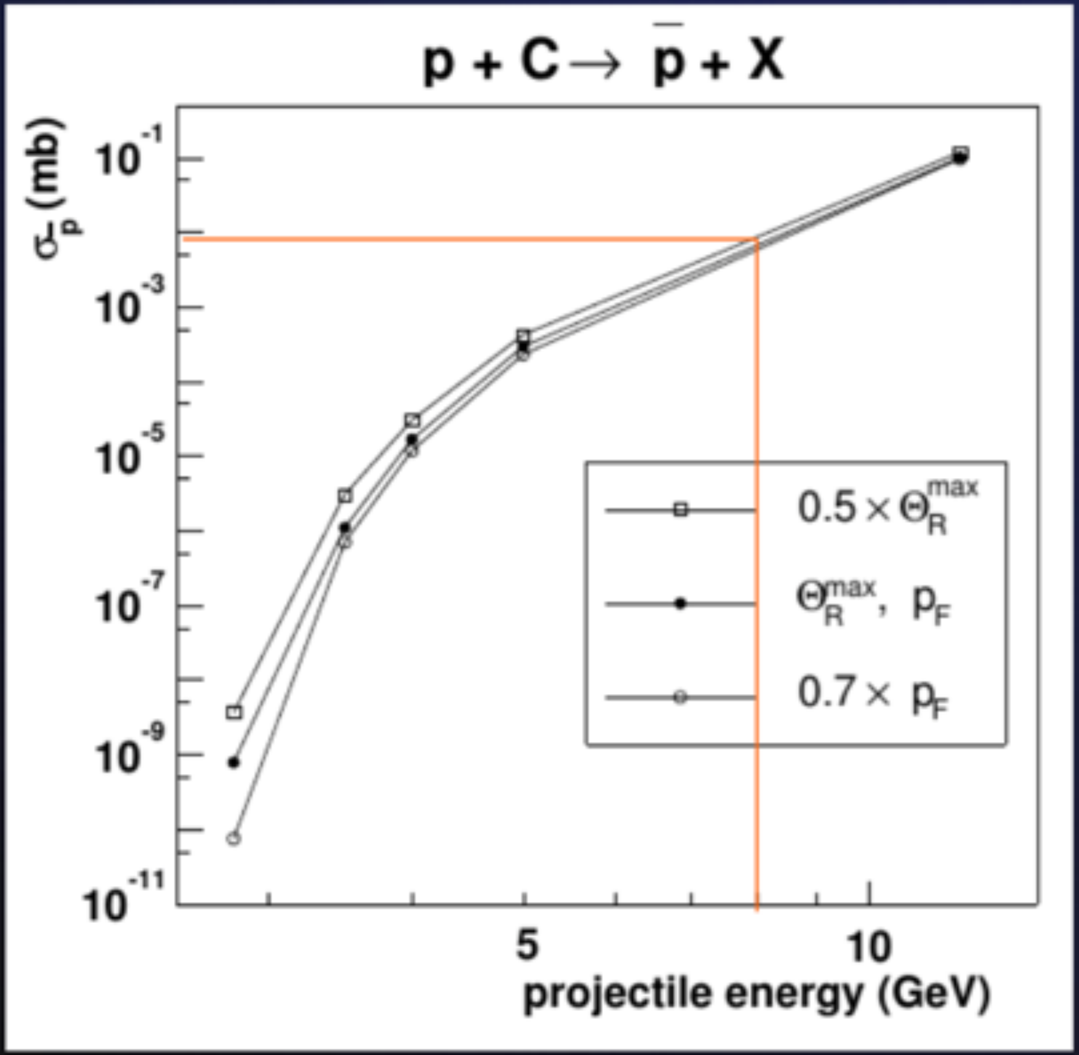

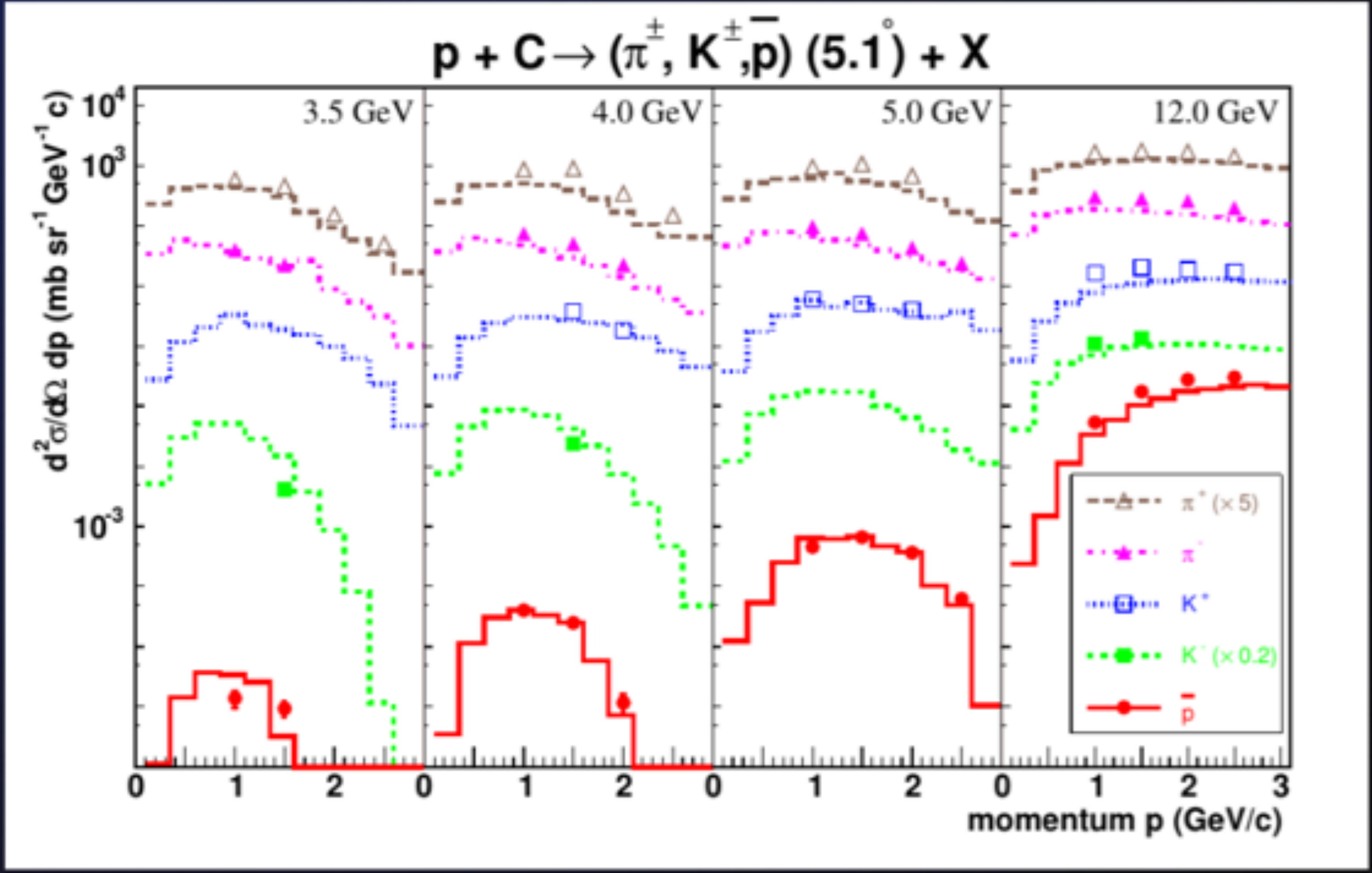

Anti-proton Backgrounds

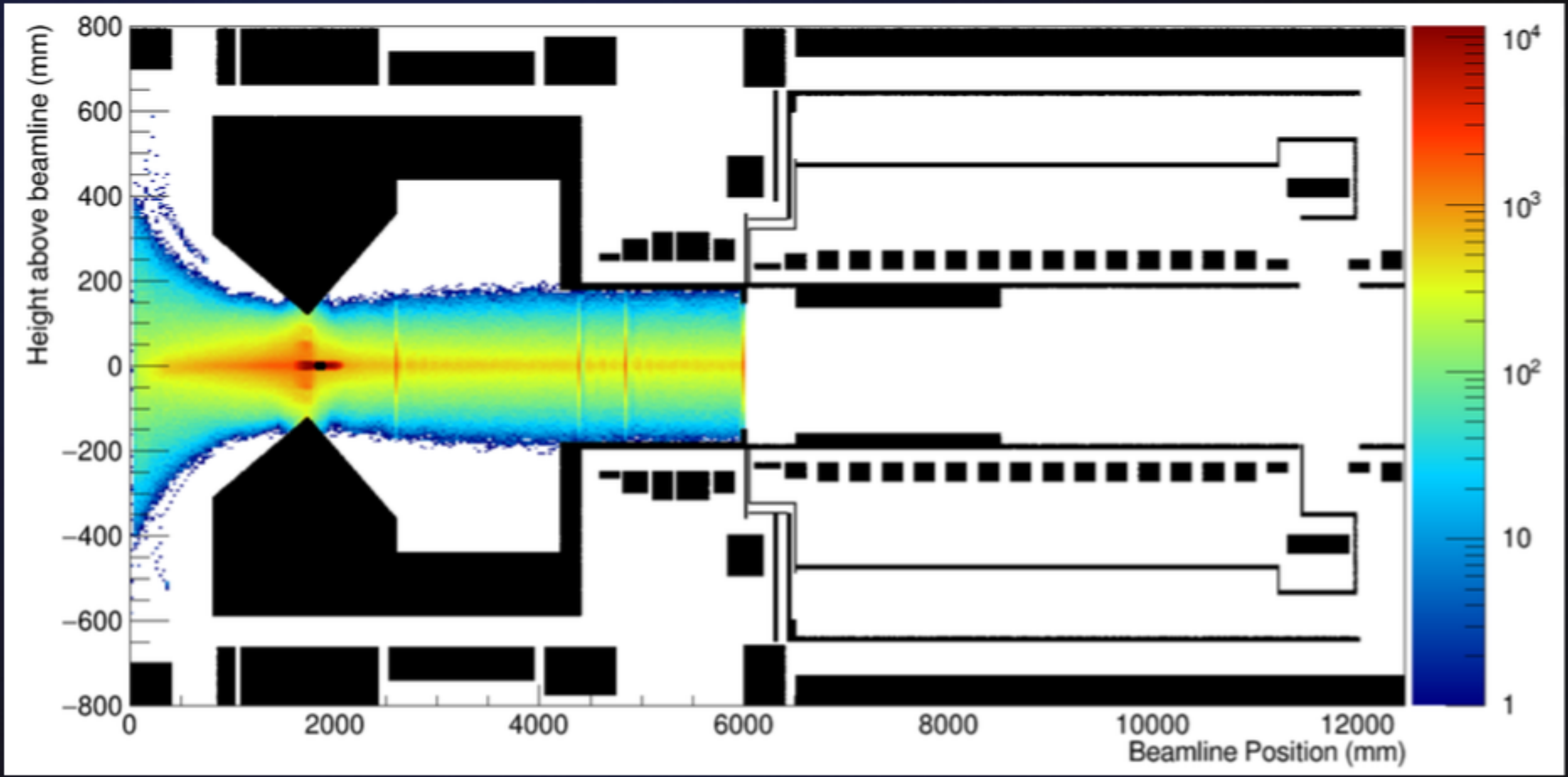

- 2e5 anti-protons with uniform kinetic energy up 10 GeV
- Isotropic and uniform at production target

Acceptance of Stopping Target Electrons

- 5e7 Electrons in stopping target
- Realistic Muon stopping position target
- Acceptance into detector if a single hit in a straw or crystal

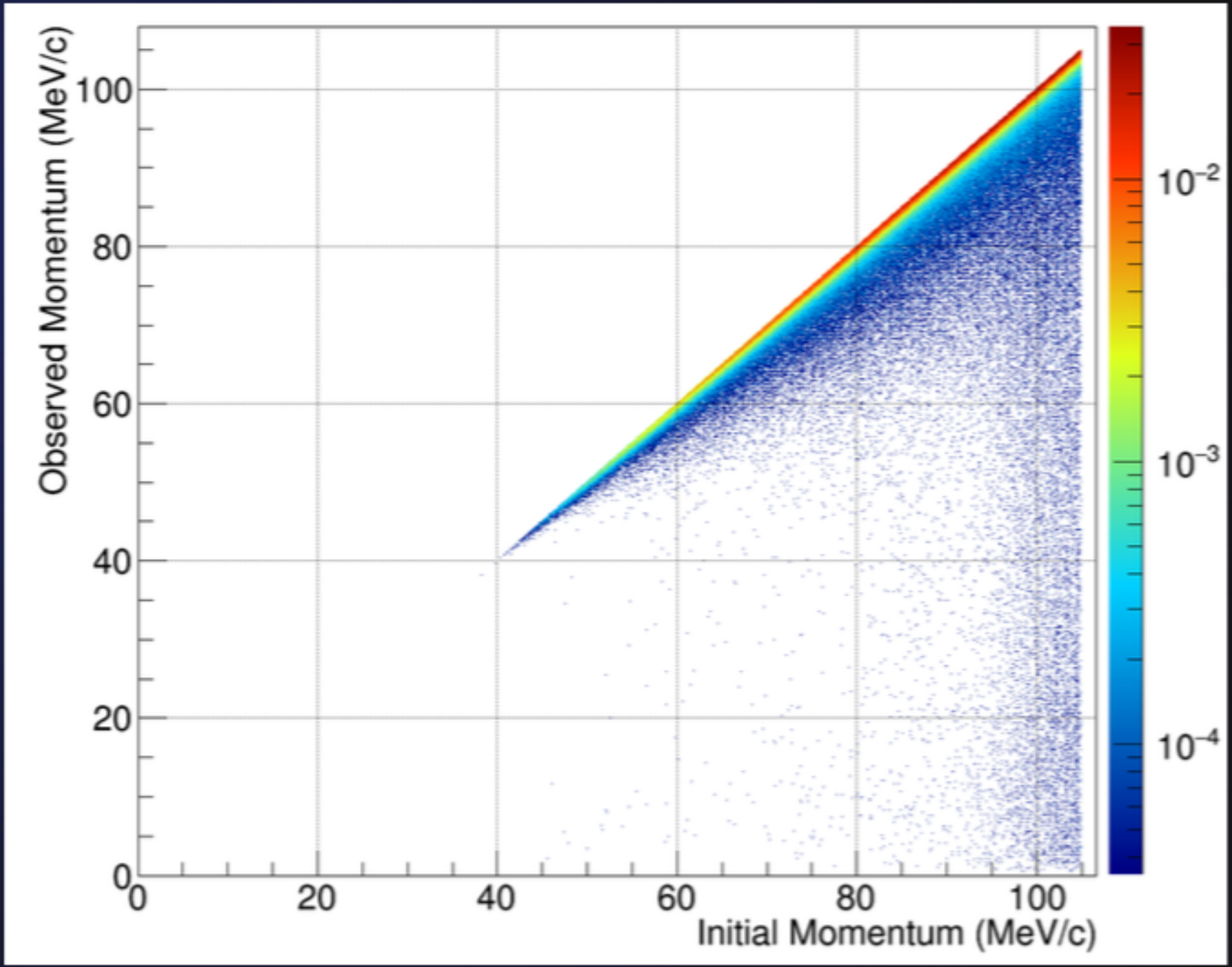

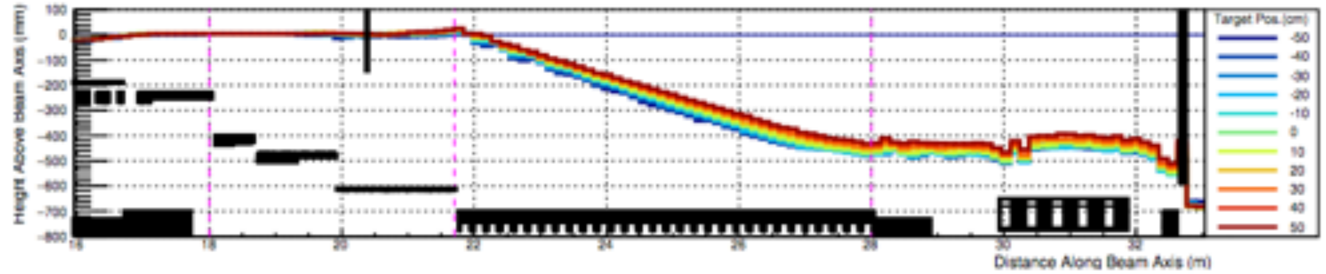

(a) Electrons from 40 to 45 MeV/c

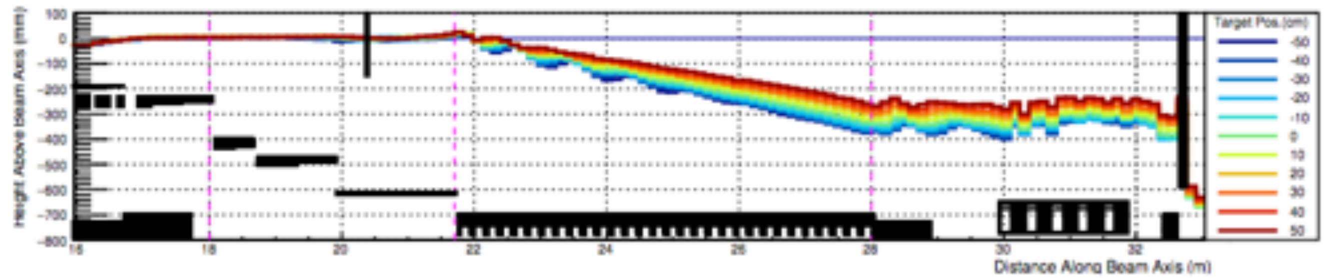

(b) Electrons from 60 to 65 MeV/c

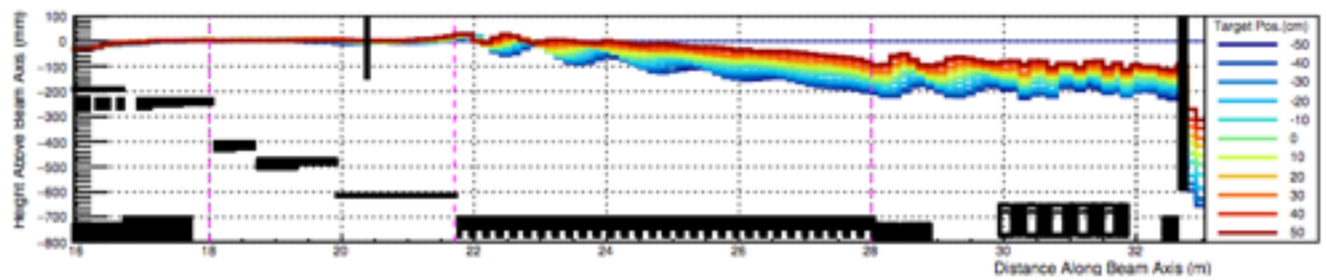

(c) Electrons from 80 to 85 MeV/c

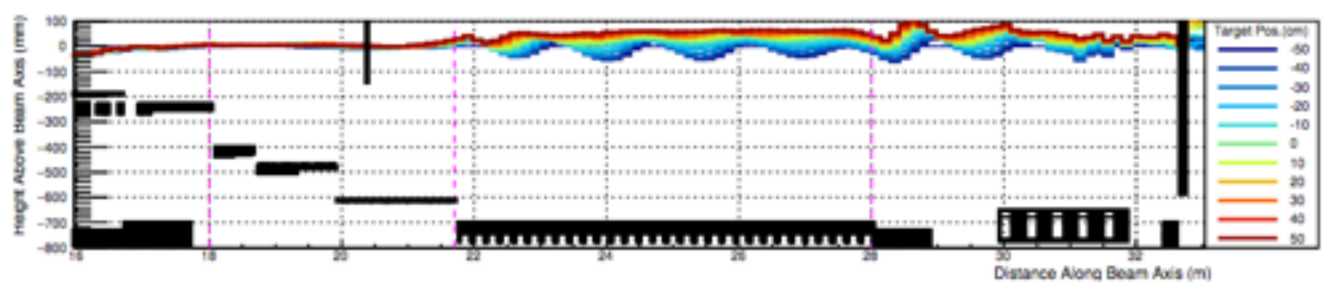

(d) Electrons from 100 to 105 MeV/c

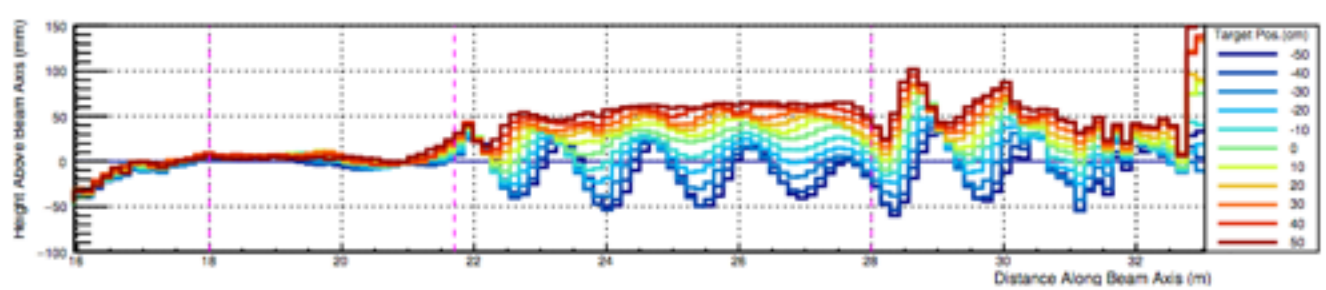

(e) Electrons from 100 to 105 MeV/c (Zoomed)

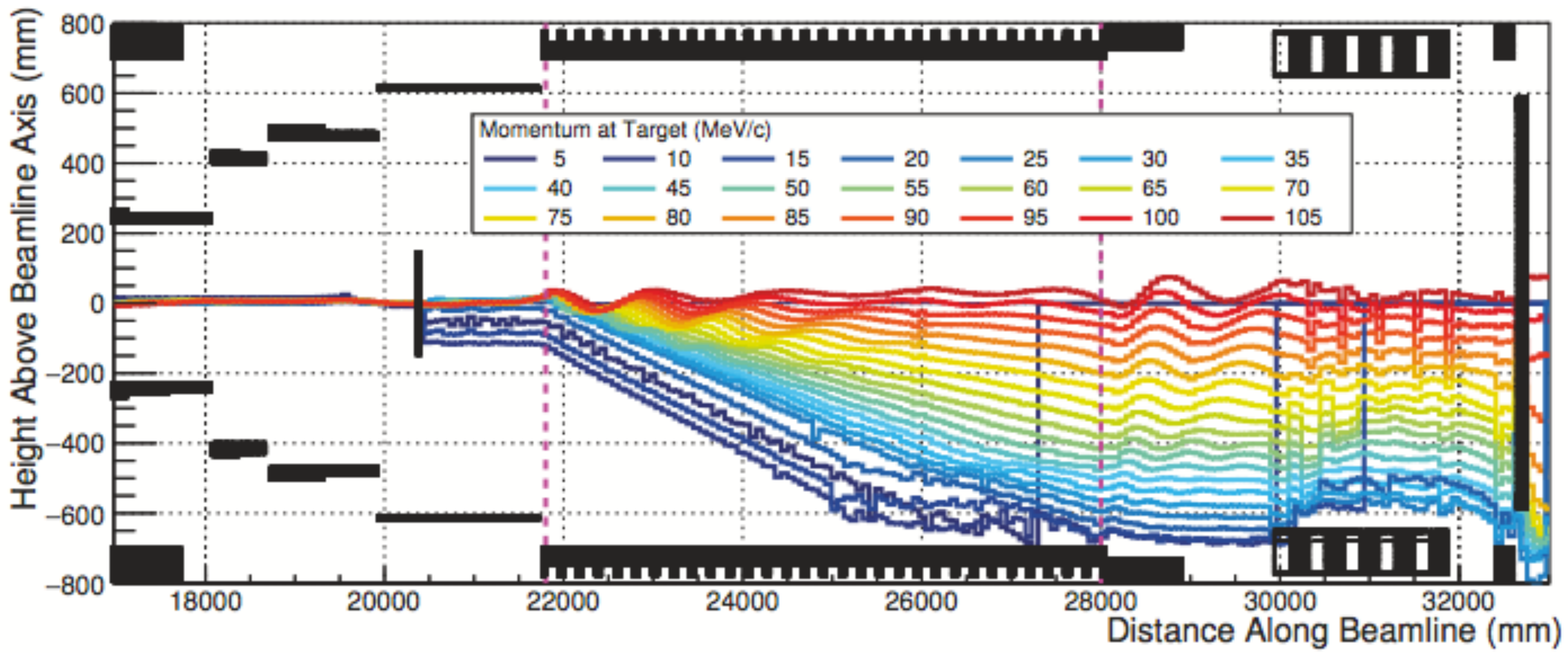

Height Above Beamline Axis (mm)
Distance Along Beamline (mm)
Momentum at Target (MeV/c)
5 10 15 20 25 30 35
40 45 50 55 60 65 70
75 80 85 90 95 100 105

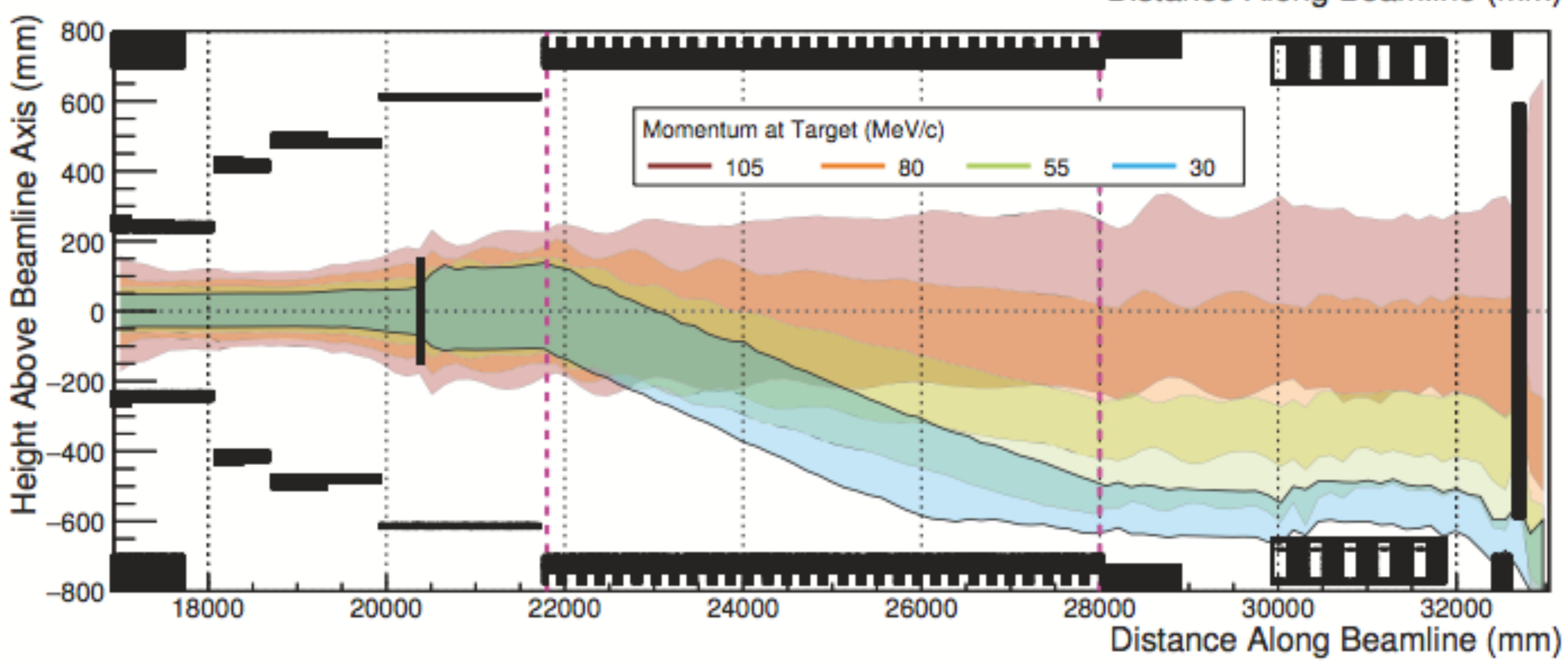

Height Above Beamline Axis (mm)
Distance Along Beamline (mm)
Momentum at Target (MeV/c)
105 80 55 30

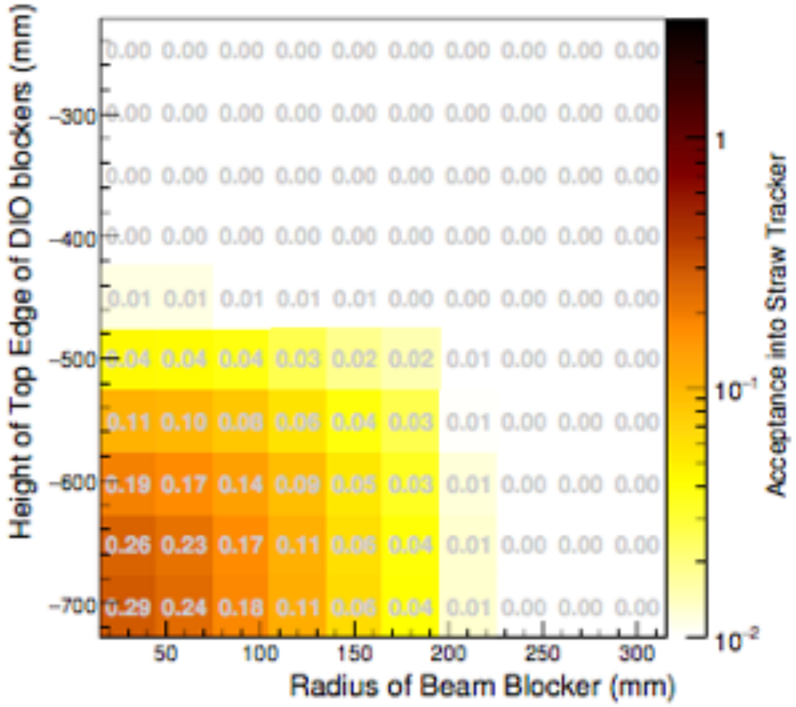

(a) 40 MeV/c

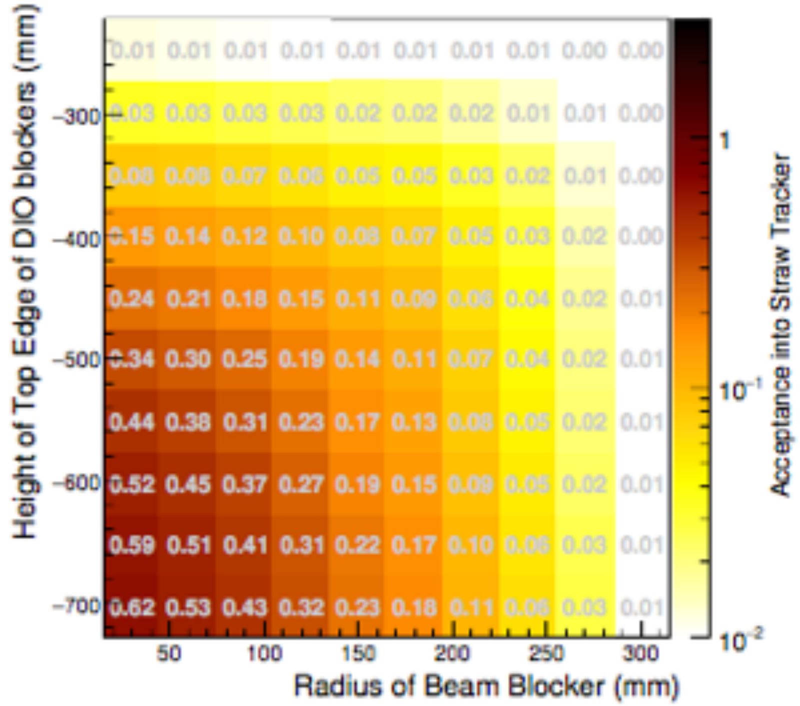

(b) 60 MeV/c

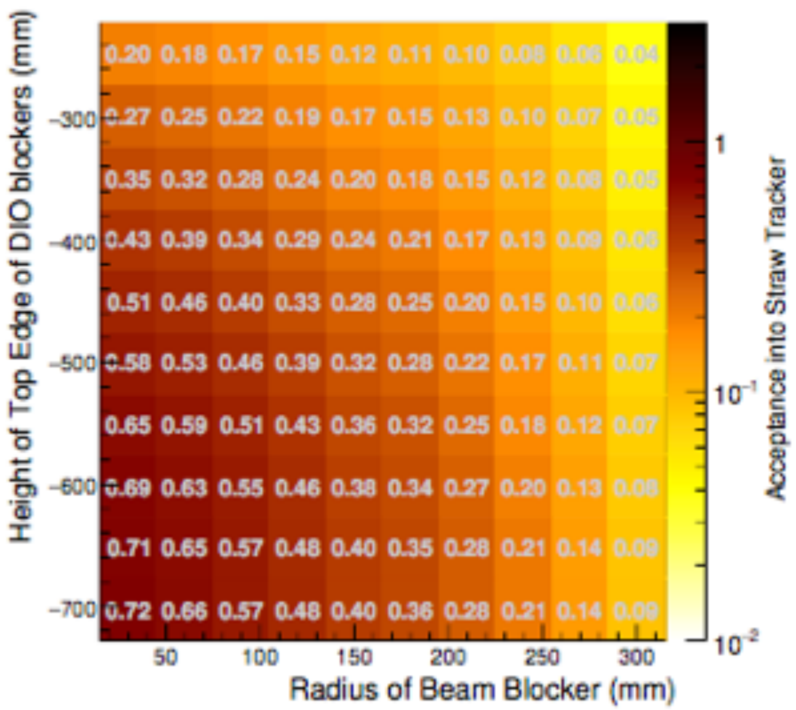

(c) 80 MeV/c

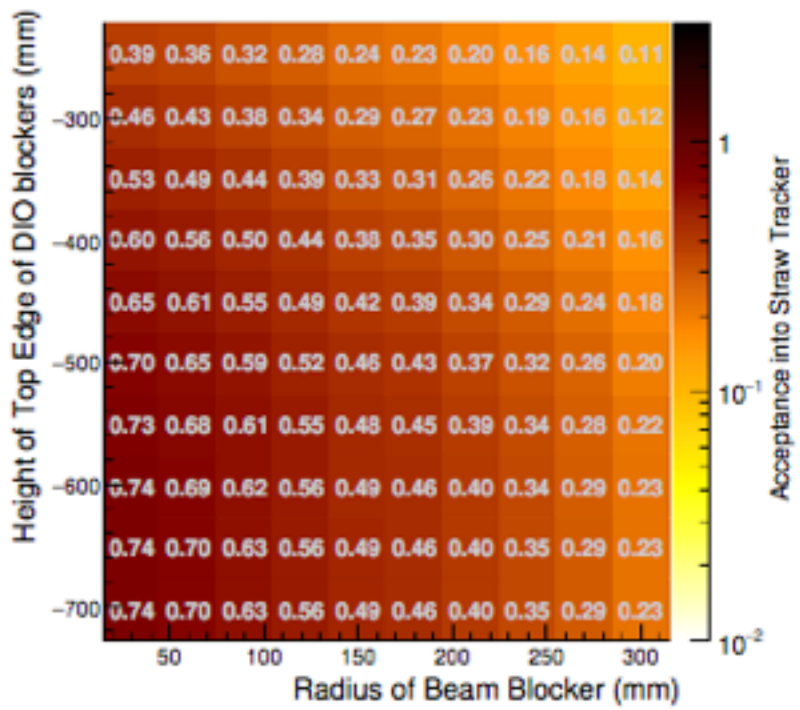

(d) 100 MeV/c

Figure 5.29: Acceptance into the straw tracker for electrons with different momentum at the stopping target as a function of the beam and DIO blocker dimensions. Note the logarithmic scale for the colour bar.

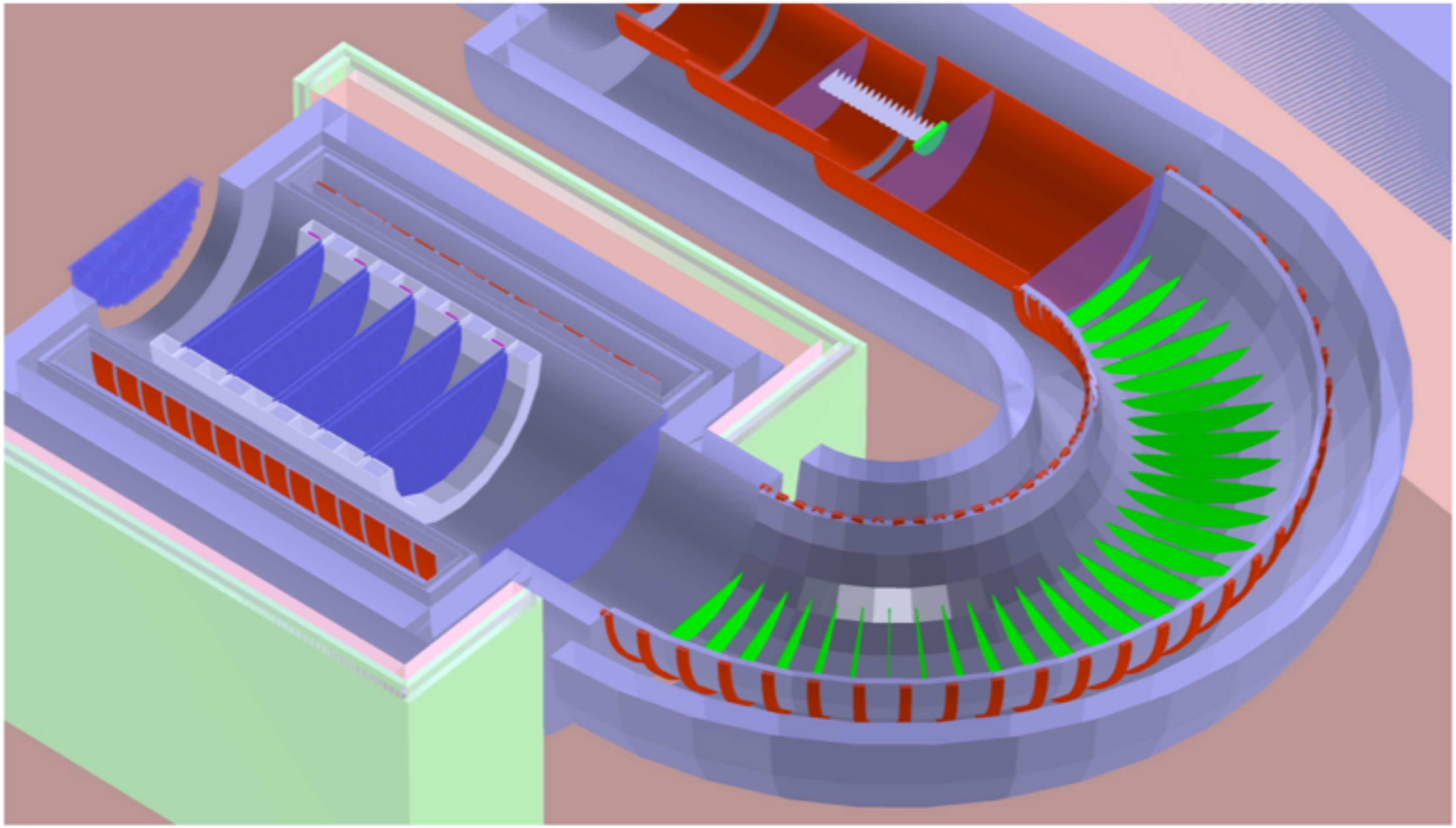

Figure 5.27: Location of the beam blocker and one possible geometry for the DIO blockers, both highlighted in dark green, shown here before optimisation.